SYSTEMATIC DESIGN OF BULK RECYCLING SYSTEMS UNDER UNCERTAINTY

A Dissertation
Presented to
The Academic Faculty

By

Jing Wei

In Partial Fulfillment
Of the Requirements for the Degree
Doctor of Philosophy in the
School of Chemical and Biomolecular Engineering

Georgia Institute of Technology

May, 2004

SYSTEMATIC DESIGN OF BULK RECYCLING SYSTEMS UNDER UNCERTAINTY

Approved by:

Dr. Matthew J. Realff, Advisor

Dr. Jane C. Ammons

Dr. Martha A. Gallivan

Dr. Jay H. Lee

Dr. F. Joseph Schork

Date Approved: May 10, 2004

DEDICATION

To my husband, Jian Gu, and parents, sister,

for their encouragement, support and love.

ACKNOWLEDGEMENTS

First, I would like to express my deepest appreciation to my thesis advisor, Dr. Matthew Realff, for giving me the support and guidance to achieve my goals and for giving me the freedom to pursue the topics that excited me.

Thanks to other thesis committee members, Dr. Jane Ammons, Dr. Martha Gallivan, Dr. Jay Lee and Dr. Joseph Schork, for giving their advice during annual committee meetings. I would also like to thank Dr. John Pelesko for discussions about electrostatics.

In addition to the many people who helped to make this dissertation possible, I could not have made it through the past five years without my friends and family. I would not have come to the U.S to pursue a Ph.D. degree without the support and love of my parents. Finally, I would like to thank my husband, Jian Gu, for his support, encouragement and love. I am so blessed to have you in my life. Thank you for loving me!

TABLE OF CONTENTS

LIST OF TABLES

LIST OF FIGURES

SUMMARY

The fast growing waste stream of electronic and other complex consumer products is making the bulk recycling problem an important environmental protection issue as many of these products contain hazardous materials such as mercury and lead and naturally non-degradable materials such as various plastics. This stream of material also contains valuable components in significantly higher proportions than raw ore streams. Mechanical recycling is potentially a more environmentally benign method than other options such as chemical recycling and energy recycling because recycled materials can be reused without significant additional investment. Many traditional mineral processing methods, such as sink-float separation, froth flotation, electrostatic separation, are now being applied to plastics separation, which is a relatively new research area compared to metals separation. The focus of this thesis is the development of systematic methods for designing systems to recover mixed plastics from electronic products such as computers and televisions.

No systematic design methodology has been proposed for the bulk recycling area. Most existing work has focused on individual experimental technologies or overall recycling strategies without using detailed unit models. Furthermore, the impact of uncertainty on the design has been ignored. This motivates the development of a systematic method that considers uncertainty from the outset.

Bulk recycling systems are similar to other chemical engineering process systems and therefore they can be synthesized and designed using the same types of techniques that have been applied to distillation and reaction systems. A widely used approach is to pose the flowsheet optimization problem under uncertainty as a stochastic Mixed Integer Nonlinear Program (sMINLP). Two major challenges arise in applying this method to bulk recycling system design.

One challenge is the efficient solution of a sMINLP. Existing work in literature solves this problem with a prefixed sample size, does not provide a way to evaluate the solution quality, and is computationally challenging. A Sample Average Approximation (SAA) method wrapped on the Outer Approximation method has been developed (Wei and Realff, 2004) in this thesis to decompose the solution of a stochastic problem into the solution of multiple smaller sample-size problems and a larger sample-size problem with fixed decision variables. The sample sizes can be adjusted based on the confidence interval of the optimality gap. The computational time is significantly reduced due to the decoupling of scenarios in the larger sample-size problem.

Another challenge is the development of unit models for bulk recycling systems. These models must account for variability in particle properties, such as the size, charge, etc., and other random factors, such as the entering position. This work modeled various plastics separation methods based on calculating the recovery as a joint cumulative distribution function and unified the models using a canonical partition curve representation. The modeling approach (Wei and Realff, 2003 a, b, c) can guide other

users to extend it to other separation methods where there are distributions in properties that must be evaluated against a cut-off value.

Finally, an overall design method is proposed in this work to decompose the overall problem into several levels and apply heuristics methods at the upper level, such as the design of size reduction step and mathematical programming at the lower level. A step-by-step design strategy is presented for an integrated design of the design of size reduction units and the separation units.

CHAPTER 1

INTRODUCTION

1.1 Introduction to bulk recycling

Recycling plays an important role in environmental protection, particularly for electronic products. Used electronic equipment is a fast-growing component of the nation's waste stream. Technological advances rapidly render formerly cutting-edge electronics obsolete. Electronic products are made from valuable resources, including precious and other metals, engineering plastics, glass, and other materials. A particular problem is the high level of lead contained in the products due to solder materials and Cathode Ray Tube (CRT) shielding. An increasing component of the electronic materials mix is engineering plastics. These are chosen as raw materials for their specific properties, design flexibility, and contribution to low manufacturing costs. It is the very fact of their low cost that makes them economically unattractive to recover, and hence provides incentive to synthesize low cost recovery processes from innovative unit operations.

1.1.1 Flow analysis

The Environmental Protection Agency (EPA) initiated some collection programs at several locations of the United States. Figure 1.1 gives the average percentage-by-type of number of items collected by five communities. It indicates that televisions accounted

for 36 percent of the products collected by five communities. Audio/Stereo equipment was the second most prevalent product (at 16%) followed by computer monitors (at 11%). The U.S. EPA analyzed the data from two residential programs – one in Somerville, MA and one in Binghamton, NY. Nearly one half of the material recovered by weight from electronic equipment was metal and one-third was plastic (Figure 1.2). CRTs (primarily glass) comprised another 12 percent of the total, wood comprised 5 percent and the remaining 1 percent consists of "other" materials.

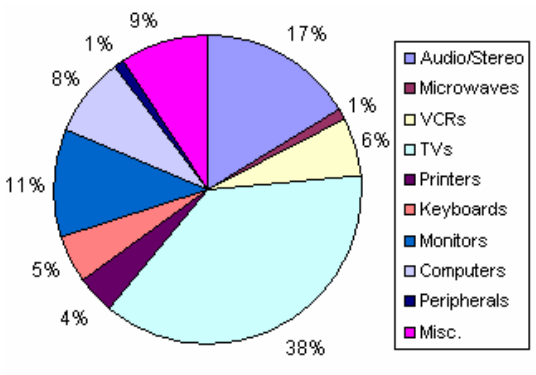

Figure 1.1 Percentage-by-type of number of items collected, weighted average of five collection events (EPA report, 1999)

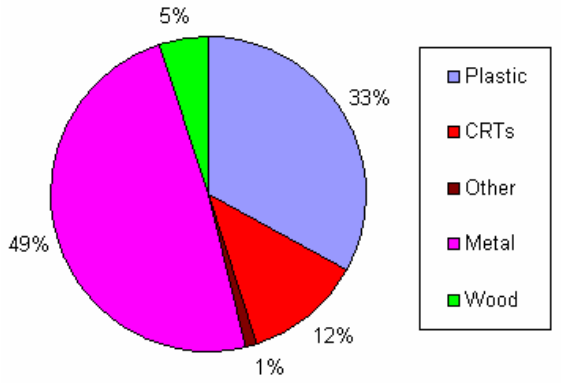

Figure 1.2 Components by weight after demanufacturing, average of two collection programs (EPA report, 1999)

Table 1.1 shows a breakdown of resins used in electrical and electronic equipment markets in North America. These six resins and their blends account for 84 percent of total resin consumption in E&E equipment, not including cable and wire. Fire retardant grades are used in some applications, which can cause a specific problem: without strict temperature control during extrusion there is a potential risk of generating dioxins and furans from some halogenated material, in particular, brominated flame retardants.

Table 1.1 Resins in electrical and electronic equipment in North America (Fisher et al., 1998)

Resin	Percentage
PS (Polystyrene)	31%
ABS (Acrylonitrile Butadiene Styrene)	16%
PP (Polypropylene)	13%
PU (Polyurethane)	10%
PC (Polycarbonate)	9%
Polyamide	5%

While the recycling of plastics bottles has become a well-established industry, there are very few recyclers processing plastics from waste electronic products due to the variety of the types plastics used and the wide range of grades. Therefore, an approach to help recyclers determine how to recover materials more economically is needed.

1.1.2 Plastics Recycling Options

Unlike metals recycling, plastics recycling has several options. These include chemical recycling, energy recovery and mechanical recycling.

(i) *Chemical Recycling*: most often refers to the thermal depolymerization of polyolefins

and substituted polyolefins into a variety of smaller hydrocarbon intermediates. One important issue with this method is the cost. Buekens and Huang (1998) estimated that for an industrial scale plant with capacity 25,000 ton/yr, the investment is around $20 million and the unit cost of plastics treatment is $250/ton. The product price is comparable to that of crude oil or Naphtha. So the economic sustainability of the system is greatly dependent of the market crude oil or Naphtha price.

(ii) *Energy Recovery*: The energy values (Table 1.2) of plastics are comparable to that of fuel oil. Pyrolysis and combustion studies have demonstrated that plastics can be safely converted to useful energy in an environmentally sound manner. Studies (Vehlow, et al., 2002) from a pilot plant have shown that 90% of the bromine in the treated waste can be recovered in the plant's gas cleaning system. Therefore, existing incinerators can be used where a bromine recovery unit is added to the scrubber system.

Table 1.2 Energy values of common materials

Plastics	BTU/lb
PP	19850
PE	19900
PS	17800
Wood	6700
Average MSW	4500
Food wastes	2600
Fuel oil	20900

(iii) *Mechanical Recycling*: Plastics separated by mechanical methods are resalable in market and can be reused. Studies (Imai, et al., 2003) have shown that plastics containing brominated flame retardants can be mechanically recycled in terms of the formation of

polybrominated dibenzodioxins/furans (PBDD/Fs) and the ability to maintain the fire safety rating after recycling loops. Therefore, it has the potential to be an economically viable approach. Mechanical separation of plastics with a different composition requires that the materials have different physical and chemical properties such as density, surface properties, electrostatic properties and spectrum, etc. This approach is discussed in more detail below.

1.1.3 Mechanical Recycling Process

In designing the electronics recycling technical program, the American Plastics Council (APC report, 1999) has addressed every step along the mechanical recycling chain (Figure 1.3).

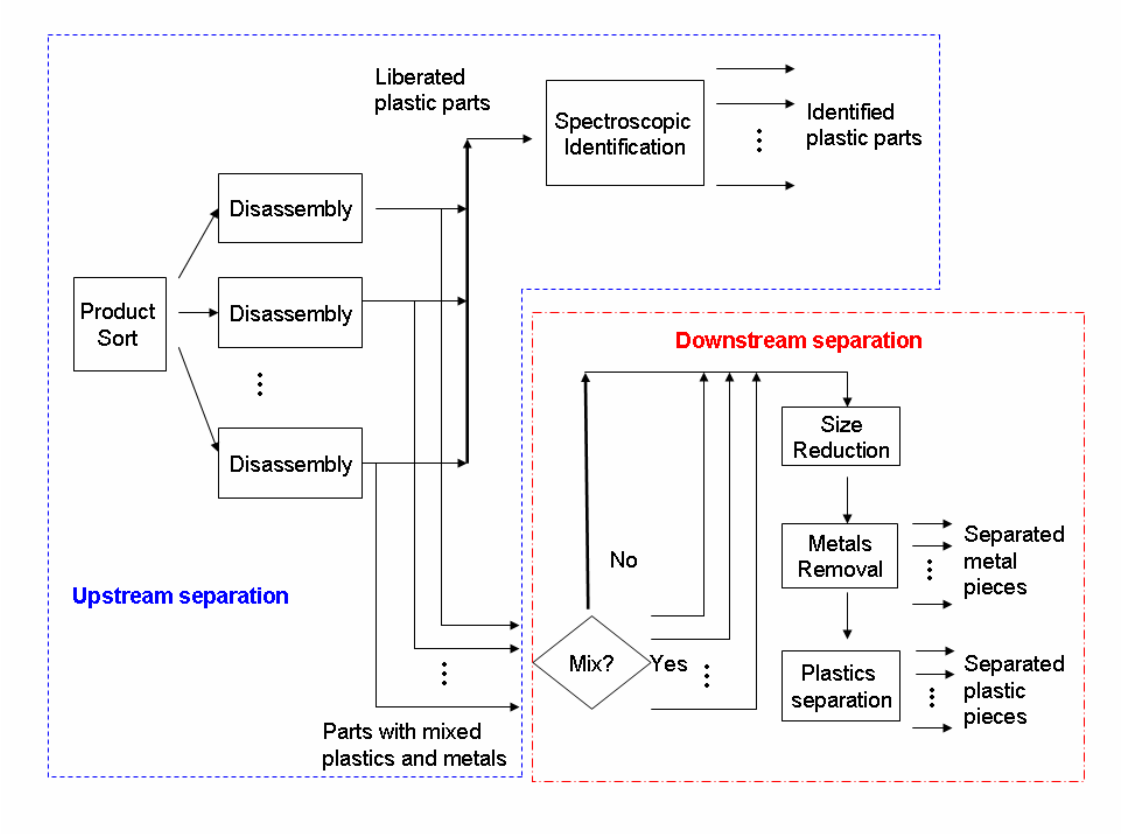

Figure 1.3 Mechanical Recycling Process (APC report, 1999)

It starts with product sorting, proceeds to dismantling/disassembly to isolate plastics-rich parts (liberated material), and on to plastic resin identification by the spectroscopic method. This is called the upstream separation. Parts with mixed plastics and metals are then sent to the downstream separation. There is a size reduction step that facilitates the liberation of non-plastic materials (mainly metals) from plastics and different plastics from each other. Then metals are removed first, followed by plastics separation. Once the plastics are separated, there is a final cleaning step, often followed by compounding and pelletizing. If the recycling process is technically and economically successful, there should now be clean and sorted post-use plastics ready to be processed and molded into new parts and products. This closes the mechanical recycling chain.

For the upstream separation, it has been shown (Rios, et al., 2003) that limited disassembly with identification does not create a bottleneck since the materials at this stage are in relatively large sizes, such as the back cover of CRT monitors or televisions. Disassembly can also separate parts that require quite different size reduction to achieve material liberation.

At the interface between upstream and downstream separation, one has to decide whether to mix the parts that come from different products or having different material liberation requirement. One can choose to classify these parts in terms of their source or the required size reduction output size range. For these classified parts, one can choose whether to use a single line to do a batch processing (in a sequential fashion) or use different lines to process them simultaneously. Of course, one can also choose to mix the parts and process them altogether. Batch processing of classified parts requires that the system can be adjusted to operate for different feed conditions at an optimal schedule.

Parallel processing of classified products requiring multiple lines therefore is an expensive option and is probably not economical when the supply is not at stable and high volume. The mixing of different parts will probably increase the difficulty of separation due to the increased number of components and require over-grinding of some parts. Therefore this option requires a more efficient use of different separation methods.

The optional equipment for each function for the downstream separation is listed in Table 1.3.

Table 1.3 Typical functional requirements and equipment

Function	Equipment
Size reduction	Jaw crusher, shear-type shredder, hammer-mill, roller-mill, rod-mill, ball-mill
Ferrous-metal separation	Drum / Belt type ferromagnetic separator
Non-ferrous metal separation	Eddy current separator
Plastics separation	Sink-float separator (Drum or cyclone) Froth flotation (Tank or column) Electrostatic separator (Free-fall or drum) Spectroscopy identification (NIR, Raman)

1.1.4 Introduction to mechanical methods for plastics separation

At the frontier of plastics recycling today is the development of accurate, high throughput separation methods to separate different types of plastics from each other and from other polymers such as rubber and elastomers.

Sink and float separation, which is a process that sorts particles on the basis of their density relative to that of the medium, is widely used. It is often the case that plastics have similar densities (PP/PE; PVC/PET; HIPS/ABS), therefore density-based separation can not be applied. Then the differences in properties other than density, such

as surface wettability and polarity can be used.

Flotation is a separation technique based on the material wettability, which can be characterized by the measurement of contact angles with water. However, most plastics are hydrophobic and floatable in water. It is possible to selectively change the wettability of plastics by various conditioning methods (chemical conditioning or physical conditioning). An overview of the applications of froth flotation is provided briefly in Table 1.4.

Table 1.4 Overview of the applications of froth flotation

Author/Inventor	Plastics	Conditioning agent
Guern (1997)	PET/PVC	Soda Ligno sulfonate
Shibata (1996)	PC/PVC/POM/PPE	Lignin sulfonate Saponin/Aerosol OT
Fraunholcz (1997)	GRPP, HIPS, ABS, PC, PA6, PMMA, PVC, POM	Non-ionic surfatant, Electrolytes Inorganic depressants Macromolecular organic depressants
Stuckrad et al. (1996) US. Patent 5566832	ABS/PC/PPO, ABS/SAN/PPO	Plasma treatment
Shen et al. (2001)	PMMA/PVC	Tannic acid
Jody et al. (1997) US. Patent 5653867	ABS/HIPS	Acetic acid + water, salt, surfactant, water

Electrostatic separation, which is widely used in mineral processing, has also been extended to the plastics separation. Plastic particles are contacted and those with higher dielectric constants become positively charged due to the electron transfer. This process is called triboelectric charging or triboelectrification. An overview of the applications of electrostatic separation is provided briefly in Table 1.5.

Table 1.5 Overview of the applications of electrostatic separation

	M.Stage	Cond.	P./D	Charging	Plastics
Yanar (1995)	1 stage	No	P.	Copper-lined cyclone	PVC/PE
Botsch (1997)	3 stages 2 stages	No	D	Rotating drum	Car dashboards (ABS-PC/ PVC) Bottles (PET/PVC)
Kamptner (1997)	2 stages	Yes	P.	Vibratory feeder, Mixing drum, Fluidized bed	Cable (PVC/EPDM/PE), PVC/PE/PS, PVC/PET
Stahl (1997)	Multiple	Yes	P	Unknown	PP-EPDM/PA, PVDF/Acetal , Cable plastics (PVC/ EPDM/ VPE), Bottles(PET/PVC)
Inculet (1998)	1 stage	No	P.	Fluidized bed, Rotating tube	PVC/PET, PP/HDPE
Xiao (1999)	Multiple	No	P.	Rotating drum	ASR(PP/PE), ESR, Refrigerators (ABS/HIPS), Bottles (PC/PVC)

M.Stage. : Multistage ; Cond.: Conditioning ; P/D: Plate or drum

Plastics identification by various spectroscopy technologies is also under research although this kind of technology has not been applied at industrial scale. A common drawback of above technologies is that the identification accuracy is easily influenced by the existence of contamination such as additives and labels. In addition, some of the technologies are expensive to build and operate.

The first type of methods (sink-float, froth flotation, electrostatic separation) separates plastics based on the particle trajectories in the separator. The separation is usually one dimensional and the boundary is determined by the system itself. Thus, the accuracy of this type of method is greatly influenced by the distribution of particle properties, especially the differentiating properties.

The second type of method (spectroscopic methods) separates plastics by identification. The separation could be multi-dimensional, i.e., spectrum data at different wave lengths. The separation boundary can be manually adjusted according to the

samples analyzed. Therefore, the accuracy increases and the negative influence of particle distribution decreases with the number of samples used to define the separation boundary. Table 1.6 is a summary of these different methods.

Table 1.6 Comparison of different mechanical separation methods

	Differentiating Property	Advantages	Disadvantages
Sink-float separation	Density	Low cost	Can not distinguish materials with overlapping densities. Medium recovery problem.
Froth flotation	Surface Wettability	Floatability can be changed by agent treatment.	Additional cost/time of conditioning.
Electrostatic separation	Polarity	Dry process. Easy/cheap operation	Charge may be widely distributed.
Spectroscopic identification	Spectrum	Low cost. High selectivity. Accuracy independent of particle size.	Low throughput. Contamination can influence accuracy.

The selection of the appropriate equipment for each function depends on the flow. Different flow requires different size output to achieve certain degree of material liberation and different separation methods depending on the components contained. Therefore, the optimal flowsheet needs to be customized for different inputs.

1.2 Research Objective and Focus

1.2.1 Research objective

The design of bulk recycling systems is an emerging field with only a few papers addressing the design of bulk recycling of electronic products. Stuart and Lu (2000a) developed a decision (reuse or recycle) model to select bulk recycling processing and reprocessing options for a take-back center that receives large quantities of similar products. They (Stuart and Lu, 2000b) also developed a refine-or-sell decision model,

which is capable of determining at what point materials are refined, and at what point they are sold. Sodhi et al. (1999) used dynamic programming to determine the sequence of operations for float-sink material separation by minimizing the total processing volume without using a detailed unit model. Reimer et al. (2000) reported on an integrated electronics recycling model and a proposed solution technique using genetic algorithms. None of these works have considered the selection of alternative separation methods and the individual unit design and operation. The interaction of the overall system design with the unit operation design is critical both from understanding the economic costs of carrying out the process steps and in ensuring that the system has the appropriate flexibility to handle the uncertainty in the waste stream.

It can be seen from our previous introduction that bulk recycling systems are similar to other chemical engineering process systems and therefore they can be synthesized and designed using the same types of techniques that have been applied to distillation and reaction systems. In particular, there is a reasonable similarity between the synthesis of plastics separation system and that of the distillation columns (Doherty and Malone, 2001) in terms of the determination of the separation sequence.

Our **research objective** is to develop a systematic approach to the design of bulk recycling systems under uncertainty. "Systematic" means that the alternatives are explicitly represented and selections made based on the economic viability and capability of the system to meet explicitly defined constraints placed on the system operation. The output will be the process flowsheet, unit sizes and products. There are two approaches to generate the output. One approach is to determine the elements of the flowsheet in a sequential way with the help of heuristic rules, such as the Douglas's hierarchical

decomposition method (Douglas, 1988). Another approach is simultaneous optimization based on mathematical programming.

The mathematical programming approach to design problems consists of three major steps: (I) the development of a representation of alternatives from which the optimum solution is selected; (II) formulation of a mathematical program that generally involves discrete and continuous variables for the selection of design and operating variables, respectively; and (III) solution of the optimization model. In the first step, the superstructure approach is widely used. A superstructure is a general flowsheet incorporating every feasible realization, from which specific designs are obtained by optimization.

A combination of these two approaches will be employed to make the systematic selection from the alternatives. In comparison to previous work in bulk recycling systems, the unit operations themselves will be explicitly modeled and the interactions between operations through the characteristics of the feed and intermediate streams captured with reasonable physical fidelity.

Due to the existence of a variety of different units in the bulk recycling system, the **scope of this research** is limited to the *plastics separation* part in the *electronics sector* of bulk recycling problems. Although the focus of this research is on the recycling of electronics, the method developed in this research can be easily extended to other applications. The size reduction and metals separations steps will not be explicitly modeled. In other words, they are not included in the superstructure. However, the influence of size reduction on the plastics separation will be discussed qualitatively and a heuristic method to incorporate the design of size reduction into plastics separation will

be presented. Since metals separation is a relatively well-understood problem, hence the incorporation of the metals separation units only makes the problem larger, but does not bring any unresolved difficulties.

However, the existing synthesis and design techniques from chemical engineering process systems can not be applied straightforwardly to the design of bulk recycling problems due to significant uncertainties in the latter.

1.2.2 Research focus

Various uncertainties include feed flowrate, component, composition as well as product prices. The variation of product prices will not make an existing recycling system infeasible, however, it could render the system uneconomical. The items generated by sector vary substantially, as do the types of collection program. The absence of a standard collection method means that the types and quantities of items collected vary substantially from program to program, making it difficult for recyclers to determine what materials will be generated, in what quantities and with what regularity and with what cost.

Uncertainties in the feed streams

An analysis of the collection programs initiated by EPA (EPA report, 1999) shows that the total weight and types of electronic products collected varies with different collection program and different time period, which means that the feed flowrate and composition to our recycling system tend to vary.

Correlation between uncertainties

The feed compositions do not vary independently. Other uncertainty parameters may also be correlated such as product prices. Product prices are influenced by market including supply and demand and the overall environment. For example, if at a time, both television and computer manufactures decide to use recycled resins then the demand for HIPS and ABS will increase, then their prices will show a positive correlation. The price of virgin materials is often correlated with the price of energy and hence the increase in cost of one virgin resin type is positively correlated with that of anther. For an empirical relationship with multiple correlation parameters, these parameters are also correlated. Correlated uncertainty parameters should be represented by a joint confidence region instead of individual confidence intervals.

For the design of bulk recycling systems, correlated uncertainties represent very important information that can not be neglected in the design procedure. There is also a need to study how correlation influences the design and the operability of a plant, irrespective of whether or not this is a bulk recycling system or another type of chemical facility.

1.3 Research Goals

To achieve the above objective, the following **three goals** need to be completed:

1. Development of an efficient solution technique for solving stochastic MINLPs
2. Development of unit models for all separation methods to be considered, and
3. Development of an overall synthesis method taking account of the interaction between size reduction and separation.

Previous work in satisfying these goals is briefly reviewed below followed by the contributions this thesis makes towards reaching them.

Design under uncertainty

Several approaches have been developed in the literature addressing the problem of design under uncertainty, such as (1) deterministic-based multi-period/scenario problem (Grossmann and Sargent, 1978; Grossmann and Halemane, 1982; Paules and Floudas, 1992); (2) probabilistic-based 2-stage stochastic programming (Pistikopoulos and Ierapetritou, 1995; Bernardo et al., 1999) and (3) flexibility analysis (Pistikopoulos and Grossmann, 1989a,b; Raspanti et al., 2000). Extensive reviews are given by Grossmann et al. (1983) and Pistikopoulos (1995). A detailed review of design under uncertainty is presented in Chapter 2.

The first approach is applied to formulate the design under uncertainty problem as a stochastic Mixed Integer Nonlinear Program. A method is to be developed to allow determination of the sample size needed to achieve certain solution confidence. Computational savings are expected as samples are used only as large as needed. Intuitively, bad solutions should be able to be eliminated without high accuracy.

Unified modeling approach for plastics separation

One should first realize that not all particles are identical. In other words, particle properties, such as size, may be widely distributed, instead of a single constant. Second, even identical particles do not have the same behavior in the separator, such as the number of contacts with other particles to generate tribo-electric charges or with bubbles

to be floated. Therefore, the development of the unit models should take account of these issues. Intuitively, the distributions of particle properties should lead to nonsharpness of the separations. Ideally, the influence of the distributions on the separation efficiency should be explicitly modeled. In this research, models for sink-float, froth flotation, electrostatic separation (free-fall and drum-type) will be developed and unified to allow others to make progress in the future. This approach is termed trajectory-based separation modeling to distinguish it from approaches in the past.

Overall synthesis method

At the overall system level the major interactions are between the separation technique and the extent of size reduction. It is important to establish how the size distribution affects the separation efficiency of different methods. Furthermore, how does the material liberation influence the choice of size reduction equipment and grinding time? The desired output particle size from size reduction will depend on the products to be processed and the separation methods to be used. Therefore, instead of grinding to a very fine size at the start of the system, it might be helpful to reduce the particle size at multiple times throughout the system and arrange the order of separation appropriately from favoring larger particles to favoring smaller ones.

Finally, a case study will be demonstrated to combine the solution technique and unit models for a plastics separation system.

1.4 Research contributions

The contributions of this research are summarized as follows. They are classified into three categories: “general” refers to process synthesis and design including the

methodology and computational implementation, "contextual" refers to the bulk recycling system, and "specific" refers to a detailed issue such as unit modeling.

General: Design Methodology and Computational Implementation

The proposed SAA method is the first approach in the MINLP area to determine the appropriate sample size based on the solution quality. The user can either adjust the sample size successively based on the calculated solution quality or calculate the solution quality based on the pre-specified sample size. The approach also provides a way to decompose the scenarios; therefore, there is no need to solve a large stochastic problem as a whole and the computational time is significantly reduced.

Contextual: Bulk recycling system design

This research is the development of the first formal and systematic approach to the bulk recycling problem. It is the first approach to account for interactions between process steps and combine structural decisions with operating decisions. It is also the first approach to consider (correlated) uncertainties in the design of bulk recycling systems.

Specific: Unit modeling

It is the first development of unified models for solids separation taking account of the influence of particle property distributions and other random factors. It also provides a basis to analyze the interactions between size reduction and separation and do an integrated design.

1.5 Summary

This chapter gives an introduction to the bulk recycling problem, which has

similarities to the distillation sequencing and design problems in chemical engineering. However, there are some salient features in the former, such as the various uncertainties and separation by different mechanisms, which make the direct application of existing synthesis and design techniques impossible. Therefore, the objective of this research is to develop a systematic method to the design of bulk recycling problems. To achieve this objective, three goals need to be completed including, a method to solve stochastic Mixed Integer Nonlinear Programs, an approach to model different separation units accounting for the distribution of particle properties, and a method to incorporate size reduction units to the optimization of the plastics separation system. The details of the research work are presented in the Chapter 2 to 6. In Chapter 2, an efficient solution technique (Sample Average Approximation method) for solving stochastic MINLPs is described. In Chapters 3 and 4, a unified approach is presented for modeling various separation units. In Chapter 5, a heuristic design method is proposed to incorporate the size reduction unit to the separation system. In Chapter 6, a case study, which combines the sample average approximation method proposed in Chapter 2 and the unit models developed in Chapters 3 and 4, is demonstrated. Finally, Chapter 7 concludes the research.

CHAPTER 2

SAMPLE AVERAGE APPROXIMATION METHODS FOR STOCHASTIC MINLPS

2.1 Introduction to process design under uncertainty

Process design under uncertainty can be formulated as multi-period or stochastic MINLPs (Halemane & Grossmann, 1983; Paules & Floudas, 1992; Pistikopoulos, 1995).

$$\begin{aligned} v^* = \min_{x,\, y, z_i} \quad & \mathrm{E}_q \left[f\left(x, y, z_i, q_i\right) \right] \\ s.t. \quad & g_j\left(x, y, z_i, q_i\right) \le 0 \quad \forall j \in J \\ & x \in X,\ z \in Z, y \in \{0,1\}^m \\ & q \in \Theta \end{aligned} \qquad \text{(SMINLP)}$$

Where y is a vector of binary 0-1 variables denoting the choice of the units or the existence of the streams, x is a vector of design variables such as unit sizes, z is a vector of control/state variables, which can vary over periods/scenarios, and q represents a vector of uncertain parameters. The objective is often to minimize the expected value of costs or maximize the expected value of profit. The constraint set J includes mass balances, unit design/operating models, design/operating specifications and some logical constraints. The exact evaluation of the expected value is difficult or even impossible when the integral cannot be computed exactly or the objective function f is not in a closed form. Then the expected value is often approximated through sample averaging. Under uncertain conditions, it is assumed that the design must remain feasible for every realization of the parameters consistent with their probability distributions. Therefore, the problem can become unmanageably large and its solution is time-consuming. Several

papers in literature have addressed the various issues of solving such problems including (i) integration methods, and (ii) sampling methods.

For the integration methods, when the exact expected value can not be computed, one usually uses a numerical integration technique or a sample average approximation method. Acevedo and Pistikopoulos (1996, 1998) compared the two approaches: Guassian Quadrature formula for numerical integration (with both a full scan of uncertainty space and evaluation of feasible region) and Monte-Carlo sampling for sample average approximation. Novak and Kravanja (1999) suggested an approximation method using extreme points (vertices), in which the objective function is calculated by the weighted average over critical points and the feasibility of the design is ensured by the constraints at critical vertices. Novak, Pintaric and Kravanja (2000) proposed a modified Box's direct search method for the design stage and a reduced dimensional stochastic procedure for the operating stage.

For sampling methods, one of the most widely used sampling techniques is the Monte Carlo method (MC), by which independent pseudo-random samples are first generated to approximate a uniform distribution and then specific values of a probability distribution are created by inverse transformation of the cumulative distribution function. However, for a uniform distribution, uniformity is more critical than randomness or independence for the samples to be more representative of the population, Kim and Diwekar (2002). To address this issue, Kalagnanam and Diwekar (1997) developed the Hammersley Sequence Sampling (HSS) technique and showed that HSS can provide much faster convergence to the true mean and variance of a distribution than MC.

Sampling-based approximation methods include two basic philosophies: internal

sampling and external sampling. The internal sampling methods perform sampling inside an algorithm with new independently, identically distributed (i.i.d.) samples generated and accumulated over iterations and the entire history of samples is used in computation at every iteration. External sampling, which is also called sample-path optimization, sample average approximation (SAA) or stochastic counterpart method, approximates the true problem by the sample average approximation problem:

$$\begin{aligned} \hat{v}_N = & \min_{x,\, z_i} \frac{1}{N} \sum_{i=1}^{N} \left[f(x, y, z_i, q_i) \right] \\ s.t. \quad & g_j(x, y, z_i, q_i) \le 0 \quad \forall i \in I_k; \forall j \in J \\ & x \in X, \; z \in Z \end{aligned} \qquad \text{(SAA-MINLP)}$$

Hence, once the sample is generated, the stochastic problem becomes a deterministic one, which can be solved by existing deterministic algorithms.

Examples of internal sampling algorithms include the "stochastic decomposition" algorithm (SD) for solving two-stage stochastic linear programs by Higle and Sen (1991) and "stochastic branch and bound" algorithm (SBB) by Norkin et al. (1998). SD solves at each iteration one subproblem to update a piecewise linear approximation of the recourse function and one master problem to generate successive iterates with increasingly large samples. In the SBB algorithm, stochastic upper and lower bounds are generated through the partitioning process and subsets are not fathomed at each iteration until a sufficiently large number of iterations are carried out. It has been shown, for both of the algorithms, that under some mild assumptions, there exists a subsequence of approximate solutions $\{x_k\}_{k=1}^{\infty}$ with accumulation point belongs to the set of optimal solutions X^*, which established the convergence of the internal-sampling algorithms (Higle and Sen, 1991 and Norkin et al., 1998).

Examples of external sampling methods include Mak et al. (1999), Linderoth et al. (2002) for stochastic linear problems and Kleywegt et al. (2001) for stochastic integer problems. The optimality gap of the objective value, estimated by the difference between an upper bound (the objective value at any candidate solution) and a lower bound (average of replicated solutions), has been used to determine the solution quality. The validity of this lower bound has been proved independently by Norkin et al. (1998) and Mak et al. (1999). Following this lower-bound generating strategy, Kleywegt et al. (2001) used a smaller sample size N to make decisions (with M replications) and a larger sample size N' to re-compute the objective value with the decisions fixed at the values obtained previously from solving the smaller problems. One alternative to evaluate solution quality is to see if the replications generate an "identical" solution and another is to test the KKT conditions. For some problems, in which the decision-making is more important than accurate estimation of the objective value, the method of identical solutions is more suitable. Convergence with probability one has been established for the external-sampling algorithms and under some assumptions the limiting distribution is normal if the solution is unique (Shapiro, 1991, King and Rockafellar, 1993).

The approach described in this chapter is wrapped around a traditional MINLP approach. Duran and Grossmann (1986) proposed the Outer Approximation (OA) method to solve deterministic MINLP problems, which is briefly introduced at the beginning of the next section. Fletcher and Leyffer (1994) proposed the Generalized Outer Approximation (GOA) method for treating infeasible primal problems. Kesavan and Barton (2000) presented a generalized branch and cut algorithm as a unified framework in which both decomposition and branch and bound algorithms are

incorporated as specific instances. The difficulty in solving stochastic MINLPs lies in the coupled discrete and continuous variables over periods. Once these coupled variables are known, the problem becomes independent at each period and can be solved easily. Intuitively, poor solutions should be capable of being eliminated with only inaccurate estimates of their quality. The goal of this work is to translate this intuition into specific modifications of an MINLP algorithm for stochastic problems. At each iteration of the OA algorithm, the SAA method is applied to each NLP subproblem and MILP master problem. In this chapter, two stopping rules are presented: one is the Optimality Gap Method (OGM), and another is the Confidence Level Method (CLM) and use examples to demonstrate that they can be more efficient than conventional fixed-sample algorithms.

2.2 The Outer Approximation algorithm

First the OA algorithm (Figure 2.1) is briefly introduced below. For a deterministic MINLP problem:

$$\begin{aligned} \min_{x,y,z_i} \quad & f(x,y,z) \\ s.t. \quad & g_j(x,y,z) \le 0 \quad \forall j \in J \\ & x \in X,\ z \in Z,\ y \in \{0,1\}^m \end{aligned} \qquad \text{(MINLP)}$$

where J is the set of constraints, the OA algorithm solves at each iteration k=1, …, K, a NLP subproblem with fixed y variables (denoted as $\tilde{y}_k$) to provide an upper bound (UB_k):

$$\begin{aligned} UB_k = \min_{x,z} \quad & f(x,\tilde{y}_k,z) \\ s.t. \quad & g_j(x,\tilde{y}_k,z) \le 0 \quad \forall j \in J \\ & x \in X,\ z \in Z \end{aligned} \qquad \text{(NLP)}$$

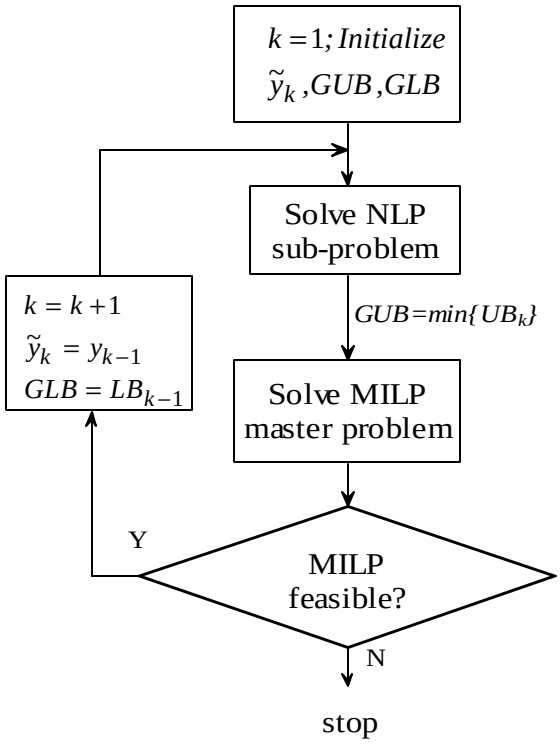

Figure 2.1 Basic steps of the OA algorithm

and an MILP master problem to provide a lower bound (LB_k) and new values of y:

$$LB_k = \min_{x,y,z} b$$

$$s.t.\ \ b \geq f\left(x_k^*, y_k^*, z_k^*\right) + \nabla f\left(x_k^*, y_k^*, z_k^*\right)\begin{bmatrix} x - x_k^* \\ y - y_k^* \\ z - z_k^* \end{bmatrix},\ k = 1, \cdots, K$$

$$g_j\left(x_k^*, y_k^*, z_k^*\right) + \nabla g_j\left(x_k^*, y_k^*, z_k^*\right)\begin{bmatrix} x - x_k^* \\ y - y_k^* \\ z - z_k^* \end{bmatrix} \leq 0,\ \ k = 1, \cdots, K;\ j \in J \qquad \text{(MILP)}$$

$$\sum_{i \in U^k} y_i - \sum_{i \in V^k} y_i \leq \left|U^k\right| - 1, \text{where } \mathrm{U^k} = \left\{i \mid y_{i,k}^* = 1\right\},\ V^k = \left\{i \mid y_{i,k}^* = 0\right\},\ \mathrm{k} = 1, \cdots, \mathrm{K}$$

$$GLB \leq b \leq G\mathrm{UB}, \quad x \in X,\ \mathrm{z} \in \mathrm{Z},\ y \in \{0,1\}^m$$

where $GLB=LB_{k-1}$ and $GUB=\min\{UB_k\}$. K is the current iteration number. The procedure is continued until the MILP master problem becomes infeasible.

The stochastic versions of the OA algorithm still employ this structure, but the NLP sub-problems and MILP master problems are stochastic. Both of the algorithms (OGM and CLM) involve solving. At each iteration,

(1) a smaller stochastic NLP sub-problem (S-NLP) M times, each at sample size N

(2) a larger stochastic NLP sub-problem (L-NLP) at sample size N' with fixed continuous decision variables $\tilde{x}$

(3) a smaller stochastic MILP master problem (S-MILP) M times, each at sample size N

(4) a larger stochastic MILP master problem (L-MILP) at sample size N', with fixed discrete and continuous decision variables $\tilde{\tilde{y}}$ and $\tilde{\tilde{x}}$ (actually a linear problem) .

The definitions for these problems are presented below. Different sample size N and N' are allowed at different iterations, therefore using a subscript k to denote the iteration number. I_k and I_k' are the sets of the samples at the kth iteration with sample size N_k and N_k', respectively.

The problem S-NLP is defined as

$$\begin{aligned} \min_{x,z_i} \ & \frac{1}{N_k} \sum_{i=1}^{N_k} \left[f\left(x, \tilde{y}, z_i, q_i\right) \right] \\ s.t. \ & g_j\left(x, \tilde{y}, z_i, q_i\right) \le 0 \quad \forall i \in I_k; \forall j \in J \\ & x \in X,\ z_i \in Z \end{aligned} \tag{S-NLP}$$

where the discrete decision variables are fixed at $\tilde{y}$.

The problem L-NLP is defined as

$$\begin{aligned} \min_{z_i} \ & \frac{1}{N_k'} \sum_{i=1}^{N_k'} \left[f\left(\tilde{x}, \tilde{y}, z_i, q_i\right) \right] \\ s.t. \ & g_j\left(\tilde{x}, \tilde{y}, z_i, q_i\right) \le 0 \quad \forall i \in I_k'; \forall j \in J \\ & z_i \in Z \end{aligned} \tag{L-NLP}$$

where both the discrete and continuous decision variables are fixed at $\tilde{y}$ and $\tilde{x}$,

respectively.

The problem S-MILP is defined as

$$
\begin{aligned}
&\min_{x,y,z_i} \; b \\
&s.t.\; b \ge \frac{1}{\overline{N}_k}\sum_{i=1}^{\overline{N}_k}\left(f\left(x_k^*,y_k^*,z_{i,k}^*,q_i\right)+\nabla f\left(x_k^*,y_k^*,z_{i,k}^*,q_i\right)\begin{bmatrix} x-x_k^* \\ y-y_k^* \\ z_i-z_{i,k}^* \end{bmatrix}\right),\; k=1,\cdots,K \\
&g_j\left(x_k^*,y_k^*,z_{i,k}^*,q_i\right)+\nabla g_j\left(x_k^*,y_k^*,z_{i,k}^*,q_i\right)\begin{bmatrix} x-x_k^* \\ y-y_k^* \\ z_i-z_{i,k}^* \end{bmatrix}\le 0,\;\; k=1,\cdots,K;\; i\in I_k\,;\; j\in J \qquad \text{(S-MILP)} \\
&\sum_{i\in U^k} y_i - \sum_{i\in V^k} y_i \le \left|U^k\right|-1,\;\; \text{where } \mathrm{U^k}=\left\{i \mid y_{i,k}^*=1\right\},\; V^k=\left\{i \mid y_{i,k}^*=0\right\},\; k=1,\cdots,K \\
&GLB \le b \le G\mathrm{UB}, \qquad x\in X,\; z_i\in Z,\; y\in\{0,1\}^m
\end{aligned}
$$

where there are no fixed variables, $\overline{\mathrm{N}}_\mathrm{k}=min\left(N_k,N_K\right),\; k=1,...,K$ and superscript * denotes the linearization points obtained from solving S-NLP or L-NLP.

The problem L-MILP is defined as

$$
\begin{aligned}
&\min_{z_i} \; b \\
&s.t.\; b \ge \frac{1}{\overline{N}'_k}\sum_{i=1}^{\overline{N}'_k}\left(f\left(x_k^*,y_k^*,z_{i,k}^*,q_i\right)+\nabla f\left(x_k^*,y_k^*,z_{i,k}^*,q_i\right)\begin{bmatrix} \tilde{\tilde{x}}-x_k^* \\ \tilde{\tilde{y}}-y_k^* \\ z_i-z_k^* \end{bmatrix}\right),\; k=1,\cdots,K \\
&g_j\left(x_k^*,y_k^*,z_{i,k}^*,q_i\right)+\nabla g_j\left(x_k^*,y_k^*,z_k^*,q_i\right)\begin{bmatrix} \tilde{\tilde{x}}-x_k^* \\ \tilde{\tilde{y}}-y_k^* \\ z_i-z_k^* \end{bmatrix}\le 0,\;\; k=1,\cdots,K;\; \mathrm{i}\in \mathrm{I}'_k\,;\; j\in J \qquad \text{(L-MILP)} \\
&\sum_{i\in U^k} \tilde{\tilde{y}}_i - \sum_{i\in V^k} \tilde{\tilde{y}}_i \le \left|U^k\right|-1,\;\; \text{where } \mathrm{U^k}=\left\{i \mid y_{i,k}^*=1\right\},\; V^k=\left\{i \mid y_{i,k}^*=0\right\},\; \mathrm{k}=1,\cdots,\mathrm{K} \\
&GLB \le b \le G\mathrm{UB},\;\; z\in Z
\end{aligned}
$$

where the discrete and continuous decision variables are fixed at $\tilde{\tilde{y}}$ and $\tilde{\tilde{x}}$, respectively,

which are obtained from solving the corresponding S-MILP. $\overline{N}'_k = min\left(N'_k, N'_K\right)$, $k = 1,...,K$. M batches of i.i.d samples are generated, each with sample size N and one batch of i.i.d (or common random numbers) of samples with a larger sample size N'. The sample sizes N and N' are increased until some stopping criterion is satisfied. Next two stopping rules are discussed.

2.3 The Optimality Gap Method (OGM)

Let *UB** denote the optimal solution of the true stochastic MINLP problem (SMINLP) and $\hat{UB}_N$ denote the optimal solution of the approximation problem (SAA-MINLP) with sample size N. According to Norkin et al. (1998) and Mak et al. (1999),

$$E\left[\hat{UB}_N\right] \leq UB^* \tag{2.1}$$

Hence a statistical lower estimate for true optimal value *v** is the expected value of the replicated SAA solutions, which can be estimated by

$$\overline{UB}_{N,M} = \frac{1}{M}\sum_{m=1}^{M} \hat{UB}_N^{(m)} \tag{2.2}$$

where $\hat{UB}_{N,M}$ denotes the average of the M replicated solutions $\hat{UB}_N^{(m)}$ (m=1, …, M) to the NLP subproblem (each with sample size N). The "lower estimate" and "upper estimate" are used to distinguish them from the "lower bound" and "upper bound" which have been reserved for the OA algorithm. $\hat{S}_{N,M}^{U\,2} / M$ is used to denote the variance of the replicated solutions:

$$\frac{\hat{S}_M^{U\,2}}{M} = \frac{1}{M(M-1)}\sum_{m=1}^{M}\left(\hat{UB}_N^{(m)} - \overline{UB}_{N,M}\right)^2 \tag{2.3}$$

So the (1-α) confidence interval of the lower estimate of the upper bound is

$$\overline{UB}_{N,M} \pm t_{M-1,\alpha/2} \frac{\hat{S}^U_{N,M}}{\sqrt{M}} \tag{2.4}$$

Where t is the student t-test with M-1 degrees of freedom and 1-α confidence level. Similarly, a confidence interval for the upper estimate of the upper bound can be constructed. Use $\hat{UB}_{N'}$ to denote a solution to the NLP subproblem with sample size N' at any $\tilde{x} \in X$. Then $\hat{UB}_{N'}$ is an upper estimate of the true value UB^*. Let $\hat{S}^{U\,2}_{N'} / N'$ denote the variance and

$$\frac{\hat{S}^{U\,2}_{N'}}{N'} = \frac{1}{N'(N'-1)} \sum_{i=1}^{N'} \left(\hat{f}_i - \hat{UB}_{N'} \right)^2 \tag{2.5}$$

Then a (1-α) confidence interval for the upper estimate of the upper bound is

$$\hat{UB}_{N'} \pm t_{N'-1,\alpha/2} \frac{\hat{S}^U_{N'}}{\sqrt{N'}} \tag{2.6}$$

Combining the confidence intervals of the lower and upper estimates, the confidence interval of the optimality gap for the upper bound is

$$\left(0, \hat{UB}_{N'} - \overline{UB}_{N,M} + t_{M-1,\alpha/2} \frac{\hat{S}^U_{N,M}}{\sqrt{M}} + t_{N'-1,\alpha/2} \frac{\hat{S}^U_{N'}}{\sqrt{N'}} \right) \tag{2.7}$$

and Mak et al. (1999) have proved that

$$P\left\{ \overline{UB}_{N,M} - t_{M-1,\frac{\alpha}{2}} \frac{\hat{S}^U_{N,M}}{\sqrt{M}} \le E\left[UB_N\right] \le UB^* \le E\left[f\left(\hat{x}, \hat{y}, z_i, q_i\right)\right] \le \hat{UB}_{N'} + t_{N'-1,\frac{\alpha}{2}} \frac{\hat{S}^U_{N'}}{\sqrt{N'}} \right\} \ge 1-\alpha \tag{2.8}$$

To make it clear, a graphical picture of this interval is given in Figure 2.2. Similarly a confidence interval of the optimality gap for the lower bound can be constructed.

$$\left(0, \hat{L}B_{N'} - \overline{L}B_{N,M} + t_{M-1,\alpha/2}\frac{\hat{S}^{L}_{N,M}}{\sqrt{M}} + t_{N'-1,\alpha/2}\frac{\hat{S}^{L}_{N'}}{\sqrt{N'}}\right) \tag{2.9}$$

where $\overline{L}B_{N,M}$ and $\hat{S}^{L}_{N,M}/\sqrt{M}$ are the mean and standard deviation of the replicated

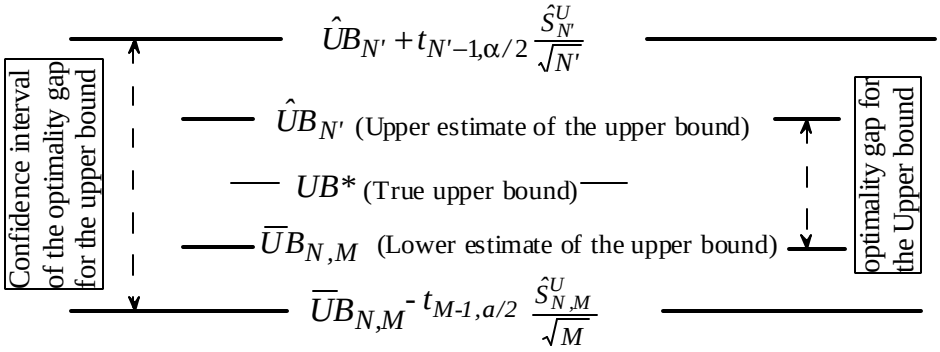

Figure 2.2 Illustration of the confidence interval for the upper bound

solutions of the S-MILP with sample size N, respectively. $\hat{L}B_{N'}$ and $\hat{S}^{L}_{N'}/\sqrt{N'}$ are the solution and standard deviation of the solution of the L-MILP problem with sample size, respectively.

The notations GUB and GLB were used in the MILP. In the deterministic case, GUB is the minimum of all upper bounds and GLB is the lower bound from the previous iteration. However, in the stochastic case there are correspondingly two values for the upper bound and lower bound, respectively: one is the average of the objective values of the replicated smaller problems and another is the objective value of the larger problem. Thus, we have $(\overline{U}B_{N,M}, \hat{U}B_{N'})$ and $(\overline{L}B_{N,M}, \hat{L}B_{N'})$ as the sequence of upper and lower bound values, respectively (Figure 2.3). It should be noted that if different values for S-MILP and L-MILP are used, one is actually solving two different problems, which make

the optimality gap estimate no longer valid. Therefore, in both S-MILPs and L-MILPs, the objective value of NLP subproblem at sample size N' is used for GUB and the objective value of MILP master problem at sample size N' for GLB, i.e.,

$$GUB = min\left\{\hat{U}B_{N'}{}^{(k)}\right\} \quad \text{and} \quad GLB = \hat{L}B_{N'}{}^{(k-1)}, \quad k = 1,2,... \tag{2.10}$$

The convergence of GUB and GLB is shown in Figure 2.3.

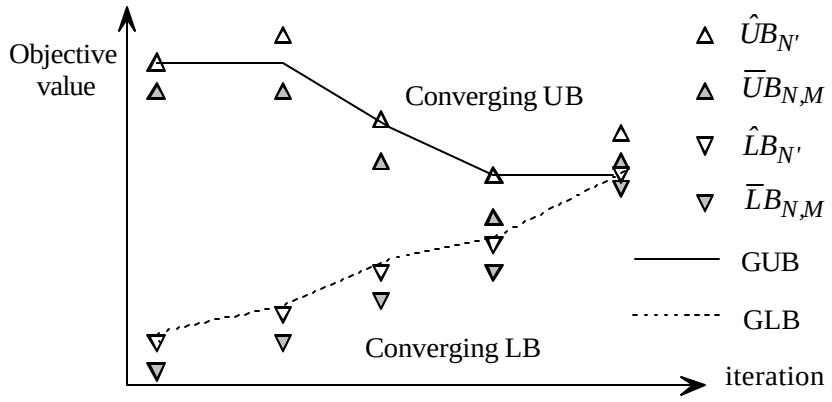

Figure 2.3 Converging upper and lower bounds

The SAA algorithm presented by Kleywegt et al. (2001) used the following stopping criterion: increase sample size N and/or N' until the gap and the variance of the gap are sufficiently small. It is apparent that the term $t_{N'-1,\alpha/2}\hat{S}^{U}_{N'}/\sqrt{N'}$ is part of the confidence interval of the optimality gap. Our approach (Figure 2.4) contains an inner loop to increase sample size N' until the term $t_{N'-1,\alpha/2}\hat{S}^{U}_{N'}/\sqrt{N'}$ is below the desired confidence interval of the optimality gap and an outer loop to increase sample size N until the confidence interval of the optimality gap is sufficiently "small". In our algorithm,

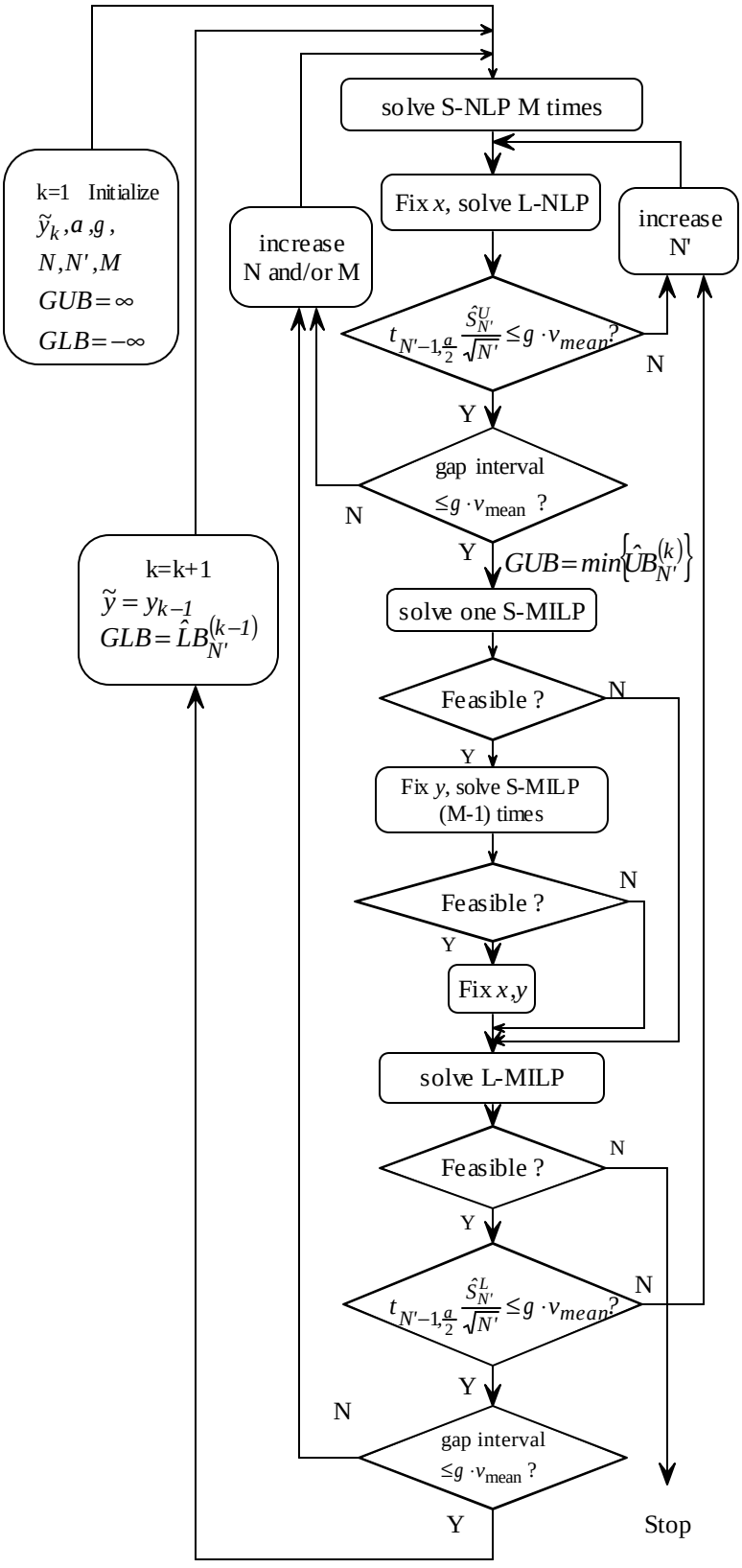

Figure 2.4 Basic steps of OGM for stochastic MINLPs

a quantitative measure of smallness is chosen, $g \cdot v_{mean}$, where γ is a small value between 0 and 1, say 0.02, and v_{mean} is the optimal value of the deterministic problem at the mean values of uncertain parameters. A consequence of using larger problem values for the S-MILPs is that the infeasibility of S-MILP does not guarantee the infeasibility of L-MILP, which will be discussed in the next section. Hence when the S-MILP becomes infeasible, one will need to solve (without fixing the decision variables) the L-MILP. The algorithm stops only when the L-MILP becomes infeasible.

2.4 The Confidence Level Method (CLM)

The optimality gap method described in the above section guarantees that at each iteration, one gets the optimal solution for the NLP subproblem or the MILP master problem with at least (1-α) confidence level. However, this does not mean that the confidence level of finding the optimal solution to the overall problem is also at least (1-α). The above strategy lacks an accuracy estimation of the final solution. Intuitively, to compare two candidate solutions, one does not necessarily need an accurate estimation of each objective value if they are "far" from each other, where a dimensionless parameter can be defined relative to the variance of the objective value. The following algorithm formalizes this idea.

Considering that the optimal solution y* can be lost during the following 3 steps:

1) Comparison of the objective values of the NLP sub-problems
2) The constraint in MILP: $b \leq GUB$
3) The constraint in MILP: $b \geq GLB$

For 1), in the deterministic case, the optimal solution is updated by comparing the upper bound of the current solution and the best upper bound found so far, if the current one is smaller, the best upper bound is updated by the current one. In the stochastic case, it should be guaranteed that at least the confidence intervals of two candidate solutions do not overlap and if they are away from each other by a certain value, it will give a higher confidence than simply using their mean values for comparison. So the rule is modified as follows: for some tolerance $\varepsilon \in (0,1)$ and y^o, the best solution found so far, to ensure either

$$\overline{U}B_{N,M}(y) > \hat{U}B_{N'}(y^o) + 2a \quad \text{if } y \text{ is worse than } y^o \tag{2.11 a}$$

$$\text{or} \quad \hat{U}B_{N'}(y) + 2a < \overline{U}B_{N,M}(y^o) \quad \text{if } y \text{ is better than } y^o \tag{2.11 b}$$

where $a^2 = \frac{s^2}{e}\left(\frac{1}{M} + \frac{1}{N'}\right)$. The definition for a is actually obtained from the derivation (see Lemma 2 in section 3) of the relationship between the probability of cutting off optimal solution at one iteration (=3ε) and the parameter a. So if y^* is already the best solution so far, y^* will be replaced by a new y only when there exists a y such that $\hat{U}B_{N'}(y) + 2a < \overline{U}B_{N,M}(y^*)$; or if y^* is still not the best solution, y^* appears to be worse than a previous y value if $\overline{U}B_{N,M}(y^*) > \hat{U}B_{N'}(y) + 2a$. If none of these can be satisfied, either the value of the parameter a or the sample sizes N and/or N' should be increased.

For 2), in order to reduce the possibility of losing y* (i.e., y^* is infeasible), the constraint is weakened as follows:

$$\overline{L}B_{N,M} \le \hat{U}B_{N'}(y^o) + 2a \tag{2.12}$$

Norkin et al. (1998) used a similar deletion rule in their stochastic branch and bound algorithm to cut off any subset when the lower bound is greater than the upper bound by a certain value. However, $\overline{L}B_{N,M}$ is an average of multiple variables which appear in different problems. Therefore, it is impossible to impose such a constraint in any MILP problem. To deal with this issue, the constraint is removed from MILP master problem. Correspondingly, a post-analysis is done after solving the S-MILP: If the above inequality is no longer satisfied, the algorithm should stop.

For 3), to reduce the possibility of losing y*, this constraint is weakened as follows:

$$b \geq \overline{L}B_{N,M}\left(y^{o}\right) - 2a \qquad \text{for S-MILP and L-MILP} \qquad (2.13)$$

These two constraints are included in the S-MILP and L-MILP, respectively. Note that since L-MILP is solved after S-MILP is infeasible, constraint (2.13) in S-MILP will not cut off the optimal solution. It will be shown in the next section that the constraints (2.11 a, b) (2.12) and (2.13) together guarantee that the probability of losing the optimal solution y* is within a tolerance, which can be adjusted by the parameter *a*, the replication number M and sample sizes N, N'.

2.5 Accuracy and convergence of the algorithms

In this section, first a few issues related to the accuracy of the algorithms are discussed, including (i) why need to solve L-MILP after S-MILP becomes infeasible (ii) justification of using the objective value from the larger sample size to compare solutions (iii) the accuracy of the confidence level method (through a proof of the probability of cutting off the optimal solution y* and a proof of the probability of having a bad solution).

In the previous section, it has been mentioned that the L-MILP needs to be solved after the S-MILP is found infeasible. The following illustration explains why this is necessary.

Figure 2.5 (a) shows the objective function curves at different sample sizes N and N'. Suppose we start from point 1' and solve the problem using a small sample size but use larger sample size to get a more accurate estimation of the upper bound. At a certain stage, say, point 2', S-MILP becomes infeasible because the upper bound UB2 is smaller than the minimum objective value of the problem at the small sample size. So in this case, the upper bound can cut off the true optimal solution. Similarly, in Figure 2.5(b), the true optimal solution can be cut off by the lower bounds generated by linearization at points of the objective function curve at larger sample size, which is greater than the curve at smaller sample size. The lower bounds (LB1 and LB2) generated by linearization at points 1 and 2 have cut off the true optimal solution. In Figure 2.5(c), for some part, the objective function at small sample size is greater than that of the larger sample size; while for some other part, this is reversed. So, both upper bound and lower bound can cut off the true optimal solution. At point 1, the linearization cuts off the true optimal solution; at point 2 the upper bound can also cut off the true optimal solution.

So, in all cases, after S-MILP becomes infeasible, it can not be guaranteed that the optimal solution has been found. Hence, it is necessary to use the larger sample size to do a precise search (i.e., solve L-MILP) to find the true optimal solution because only the infeasibility of L-MILP can indicate that there is no better solution than the current upper bound, but the advantage is that this is done only at the last few iterations.

Next, the second issue of this section is discussed. Assume that the objective

values with sample size N' are exact and use the objective values from the larger sample size to compare solutions and solve master problems. After the S-MILP is found infeasible, solve the L-MILP until L-MILP is found infeasible.

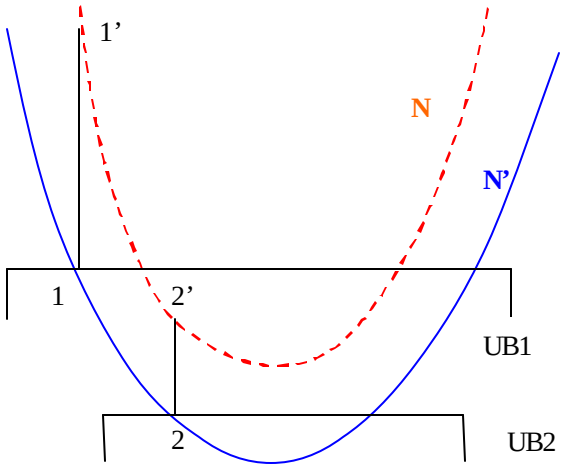

Figure 2.5 (a). Case I
objective function at large sample size
< objective function at small sample size

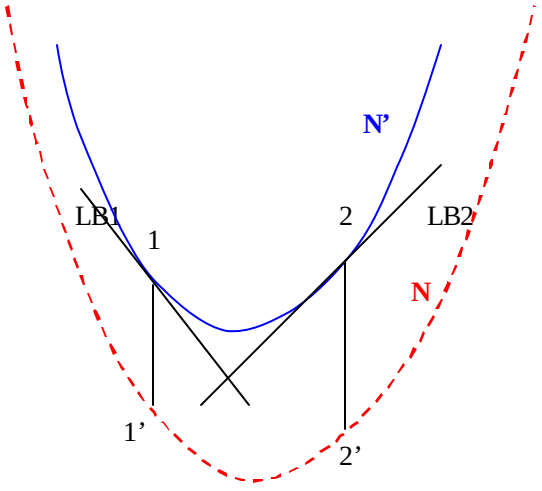

Figure 2.5 (b). Case II
objective function at large sample size
> objective function at small sample size

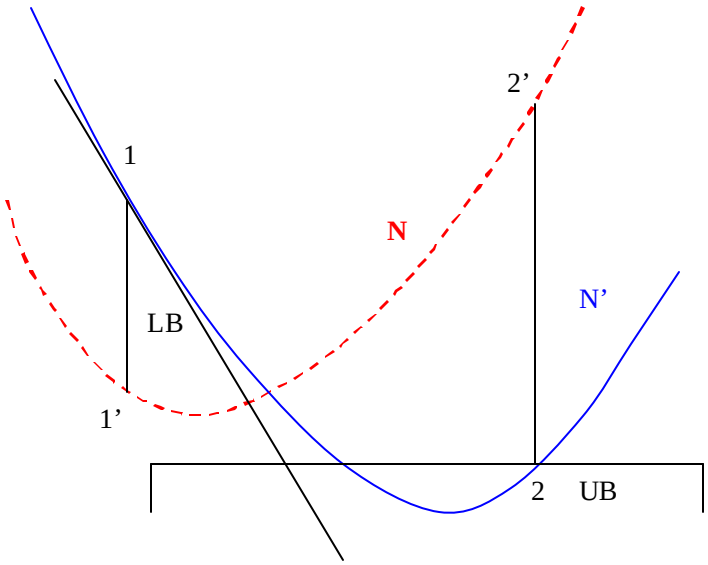

Figure 2.5 (c). Case III.
objective functions at two sample sizes cross each other

Lemma 1: the optimal solution y* will not be eliminated.

Proof (by contradiction)

Assuming the true optimal solution y^* is lost. Case a) y* appears in the sequence of y values but there is at least another y in the sequence with a smaller objective value. Since $\hat{v}_{N'}$ is used to compare the solutions and have assumed that $\hat{v}_{N'}$ are exact, this is a contradiction. Case b) y^* has been cut off because of the two constraints ($b \le GUB$ and $b \ge GLB$) in L-MILP. (i.e. y^* does not appear in the sequence of iterations). As the L-MILP becomes infeasible, we must have $b_{N'}(y^*) > GUB$ or $b_{N'}(y^*) < GLB$. Since $b_{N'}(y^*)$ is a lower bound, a contradiction is reached that a lower bound is greater than an upper bound, i.e., the first inequality can not happen. Also, since y^* is an optimal

solution, y^* should have a maximal lower bound which is greater than any other lower bounds generated at previous y values in the sequence. This means that $b_{N'}(y^*) < GLB$ can not happen either. Combining the two cases, y^* can not be lost in either way.

(*End of proof*).

The above states that if the bound estimates are exact, the optimal solution y^* will be found. However, the bounds are random variables, i.e. they are not 100% exact. For the algorithm based on the optimality gap method, a quantitative estimate of the overall accuracy can not be provided. Qualitatively, the overall accuracy increases as the tolerance on the optimality gap interval decreases. For the confidence level method, a bound for the probability that the solution y* will be lost can be derived.

Lemma2: **Assume the variances of all upper and lower bounds are bounded by the value s^2. It can be shown that by guaranteeing (2.11a, b), (2.12) and (2.13), the probability that y^* is lost will be no greater than $3Ke$, where K is the number of iterations at which the bounds are updated.**

Proof:

Assume $\{y^{(k)}\}$ is a sequence of y values that have been examined.

$$
\begin{aligned}
&P\{y^* \text{ is lost at one iteration}\} = \\
&\quad P\{y^* \in \{y^{(k)}\} \text{ but is lost during the comparison with another } y \in \{y^{(k)}\} \\
&\qquad + \; y^* \notin \{y^{(k)}\} \text{ because of constraint 2.12} \\
&\qquad + \; y^* \notin \{y^{(k)}\} \text{ because of constraint 2.13 }\} \qquad (2.14) \\
&\leq \\
&\quad P_1\{y^* \in \{y^{(k)}\} \text{ but is lost during the comparison with another } y \in \{y^{(k)}\} \\
&\quad + \; P_2\{y^* \notin \{y^{(k)}\} \text{ because of constraint 2.12 }\} \\
&\quad + \; P_3\{y^* \notin \{y^{(k)}\} \text{ because of constraint 2.13 }\}
\end{aligned}
$$

Where

$$P_1 = P\left\{\overline{U}B_{N,M}(y^*) > \hat{U}B_{N'}(y) + 2a \quad \text{or} \quad \hat{U}B_{N'}(y) + 2a < \overline{U}B_{N,M}(y^*)\right\} \tag{2.15}$$

$$\begin{aligned} &P\left\{\overline{U}B_{N,M}(y^*) > \hat{U}B_{N'}(y) + 2a\right\} \\ &= P\left\{\overline{U}B_{N,M}(y^*) - E[UB(y^*)] > \hat{U}B_{N'}(y) - E[UB(y^*)] + 2a\right\} \\ &\le P\left\{\overline{U}B_{N,M}(y^*) - E[UB(y^*)] - a > 0\right\} + P\left\{\hat{U}B_{N'}(y) - E[UB(y^*)] + a < 0\right\} \end{aligned} \tag{2.16}$$

For the 1st term, Norkin et al. (1998) showed that

$$P\left\{\overline{U}B_{N,M}(y^*) - E[UB(y^*)] - a > 0\right\} \le \frac{Var\left(UB_N^{(m)}(y^*)\right)}{a^2 M} \le \frac{s^2}{a^2 M} \tag{2.17}$$

where the first inequality is by the Chebyshev inequality (if a random variable x has a finite mean μ and finite variance σ^2, then $\forall\, k \ge 0$, we have $P\{|x - m| \ge k\} \le s^2 / k^2$) and the 2nd one is by the assumption in Lemma 2.

For the 2nd term,

$$\begin{aligned} &P\left\{\hat{U}B_{N'}(y) - E[UB(y^*)] + a < 0\right\} \\ &= P\left\{\hat{U}B_{N'}(y) - E[UB(y)] + a < E[UB(y^*)] - E[UB(y)]\right\} \\ &\le P\left\{\hat{U}B_{N'}(y) - E[UB(y)] + a < 0\right\}, \text{ since } \; E[UB(y^*)] < E[UB(y)] \\ &\le \frac{Var\left(UB_{N'}(y)\right)}{a^2 N'} \le \frac{s^2}{a^2 N'} \quad \text{(again, by Chebyshev inequality and the assumption)} \end{aligned} \tag{2.18}$$

Therefore,

$$P\left\{\overline{U}B_{N,M}(y^*) > \hat{U}B_{N'}(y) + 2a\right\} \le \frac{s^2}{a^2}\left(\frac{1}{M} + \frac{1}{N'}\right) = e \tag{2.19}$$

Parameter a can be defined by setting the right hand side equal ε. Similarly, we have

$$P\left\{\hat{U}B_{N'}(y) + 2a < \overline{U}B_{N,M}(y^*)\right\} \le e \tag{2.20}$$

However, since the two events $\left\{\overline{U}B_{N,M}(y^*) > \hat{U}B_{N'}(y) + 2a\right\}$ and $\left\{\hat{U}B_{N'}(y) + 2a < \overline{U}B_{N,M}(y^*)\right\}$ can not occur simultaneously, so we have

$$P_1 \le e \tag{2.21}$$

Similarly, for P_2, we have

$$\begin{aligned}
P_2 &= P\left\{\overline{L}B_{N,M}(y^*)) > \overline{U}B_{N'}(y) + 2a\right\} \\
&= P\left\{\overline{L}B_{N,M}(y^*) - E[UB(y)] - a > \overline{U}B_{N'}(y) + a - E[UB(y)]\right\} \\
&\le P\left\{\overline{L}B_{N,M}(y^*) - E[UB(y)] - a > 0\right\} + P\left\{\overline{L}B_{N'}(y) + a - E[UB(y)] < 0\right\} \\
&\le P\left\{\overline{L}B_{N,M}(y^*) - E[LB(y^*)] - a > 0\right\} + P\left\{\overline{L}B_{N'}(y) + a - E[UB(y)] < 0\right\} \\
&\le \frac{var\left(LB_N{}^{(m)}(y^*)\right)}{M \cdot a^2} + \frac{var\left(\hat{U}B_{N'}(y)\right)}{N' \cdot a^2} \le \frac{s^2}{a^2}\left(\frac{1}{M} + \frac{1}{N'}\right) = e
\end{aligned} \tag{2.22}$$

and for P_3, we have

$$\begin{aligned}
P_3 &= P\left\{\hat{L}B_{N'}(y^*) < \overline{L}B_{N,M}(y) - 2a\right\} \\
&= P\left\{\overline{L}B_{N'}(y^*) - E[LB(y^*)] + a < \overline{L}B_{N,M}(y) - a - E[LB(y^*)]\right\} \\
&\le P\left\{\overline{L}B_{N'}(y^*) - E[LB(y^*)] + a < 0\right\} + P\left\{\overline{L}B_{N,M}(y) - a - E[LB(y^*)] > 0\right\} \\
&\le P\left\{\overline{L}B_{N'}(y^*) - E[LB(y^*)] + a < 0\right\} + P\left\{\overline{L}B_{N,M}(y) - E[LB(y)] - a > 0\right\} \\
&\le \frac{var\left(\hat{L}B_{N'}(y^*)\right)}{N' \cdot a^2} + \frac{var\left(LB_N{}^{(m)}(y)\right)}{M \cdot a^2} \le \frac{s^2}{a^2}\left(\frac{1}{M} + \frac{1}{N'}\right) = e
\end{aligned} \tag{2.23}$$

Therefore, combining (2.14) and (2.21~2.23), we have

$$\text{P}\{y^* \text{ is lost at one iteration}\} \le 3e \tag{2.24}$$

If there are K iterations at which bounds are updated (i.e., exclude those iterations where NLP subproblems are infeasible for the given y values), the total probability of losing the optimal solution is

$$\text{P}\{y^* \text{ is lost finally}\} \le 3Ke \tag{2.25}$$

(End of proof)

First it should be noted that the error is proportional to the square of the ratio (σ/a), therefore if a can be chosen a large value, i.e., objective values at different decisions are far from each other, a large variance σ^2 can be tolerated, which means small sample sizes N, N' or replication number M might be sufficient to obtain a small probability of error. Second, since the overall error is also proportional to the number of iterations, if the iteration number K is large, the overall error could be large due to the error accumulation over the iterations. The problem of error accumulation exists if one applies the SAA method to each subproblem and master problem. However, the number $3K\varepsilon$ is just a conservative estimate, i.e., the actual error might be much smaller.

It is also important to establish bounds on the probability of having a very bad solution (i.e., the probability that the objective value is greater than the true optimal value by a certain number if a wrong solution y^o is reached instead of y^*). Consider the worst case: for a sequence $\{y_k\}$, k=1,…, K, the true objective values are ordered as: $v(y_1) < v(y_2) < \cdots < v(y_K)$; but the CLM algorithm generates a reverse order: $\hat{v}(y_1) > \hat{v}(y_2) > \cdots > \hat{v}(y_K)$, so there is an incorrect comparison of objective values at each iteration and we end up with a wrong solution $y^o=y_K$ while the true optimal solution is $y^*=y_1$. We must have in the algorithm:

$$\hat{UB}_{N'}(y_k) + 2a < \overline{UB}_{N,M}(y_{k-1}), \text{ for k=2, …, K} \qquad (2.26)$$

The problem becomes: given (2.26), what is the probability of $v(y^o) - v(y^*) \geq 2(K-1)d$, where δ is a parameter.

Lemma 3: for the problem stated above, we have

$$P\left\{v\left(y^{o}\right)-v(y^{*})\geq 2(K-1)d\right\}\leq (K-1)\left(\frac{1}{M}+\frac{1}{N'}\right)\frac{s^{2}}{(d+a)^{2}}=e' \tag{2.27}$$

Proof: since $y^{o}=y_{K}$ and $y^{*}=y_{1}$

$$\begin{aligned}
&P\left\{v\left(y^{o}\right)-v(y^{*})\geq 2(K-1)d\right\}\\
&=P\left\{v\left(y_{K}\right)-v\left(y_{1}\right)\geq 2(K-1)d\right\}\\
&=P\left\{v\left(y_{K}\right)-v\left(y_{K-1}\right)+v\left(y_{K-1}\right)-v\left(y_{1}\right)\geq 2(K-1)d\right\}\\
&\leq P\left\{v\left(y_{K}\right)-v\left(y_{K-1}\right)\geq 2d\right\}+P\left\{v\left(y_{K-1}\right)-v\left(y_{1}\right)\geq (K-2)2d\right\}
\end{aligned} \tag{2.28}$$

By induction

$$\begin{aligned}
&P\left\{v\left(y_{K}\right)-v\left(y_{1}\right)\geq 2(K-1)d\right\}\\
&\leq P\left\{v\left(y_{K}\right)-v\left(y_{K-1}\right)\geq 2d\right\}+P\left\{v\left(y_{K-1}\right)-v\left(y_{K-2}\right)\geq 2d\right\}+\cdots\\
&\quad+P\left\{v\left(y_{2}\right)-v\left(y_{1}\right)\geq 2d\right\}\\
&=\sum_{k=2}^{K}P\left\{v\left(y_{k}\right)-v\left(y_{k-1}\right)\geq 2d\right\}
\end{aligned} \tag{2.29}$$

Next, the probability $P\{v(y_{k})-v(y_{k-1})\geq 2d\}$ can be calculated.

$$\begin{aligned}
&P\{v(y_{k})-v(y_{k-1})\geq 2d\}\\
&=P\left\{\left[v(y_{k})-\hat{U}B_{N'}(y_{k})-d\right]-\left[v(y_{k-1})-\overline{U}B_{N,M}(y_{k-1})+d\right]\geq\left[\overline{U}B_{N,M}(y_{k-1})-\hat{U}B_{N'}(y_{k})\right]\right\}
\end{aligned} \tag{2.30}$$

From inequality (2.26), we have

$$\begin{aligned}
&P\left\{\left[v\left(y_{k}\right)-\hat{U}B_{N'}\left(y_{k}\right)-d\right]-\left[v\left(y_{k-1}\right)-\overline{U}B_{N,M}\left(y_{k-1}\right)+d\right]\geq\left[\overline{U}B_{N,M}\left(y_{k-1}\right)-\hat{U}B_{N'}\left(y_{k}\right)\right]\right\}\\
&\leq P\left\{\left[v\left(y_{k}\right)-\hat{U}B_{N'}\left(y_{k}\right)-d\right]-\left[v\left(y_{k-1}\right)-\overline{U}B_{N,M}\left(y_{k-1}\right)+d\right]\geq 2a\right\}\\
&\leq P\left\{v\left(y_{k}\right)-\hat{U}B_{N'}\left(y_{k}\right)-d-a\geq 0\right\}+P\left\{v\left(y_{k-1}\right)-\overline{U}B_{N,M}\left(y_{k-1}\right)+d+a\leq 0\right\}
\end{aligned} \tag{2.31}$$

where

$$P\left\{v\left(y_{k}\right)-\hat{U}B_{N'}\left(y_{k}\right)-d-a\geq 0\right\}\leq\frac{s^{2}}{N'(d+a)^{2}} \tag{2.32}$$

and

$$P\left\{v\left(y_{k-1}\right)-\overline{U}B_{N,M}\left(y_{k-1}\right)+d+a\le 0\right\}\le\frac{s^2}{M(d+a)^2} \tag{2.33}$$

so, the overall probability is

$$P\left\{v\left(y^o\right)-v(y^*)\ge 2(K-1)d\right\}\le(K-1)\left(\frac{1}{M}+\frac{1}{N'}\right)\frac{s^2}{(d+a)^2}=e', \text{ (defined as } \varepsilon\text{')} \tag{2.34}$$

(End of proof)

Having established that the error can be controlled by increasing the sample sizes, it is necessary to demonstrate that the algorithm will terminate. For each stochastic NLP subproblem and MILP master problem, a strong convergence of the SAA algorithm has been established for both the solution and the objective value. Under some mild assumptions [see the theorems 1 and 2, page 332-334 in Birge (1997), also theorem 3.2 in King and Rockafellar (1993) and theorem 3.3 in Shapiro (1991)], the sequences of solution and the objective value converge to the optimal solution and optimal value, respectively, w.p.1 as the sample size N$\to\infty$. Moreover, if the solution is unique, we have $\sqrt{N}\left(\hat{v}_N-v^*\right)$ converges in distribution to a normal $N\left(0,s^2\right)$. The strong convergence result also applies to our algorithms: since the OA algorithm converges and at each iteration the subproblem and master problem converge to their respective true problems, the solution to the SAA problem must converge to the true optimal solution w.p.1 as the sample sizes N and N' $\to\infty$.

2.6 Case Studies

In this section, two case studies are presented to compare the two algorithms and demonstrate their efficiencies over a single sample size algorithm. The first example is

used to compare the two algorithms (OGM and CLM) and their efficiencies with that of the conventional fixed-sample algorithm. The second example is used to show the computational efficiency. Instead of solving the problem by the OGM with a pre-specified optimality gap tolerance, the optimality gap intervals are computed by the CLM algorithm. If any of the gap intervals is larger than the tolerance, the sample sizes required by OGM are larger than that by CLM. All examples were coded in AMPL. NLP sub-problems and MILP master problems were solved using SNOPT 5.3-4 and CPLEX 7.0, respectively, on a PC with 2.5 GHZ CPU and 1G memory.

Example 1

$$\min_{x,y,z} E_q \left\{ \begin{array}{l} 0.130(e^{5x_{1,1}} + e^{4x_{2,1}}) + 131y_1 + 80?_1^2 z_1 \\ + 0.155(e^{5x_{1,2}} + e^{4x_{2,2}}) + 172y_2 + 120?_2^2 z_2 \\ + 0.145(e^{5x_{1,3}} + e^{4x_{2,3}}) + 150y_3 + 145?_3^2 z_3 \\ + 0.085(e^{5x_{1,4}} + e^{4x_{2,4}}) + 110y_4 + 80?_1^2 z_4 \\ + 0.140(e^{5x_{1,5}} + e^{4x_{2,5}}) + 172y_5 + 100?_2^2 z_5 \\ + 0.160(e^{5x_{1,6}} + e^{4x_{2,6}}) + 272y_6 + 85?_3^2 z_6 \end{array} \right\}$$

s.t.

$$\begin{array}{l} y_1 + y_2 + y_3 \geq 1, \qquad y_4 + y_5 + y_6 \geq 1 \\ y_1 + y_4 \leq 1, \qquad y_1 + y_2 \geq 1 \\ z_j + x_{1,j} + x_{2,j} \geq q_j y_j \qquad \forall \, j = 1, \cdots, 3 \\ z_j + x_{1,j} + x_{2,j} \geq q_{j-3} y_j \qquad \forall \, j = 4, \cdots, 6 \\ z_1 + z_2 + \cdots + z_6 \leq 5 \\ 0.2 y_j \leq x_{i,j} \leq 1.5 y_j \qquad \forall \, i, j = 1, \cdots, 6 \\ 0.4 y_j \leq z_j \leq 3.0 y_j \qquad \forall \, j = 1, \cdots, 6 \\ q_1 \sim log\, n(1.0, 0.2) \quad q_2 \sim log\, n(0.8, 0.2) \quad q_3 \sim log\, n(1.0, 0.1) \\ e^{0.4} \leq q_1 \leq e^{1.6}, e^{0.2} \leq q_2 \leq e^{1.4}, e^{0.7} \leq q_3 \leq e^{1.3} \end{array}$$

The purpose of this example is to compare the two algorithms (OGM and CLM). This example has 12 continuous decision variables $x_{i,\ j}$ (i=1..2, j =1,…,6), 6 binary decision variables y_j (j=1,…,6), 6 control variables z_j (j=1..6) and 3 uncertain parameters q_k (k=1..3) which are log normally distributed with their respective mean and variance.

The result is shown in Table 2.1. The problem was first solved using the CLM algorithm with a=30, M=40, N=600 and N'=10000. To calculate the probability of cutting off optimal solution y*, the value of σ^2 is estimated by the maximum variance of all upper and lower bounds. In this problem, the maximum variance (54.41) is generated for the lower bound $var\left(\hat{L}B_{N'}\right)$ at the 4th iteration. Hence, an estimate of the probability of cutting off the optimal solution is

$$3*\ 5*\ 55\ /30^2*(1/40+1/10000) \approx 2.3\ \%$$

, and the probability of having a bad solution (with $v(y^*) \approx 1230$) is

$$(5\text{-}1)*55\ /(0.05*1230/2/4+30)^2*(1/40+1/10000) \approx 0.39\ \% \quad \text{for } 2(K\text{-}1)\delta=5\%\cdot v(y^*)$$

$$(5\text{-}1)*55\ /(0.01*1230/2/4+30)^2*(1/40+1/10000) \approx 0.56\ \% \quad \text{for } 2(K\text{-}1)\delta=1\%\cdot v(y^*)$$

The gap in Table 2.1 is the size of the 99.9% confidence level of the optimality gap, which is estimated according to the Equation (2.7). The maximum of the gap intervals decreased from 57 to 34 as the smaller sample size is increased from 600 to 1000 (Table 2.1, part a and b). However, one can see that the mean values of the upper bounds have not been improved significantly and the optimal solution stays the same while the computational time significantly increased. Kleywegt et al. (2001) have pointed that the optimality gap estimator used here is a weak one: sometimes the optimality gap is still very large while a good solution has been found. Therefore, the stopping rule of sufficiently small optimality gap seems to be a subjective one.

Table 2.1 Results for example 1

Part a: M=40, N=600, N'=10000, CPU time = 16 min 10 sec						
Y	$\overline{UB}_{N,M}$	$\hat{UB}_{N'}$	Gap of UB	$\overline{LB}_{N,M}$	$\hat{LB}_{N'}$	Gap of LB
010001	1197.90	1203.58	22.91	167.19	198.43	57.13
100010	1104.25	1108.82	32.87	545.74	551.84	27.87
010010	**1031.41**	**1038.57**	**36.14**	**733.96**	**756.31**	**46.35**
010100	1101.96	1107.31	33.85	929.82	932.73	35.48
100001	1270.73	1273.82	28.66	Infeasible		

Part b: M=40, N=1000, N'=10000, CPU time= 43 min 9 sec

Y	$\overline{UB}_{N,M}$	$\hat{UB}_{N'}$	Gap of UB	$\overline{LB}_{N,M}$	$\hat{LB}_{N'}$	Gap of LB
010001	1197.34	1202.48	20.46	169.23	178.57	32.61
100010	1105.28	1107.82	29.84	539.43	543.40	23.08
010010	**1031.58**	**1036.44**	**30.44**	**736.04**	**747.61**	**34.23**
010100	1102.99	1106.13	30.38	919.34	921.62	33.51
100001	1271.04	1273.86	27.71	Infeasible master problem		

Part c: M=100, N=600, N'=10000, CPU time= 37 min 29 sec

Y	$\overline{UB}_{N,M}$	$\hat{UB}_{N'}$	Gap of UB	$\overline{LB}_{N,M}$	$\hat{LB}_{N'}$	Gap of LB
010001	1196.89	1203.58	20.52	169.21	180.89	31.70
100010	1104.65	1108.82	28.03	558.36	564.51	23.96
010010	**1030.44**	**1038.57**	**31.13**	**735.14**	**738.03**	**23.15**
010100	1102.25	1107.31	28.95	908.40	910.65	30.89
100001	1271.10	1273.82	24.42	Infeasible master problem		

Part d: M=40, N=600, N'=20000, CPU time= 16 min 31 sec

Y	$\overline{UB}_{N,M}$	$\hat{UB}_{N'}$	Gap of UB	$\overline{LB}_{N,M}$	$\hat{LB}_{N'}$	Gap of LB
010001	1197.90	1200.36	16.69	167.19	194.10	48.96
100010	1104.25	1103.31	22.14	545.74	549.51	21.86
010010	**1031.41**	**1035.32**	**28.03**	**733.96**	**751.04**	**36.51**
010100	1101.96	1101.65	22.94	929.82	927.95	23.79
100001	1270.73	1268.35	18.43	Infeasible master problem		

Part e: using a fixed sample size N= 5000, CPU time = 1 hr 2 min 46 sec

Optimal solution: 010010, optimal objective value= 1028.46

Since the parameter a can not be arbitrarily large, to get an even smaller probability, one option is to increase the number of replications M; another option is to increase the sample size N or N', depending on whether the current maximum variance is from the larger problem or the replication of smaller problems. If the value of M is

increased to 100 (Table 2.1: part c), then the probability of cutting off the optimal solution is

$3* 5* 53 /30^2*(1/100+1/10000) \approx 0.89$ %

and the probability of having a bad solution (with $v(y^*) \approx 1230$) is

$(5-1)*53 /(0.05*1230/2/4+30)^2*(1/100+1/10000) \approx 0.15$ %, for $2(K-1)\delta=5\% \cdot v(y^*)$

$(5-1)*53 /(0.01*1230/2/4+30)^2*(1/100+1/10000) \approx 0.22$ %, for $2(K-1)\delta=1\% \cdot v(y^*)$

Of course, a tradeoff of this is the significantly increased computational time.

If the value M is kept the same but the sample size N' is increased to 20000 (Table 2.1: part d), the maximum variance is reduced to 27 and the probability of cutting off the optimal solution is

$3* 5* 27 /30^2*(1/40+1/20000) \approx 1.13$ %

and the probability of having a bad solution (with $v(y^*) \approx 1230$) is:

$(5-1)*27 /(0.05*1230/2/4+30)^2*(1/40+1/20000) \approx 0.19$ %, for $2(K-1)\delta=5\% \cdot v(y^*)$

$(5-1)*27 /(0.01*1230/2/4+30)^2*(1/40+1/20000) \approx 0.27$ %, for $2(K-1)\delta=1\% \cdot v(y^*)$

However, there is only a slight increase of the computational time. Therefore, whenever the maximum variance comes from the larger problems, increasing the larger sample size seems to be a better choice than increasing the replication number. However, this would not be the case if parallel computing is available to solve M problems simultaneously.

Compared with using a fixed sample size (part e), the new algorithms provided fairly close optimal value while reducing the computational time significantly.

Example 2

This example is taken from Acevedo and Pistikopoulos (1998) with modified

yield model and parameter values. The problem (Figure 2.6) is to produce 5 products from 5 raw materials with 11 processes, each of which is optional. The uncertainties are the availabilities of raw materials and demands for products, i.e., 10 uncertainty parameters. The continuous decision variables are the capacities Q_k for the processes k=1...11. The complete model and parameter values are shown in Table 2.2 and Table 2.3 respectively.

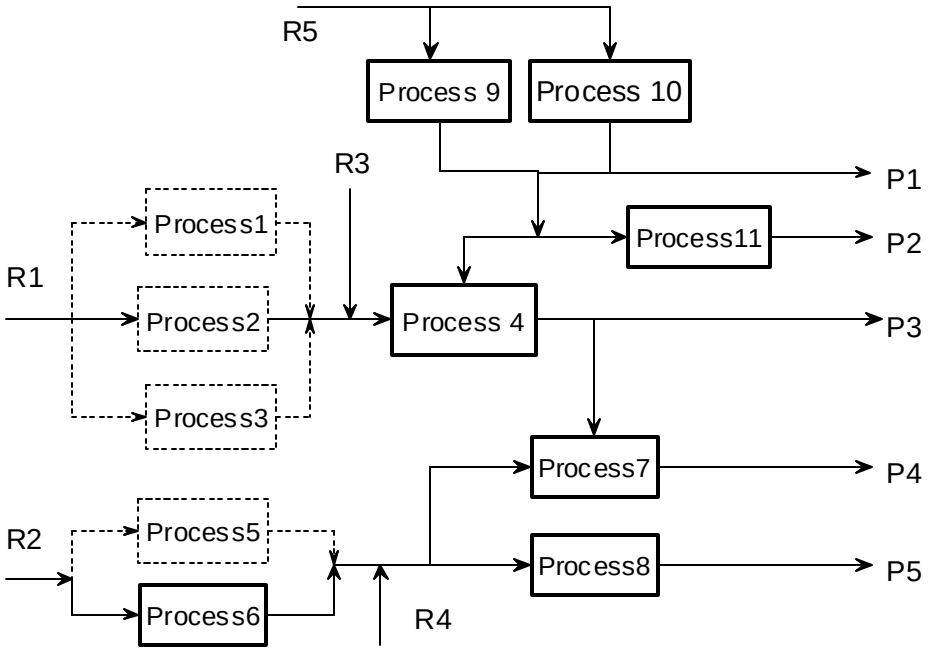

Figure 2.6 Process flowsheet for example 2 (Solid lines show the optimal choice)

It should be noted that in this problem since there are 10 uncertain parameters, theoretically the smaller sample size would be at least $2^{10} \approx 1000$ to include all vertices. However, in this case, including the worst case parameter values in samples for the smaller problem can guarantee that the larger problem is feasible. This worst case occurs

when the demands for all products are at their highest values (35) and the availabilities of all raw materials are at their lowest values (29).

The problem was first solved using the confidence level method with M=20, N=200, N'=1000 and a=1000 and the result in shown in part a of Table 2.4. The maximum variance (~10000) came from the replicated solutions of the smaller master problem at the 1st iteration. At the 2nd iteration, the NLP sub-problem is infeasible, hence

Table 2.2 Model for example 2

Objective function	$max\, E_q\left[\sum_{i=1}^{5} b_i \times P_i - \sum_{j=1}^{5} a_j \times RM_j - \sum_{k=1}^{11} OC_k \times IS_k\right] - \sum_{k=1}^{11}\left[DC_k \times Q_k + FC_k \times y_k\right]$	
Constraints		
1. Yield relations	$OS_k \pounds Pc_k\, ln(1+IS_k/K_k)$	$k=1, ...,11$
2. Desired production	$P_i \pounds D_i$	$i=1,\ldots, 5$
3. Availability of raw material	$RM_j \pounds MaxRM_j$	$j=1, ..., 5$
4. Logical constraints	$IS_k \pounds MI_k Q_k$	$k=1,\ldots,11$
	$Q_k \pounds y_k\, MaxQ_k$	$k=1,\ldots,11$
5. Flowrate balances	(not shown here)	

Notation:

D_i	Uncertain demand of product I
DC_k	Design cost for process k
FC_k	Fixed cost of process k
K_k	Parameter in yield relation for process k
$MaxRM_j$	Uncertain maximum availability of raw material j
$MaxQ_k$	Maximum capacity of process k
MI_k	Flow to volume relation for process k
IS_k	Input stream to process k
P_i	Flowrate of product i
Pc_k	Parameter in yield relation for process k
Q_k	Capacity of process k
OC_k	Operating cost for process k
OS_{kt}	Output stream from process k
y_k	Binary variable denoting the existence of process k
a_j	Cost of raw material j
b_I	Price of product i

no upper and lower bound were updated and the only action performed in this iteration was to find a y value for the next iteration. Therefore, only the 1st and 3rd iterations may have influence on the probability of losing the optimal solution. The probability of cutting off the optimal solution is calculated as below:

$$3*2*10000/1000^2*(1/20+1/5000) \approx 0.4\%.$$

and the probability of having a bad solution (with $v(y^*) \approx 27920$) is:

$$(2-1)*10000 /(0.05*27920/2/1+1000)^2*(1/20+1/5000) \approx 0.017\ \%, \text{ for } 2(K-1)\delta=5\%\cdot v(y^*)$$

Although the gap intervals are large, the probability of losing y* is low enough due to the large difference between the objective values. Again the problem was also solved using a fixed sample size (part b in Table 2.4) and the computational efficiency of the proposed algorithm is apparent.

Table 2.3 Parameter values for example 2

Proc. k	1	2	3	4	5	6	7	8	9	10	11
PC_k	13	15	17	14	10	15	16	11	13	15	17
K_k	1.0	1.2	1.7	1.5	1.8	1.4	1.5	1.3	1.1	1.2	1.8
MI_k	18	20	15	20	20	21	15	15	25	15	20
OC_k	400	400	400	400	400	400	400	400	400	400	400
DC_k	2500	2500	2500	2500	2500	2500	2500	2500	2500	2500	2500
FC_k	4000	2500	3500	3000	4500	2500	3000	2200	2800	2700	2500
$MaxQ_k$	3.0	3.0	3.0	3.0	3.0	3.0	3.0	3.0	3.0	3.0	3.0
Prod. I	1	2	3	4	5						
β_I	600	650	500	400	700						
D_i	Normal distribution ~ N (30, 1.5), $25 \le D_i \le 35$										
Raw j	1	2	3	4	5						
α_j	200	320	230	250	300						
$MaxRM_j$	Normal distribution ~ N(35, 1.5), $29 \le MaxRM_j \le 41$										

Table 2.4 Results for example 2

Part a: M=20, N=200, N'=5000, CPU time = 59 min						
Y	$\overline{UB}_{N,M}$	$\hat{UB}_{N'}$	Gap of UB	$\overline{LB}_{N,M}$	$\hat{LB}_{N'}$	Gap of LB
11111111111	-16189.72	-15287.26	1072.05	-37900.63	-28753.16	29498.70
00010011101	Infeasible NLP					
00010111111	-28612.15	-27733.56	1045.71	Infeasible master problem		
Part b: using a fixed sample size N=5000, CPU time = 4 hr 50 min						
optimal solution: 00010111111, optimal objective value= -27919.66						

2.7. Conclusions

This chapter describes two new algorithms that combine the SAA method (with bounding techniques) and OA algorithm to solve stochastic MINLPs. In both algorithms, a smaller sample size N is used to make decisions (with several replications) and a larger one is used to re-evaluate the objective value with the decision variables fixed. The sample sizes and replication number are increased until a stopping criterion is satisfied. In the OGM algorithm, the sample sizes are increased until the optimality gap of each upper and lower bound is sufficiently small; in the CLM algorithm, the sample sizes are increased until an overall accuracy probability is within a certain tolerance. The case study showed that the algorithm based on optimality gap is sometimes not efficient because the optimality gap estimator is too weak to be a good indicator of finding the optimal solution. It was also shown that the proposed algorithms could result in significant computational time savings compared with that of using a fixed sample size for the same required confidence. This improvement will enable the solution of larger stochastic MINLPs and hence broaden the range of application of this method to process design problems. This work has been published in Wei and Realff (2004).

CHAPTER 3

UNIT MODELING I

¾ DESIGN AND OPTIMIZATION OF FREE-FALL ELECTROSTATIC SEPARATORS FOR PLASTICS RECYCLING

3.1 Introduction

Electrostatic separation provides many advantages over other separation methods (such as froth flotation and sink-float separation): low energy consumption, a dry process, independence of particle shape and it is often simpler, cheaper and easier to control than froth flotation and other wet medium techniques. Therefore, it is a very important separation operation whose design should be treated systematically to explore its full potential.

When two different plastics come into contact and are subsequently separated, electrons are transferred from one to the other. Thus different particles acquire opposite charges and can be separated in a high voltage field (usually 30~60 kV). In general, particles with higher dielectric constant are charged positively against particles with a lower constant. Table 3.1 shows the relative triboelectric charging sequence of common plastics. It should be pointed out that the relative positions of plastics in the sequence depend on the experimental condition, hence the table is only for general reference. For further details about the basics of triboelectrification, readers may refer to Lowell et al. (1980), Inculet (1984), Botsch et al. (1997) and Kwetkus (1998).

Table 3.1 Triboelectric series of plastics (Stahl et al., 1997)

Material	PUR	POM	PC	PA	ABS	PS	PE	PP	PET	PVC	PVDF
Series	+									–	

Besides the electric properties of the materials, the triboelectric charging process can be influenced by many other factors, such as the frequency of collision (contact), humidity, material ratios, pretreatment, etc. Kamptner et al. (1997) demonstrated several successful examples of using surfactants. It has been shown that it is possible to change the charge sign of PE in the mixture of PVC/PE/PS by surface treatment, while the sign of PVC and PS charging remains unchanged. Since the charging is affected by so many factors, the charges carried by the particles are difficult to predict. Lowell (1980) found that the standard deviation is about 1/3 of the mean even to the extent that wrong sign charges are seen. It appears that a wide charge distribution may be fundamental to insulator charging, and must be accounted for in any design procedure.

Figure 3.1 shows the schematic of the separation process.

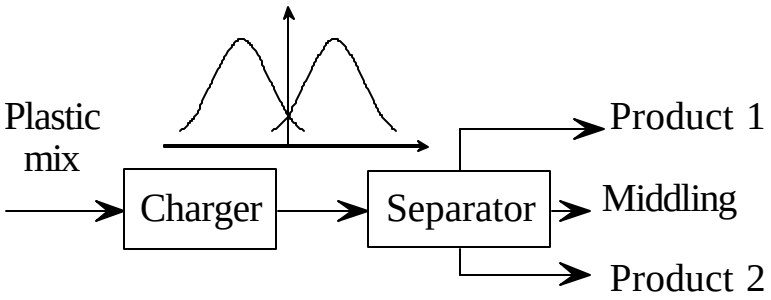

Figure 3.1 Schematic of the separation process

First a plastic mix is charged in a charging device and then fed to the separator with

usually several bins to collect the products and middling. The overlapping curves represent the distribution of particle charges. Due to the various factors mentioned above that might have influence on the charging process, it is reasonable to assume that different types of plastic particles have normal charge distributions with their respective mean and variance.

There are several methods of contacting particles together to generate triboelectric charging. Commonly used devices are an inclined rotating drum (Inculet et al., 1998), fluidized bed (Inculet et al., 1998), cyclone (Yanar and Kwetkus, 1995) and vibrating feeder (Higashiyama et al., 1997). For the separation process after charging, free-fall between two plates or a rotating drum are the most common designs. The free-fall design is simpler, eliminating moving parts. However, a rotating drum might be able to provide a higher throughput.

There are few papers addressing the modeling and design of electrostatic separators. Vlad et al. (2000) modeled the behavior of charged conductive particles in plate-type (a single inclined plate with particles sliding down) electrostatic separator. The detachment points of particles were simulated and the detachment voltage at fixed point was calculated and verified by experiments. Mihailescu et al. (2000) demonstrated a computer-assisted experimental design for optimizing the separation process. Most of the previous research on modeling electrostatic separation processes focused on single particle behavior, instead of the overall separation efficiency (such as recoveries and grades of the products). A model-based design and optimization procedure would be helpful as a guide to the preliminary design, which could then be verified by experiments. The aim of this work is to present a systematic method which can be used to design and

optimize an electrostatic separator system. The system should distinguish among several design options (single or two-stage, with or without recycle etc). For this purpose, unit separation models for each design option were developed. These were then used within nonlinear optimization procedure to find optimized designs.

3.2 The trajectory model of free-fall electrostatic separators

The schematic of free-fall electrostatic separators is shown in Figure 3.2.

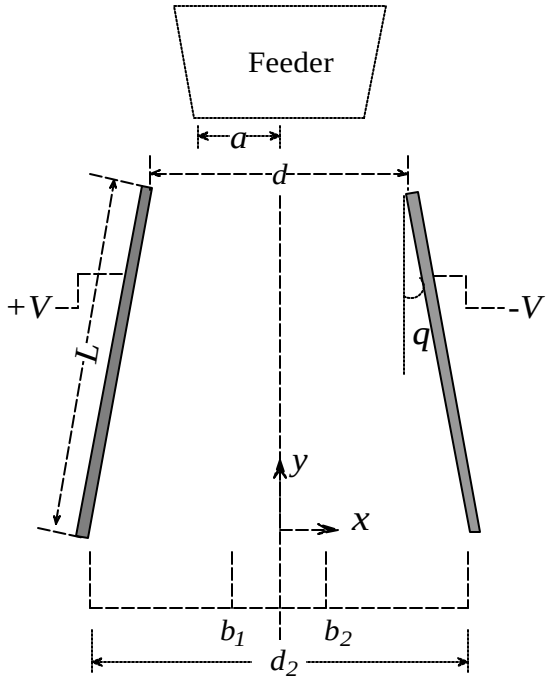

Figure 3.2 Schematic of a free-fall electrostatic separator

The two plates, with feed gap d, end gap d_2 and length L, are inclined at angle q and charged at constant voltage $\pm V$. Particles enter the electrical field from a feeder with feeding gap $2a$, hence the initial position of a particle is a random variable with uniform

distribution U(-*a*, *a*). Three collection bins (two side bins for the products and one middle bin for the middling) are placed at the bottom with the separating positions b_1 and b_2 as indicated in the figure. First, the assumptions that have been used to develop the trajectory model are described below.

3.2.1 Assumptions

1. Pairwise particle-particle interaction (Coulomb force) is negligible

This is supported by the following quick calculation: for two particles with same diameter 5 mm and same charge 7.2e-10 C in an electrical field (4×10^5 V/m), the pairwise particle-particle interaction is 1.35 μN, which is insignificant compared to the average electrostatic force of 288 μN.

2. Air drag force is negligible

For a spherical particle with density 1100 kg/m^3 and diameter 5 mm in the air with density 1.2 kg/m^3 and viscosity 1.8e-5 pa·s, a numerical calculation showed that the differences of the time for particles to hit the bottom with or without drag force is only 0.015 second, which generates a difference of the particle horizontal position at the bottom only 0.3 cm. For flat pieces, with length to width ratio less than 2.0, the drag coefficient in the turbulent region is approximately 1.15 and the difference of the horizontal position is less than 2.4 cm, which is also not large enough to generate significant error. Therefore, this assumption is justified.

3. Inter-particle collisions are negligible

A simple Monte Carlo simulation showed that the inter-particle collisions have insignificant influence on the recoveries. First, the average number of particles in the separator was computed based on the mass flow rate and the residence time of particles in the separator. These stationary particles were uniformly distributed and placed at the center of each cell. One positive particle with random charge and initial position was allowed to fall and move toward the right side bin. 20,000 such samples were generated and the procedure was repeated 10 times. If during its travel, the perpendicular distance of any stationary particle to the trajectory of the moving particle was less than 1.1 the particle diameter, there was a collision and the position was recorded. It turned out that, for a mass flowrate of 1000 kg/hr and mean particle charge (mass to charge ratio) 3.0 μC/kg and standard deviation 0.4, there were an average of 19158 collisions. However, most of them are ineffective with regards to changing the final classification of the particles for the following reasons:

(1) There are an average of 1348 collisions in region I (space above the left side bin) which are negligible because the positive moving particle has very small velocity, the collision has little effect on its trajectory.

(2) There are an average of 11247 collisions in region III (space above the right side bin) which are mostly negligible because positive particle collides mostly with another positive particle, which does not change the classification of both particles.

(3) There are an average of 6563 collisions in region II (space above the middle bin). Assume half of the collisions are between the positive particle and a positive particle, and another half between the positive particle and a negative particle. Again, the collisions between two positive particles do not change their final classifications. Assuming elastic

collision between a positive particle and a negative particle, the positive moving particle took the velocity of the negative particle after collision. The simulation showed that only 1083 on average changed the classification of the positive particle (from the right side bin to the middle or even the left side bin).

Therefore, only 5.6% (1083/19158) of the total collisions affects the recoveries. The percentage is reduced as flowrate decreases and mean charge increases. This simulation ignores the real distribution of particles in the separator and the effect of collisions on this and thus represents a first order attempt to characterize the effect of collisions.

4. *Plate inner walls are inelastic, hence particles drop to the side bins after impinging against the walls.*

This assumption is supported by industrial practice. Some industrial designs used box electrodes consisting of a perforated plate and a solid back plate (Yan et al., 2001) or parallel tubular electrodes (Norbert and Ingo, 1997) so that the particles can fly through after reaching the walls.

5. *Edge effects of the electrical field are negligible.*

It implies that the plate width and length are both sufficiently large to confine fringing effects to a small portion of the separation.

6. *The plate height is much longer than the plate gap, i.e., $L_x \cos\theta >> d$*

7. *The total charge on the particles is negligible, i.e., the presence of the particles does not change the electric field.*

This is supported by the calculations of assumption (1).

Since the air drag force is negligible, the separation process is independent of particle size and shape, with the gravitational and electrostatic forces both proportional to the particle mass. The above assumptions enable a reasonably simple, analytical model of the particle trajectory to be derived and used in a design model. The translation of the single particle trajectory model into a recovery model is carried out through a probabilistic argument based on the random variables of particle charge and initial position.

3.2.2 Model derivation

The potential is related to the charge density by Poisson's Equation:

$$\nabla^2 j = -\frac{r_c}{e_0} \tag{3.1}$$

and the electric field is related to the electric potential as follows:

$$E = -\nabla j \tag{3.2}$$

Based on assumption 7, in a charge-free region between two plates, Equation 3.1 becomes the Laplace Equation in the 2-dimensional space:

$$\frac{\partial^2 j}{\partial x^2} + \frac{\partial^2 j}{\partial y^2} = 0 \tag{3.3}$$

By assumption 6, the second term of the above equation can be dropped since it is much smaller than the first term and the model is simplified to an ODE:

$$d^2 j / dx^2 = 0 \tag{3.4}$$

After scaling $\tilde{x} = x / L\cos q$ and defining $g = d / L\cos q$, which is the ratio of feed gap to plate height, the plate positions were determined as:

$$\tilde{x}_L = -\frac{g}{2} - (1-\tilde{y})tanq, \qquad \tilde{x}_R = \frac{g}{2} + (1-\tilde{y})tanq \tag{3.5}$$

So, the boundary values to Equation (3.4) are:

$$\tilde{j}\big|_{\tilde{x}=\tilde{x}_R} = -1 \ and \ \ \tilde{j}\big|_{\tilde{x}=\tilde{x}_L} = 1 \tag{3.6}$$

The solution to Equations (3.4) (3.6) is

$$\tilde{j} = \frac{-\tilde{x}}{\frac{g}{2} + (1-\tilde{y})tanq} \tag{3.7}$$

and

$$\tilde{E}_x = -\frac{\partial \tilde{j}}{\partial \tilde{x}} = \frac{1}{\frac{g}{2} + (1-\tilde{y})tanq} \tag{3.8}$$

In the *x* direction, by Newton's 2nd law and scaling $\tilde{t} = t / \sqrt{2L\cos q / g}$, we have:

$$\begin{cases} \dfrac{d^2\tilde{x}}{d\tilde{t}^2} = \dfrac{2A}{1 + B\tilde{t}^2} \\ \tilde{x}\big|_{\tilde{t}=0} = \tilde{x}_0 \ and \ \tilde{x}'\big|_{\tilde{t}=0} = 0 \end{cases} \tag{3.9}$$

There are two dimensionless parameters: A= $\left(\frac{2V}{d}q\right)/(mg)$, which is the ratio of electrostatic force to the gravitational force and B= $2tanq / g$, which is the ratio of the gap increment (equals 0 for two parallel plates) at the bottom to the feed gap. The term $1/\left(1 + B\tilde{t}^2\right)$ represents the ratio of the feed gap to the gap at the particle position. The solution to Equation (3.9) is:

$$\tilde{x} = \tilde{x}_0 + 2\frac{A}{B}\left[\sqrt{B}\tilde{t}\ arctan\sqrt{B}\tilde{t} - ln\sqrt{1+B\tilde{t}^{\,2}}\right] \tag{3.10}$$

Since $\tilde{t} = \sqrt{1-\tilde{y}}$, the particle trajectory is

$$\tilde{x} = \tilde{x}_0 + 2\frac{A}{B}\left[\sqrt{B(1-\tilde{y})}\ arctan\sqrt{B(1-\tilde{y})} - ln\sqrt{1+B(1-\tilde{y})}\right] \tag{3.11}$$

and the particle position at the bottom is

$$\tilde{x} = \tilde{x}_0 + 2\frac{A}{B}\left[\sqrt{B}\ arctan\sqrt{B} - ln\sqrt{1+B}\right] \tag{3.12}$$

For two parallel plates (θ=0 and B=0), the particle trajectory is

$$\tilde{x} = \tilde{x}_0 + A(1-\tilde{y}) \tag{3.13}$$

and the particle position at the bottom is

$$\tilde{x} = \tilde{x}_0 + A \tag{3.14}$$

Now that we have the equation for particle position at the bottom as a function of the initial position, particle charge, and electrostatic design variables, the recovery model can be derived, which is presented in the next section.

3.3 The recovery model of the 1-stage and 2-stage free-fall electrostatic separators

One of the objectives of this work is to compare the following design options (Figure 3.3):

(a) 1-stage without recycle

(b) 1-stage with recycle (middling is sent back to the charging device and recharged)

(c) 2-stage with recharge (middling of the 1st stage is sent to the 2nd stage after recharging)

(d) 2-stage without recharge (middling of the 1st stage is sent to the 2nd stage for separation directly)

For this purpose, recovery models need to be derived. The problem is stated as: given a separator, the particle charge distribution and the distribution of the entering position, what would be the recovery of each type of particle in each bin? The particle charge-to-mass ratio q_m is assumed to be normally distributed with mean μ and standard deviation σ and the particle entering position x_0 is assumed to be uniformly distributed within ($-a$, a). Once the recovery model for option (a) is derived, the derivation for option (b) or (c) is straightforward, assuming for option (b), the recycled portion has the same distribution as the fresh feed after recharging and for option (c), the feed to the 2nd stage has the same distribution as the feed to the 1st stage. However, for option (d), the model is more complicated because the feed to the 2nd stage has different distribution from the feed to the 1st stage. Next, the recovery models for design (a) and (d) are derived.

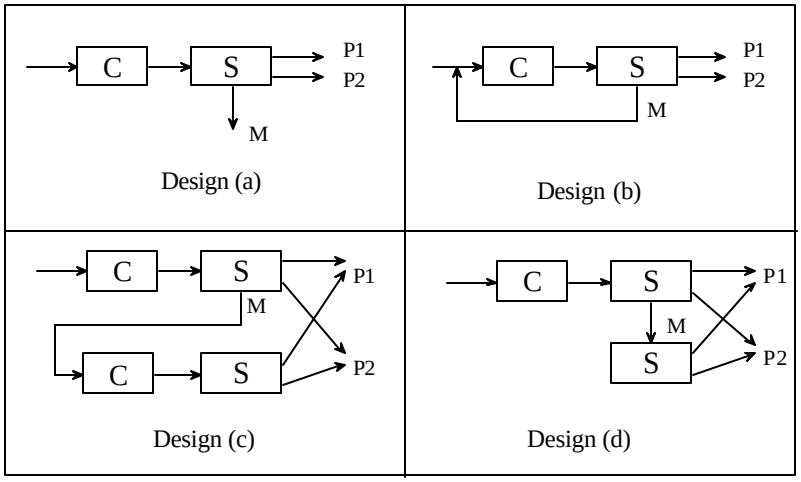

C: Charging device; S: separator; P1, P2: products; M: middling

Figure 3.3 Illustration of four design options

3.3.1 The recovery model for design(a)

The recovery of any type of particles to the left side bin is the probability of the particle position at the bottom being less than b_1, i.e., $Pr\{x < b_1\}$ which is a function of the initial position by Equation (3.12)

$$Pr\left\{x_0 + \frac{2Vq}{mg\ tanq}\left[\sqrt{B}\ arctan\sqrt{B} - ln\sqrt{1+B}\right] < b_1\right\} \tag{3.15}$$

Define

$$M = \begin{cases} \dfrac{1}{\dfrac{2V}{g\ tanq}\left[\sqrt{B}\ arctan\sqrt{B} - ln\sqrt{1+B}\right]}, & q > 0 \\ \dfrac{gd}{2VL}, & q = 0 \end{cases} \tag{3.16}$$

and note that M is always nonnegative, then Equation (3.15) can be written as:

$$r_1 = Pr\{q_m < (b_1 - x_0)M\} \tag{3.17}$$

Similarly, the recovery of any type of particle to the right side bin is the probability of the particle position at the bottom being greater than b_2, i.e.,

$$r_2 = Pr\{q_m > (b_2 - x_0)M\} \tag{3.18}$$

Note that q_m, $(b_1\text{-}x_0)$ and $(b_2\text{-}x_0)$ are all random variables and that only the case for $q_m < (b_1 - x_0)M$ needs to be examined since the other case can be found by subtraction. Assuming particle charge to mass ratio is normally distributed with mean μ and standard deviation σ and the displacement $(b_1 - x_0)$ is uniformly distributed from b_1-a to b_1+a, we have

$$Z = q_m \sim N(m, s) \quad \text{and} \quad Y = (b_1 - x_0) \sim U(b_1 - a, b_1 + a) \tag{3.19}$$

From Figure 3.4, the probability can be computed as:

$$Pr(Z < YM) = F(M) = \int_{b_1-a}^{b_1+a} \int_{-\infty}^{yM} f_{yz}(y,z)\,dz\,dy \tag{3.20}$$

Where f_{yz} is the joint probability density function of Z and Y, which is simply the product of their respective probability density functions since they are independent.

$$f_y = \frac{1}{2a},\ f_z = \frac{1}{\sqrt{2p}\,s} e^{-\frac{1}{2}\left(\frac{z-m}{s}\right)^2} \text{ and } f_{yz} = \frac{1}{2\sqrt{2p}\,as} e^{-\frac{1}{2}\left(\frac{z-m}{s}\right)^2} \tag{3.21}$$

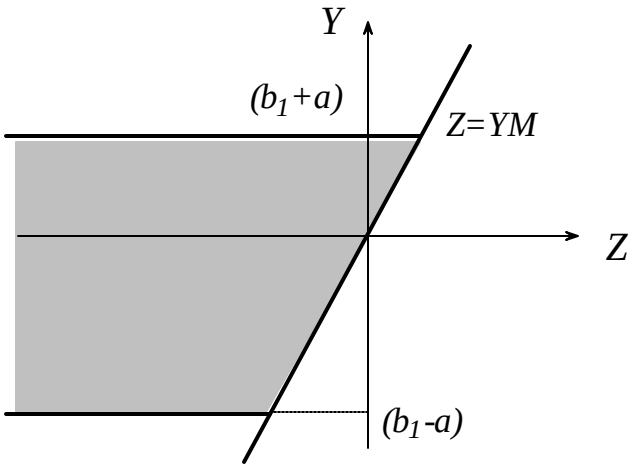

Integrate over the shaded region to obtain *Pr(Z<YM)*

Figure 3.4 The probability of one random variable less than a function of another random variable

The integral gives the recovery to the left side bin:

$$r_{1,l} = \frac{1}{2} + \frac{Y(g_2) - Y(g_1)}{2(g_2 - g_1)} \tag{3.22}$$

the recovery to the right side bin:

$$r_{1,r} = \frac{1}{2} - \frac{Y(g_4) - Y(g_3)}{2(g_4 - g_3)} \tag{3.23}$$

the recovery to the middle bin:

$$r_{1,m} = \frac{Y(g_4) - Y(g_3) - Y(g_2) + Y(g_1)}{2(g_2 - g_1)} \tag{3.24}$$

where

$$g_1 = \frac{M(b_1 - a) - m}{\sqrt{2}s} \qquad g_2 = \frac{M(b_1 + a) - m}{\sqrt{2}s}$$
$$g_3 = \frac{M(b_2 - a) - m}{\sqrt{2}s} \qquad g_4 = \frac{M(b_2 + a) - m}{\sqrt{2}s} \tag{3.25}$$

and

$$Y(x) = x \cdot erf(x) + e^{-x^2} / \sqrt{p} \tag{3.26}$$

3.3.2 The recovery model for design (d)

Before applying the Equation (3.20) to the 2nd stage, the particle charge distribution of the middling from the 1st stage is derived:

$$\frac{\left\{ min\left[max\left(\frac{Z/M_1 - (b_1 - a)}{(b_1 + a) - (b_1 - a)}, 0 \right), 1 \right] - min\left[max\left(\frac{Z/M_1 - (b_2 - a)}{(b_2 + a) - (b_2 - a)}, 0 \right), 1 \right] \right\} \frac{e^{-\frac{1}{2}\left(\frac{Z-m}{s}\right)^2}}{\sqrt{2p}\,s}}{r_{1,m}} \tag{3.27}$$

where $r_{1,m}$ is the recovery to the middle bin at the 1st stage (Equation 3.24).

Since there are three different density regions (I, II and III in Figure 3.5), the recovery integral depends on how the line $Z=YM_2$ intersects the regions. Now let the 2nd stage feeder width be $2c$ and the collection bin positions be d_1 and d_2. And let Z represents the distribution by Equation (3.27) and Y is the uniform distribution within (d_1-c, d_1+c). In Figure 3.5, the three density regions are defined by the Y-values from d_1-c to d_1+c and Z-values in region I from $M_1(b_1\text{-}a)$ to $M_1(b_2\text{-}a)$, region II from $M_1(b_2\text{-}a)$ to $M_1(b_1\text{+}a)$ and region III from $M_1(b_1\text{+}a)$ to $M_1(b_2\text{+}a)$, respectively. The integral for the recovery to the left bin covers the density area at the left hand side of the line $Z=YM_2$. The intersection points of the line $Z=YM_2$ with the top and bottom boundary of the regions have the values ($M_2(d_1\text{-}c)$, d_1-c) and ($M_2(d_1\text{+}c)$, d_1+c). The left intersection point

can be on the bottom boundary of region II, on the bottom boundary of region I or on the left boundary of region I. Similarly, the right intersection point can be on the top boundary of region II, on the top boundary of region III or on the right boundary of region III. Therefore, there are 9 scenarios (i.e., a combination of above 3 by 3 cases). t_1 is defined as the difference of the Z-values of the left intersection point and the left boundary of region I, t_2 as the difference of the Z-values of the left intersection point and the left boundary of region II, t_3 as the difference of the Z-values of the right intersection point and the right boundary of region II and t_4 as the difference of the Z-values of the right intersection point and the right boundary of region III. So, we have the following formulae:

$$t_1 = M_2(d_1 - c) - M_1(b_1 - a) \qquad t_2 = M_2(d_1 - c) - M_1(b_2 - a)$$
$$t_3 = M_2(d_1 + c) - M_1(b_1 + a) \qquad t_4 = M_2(d_1 + c) - M_1(b_2 + a) \tag{3.28}$$

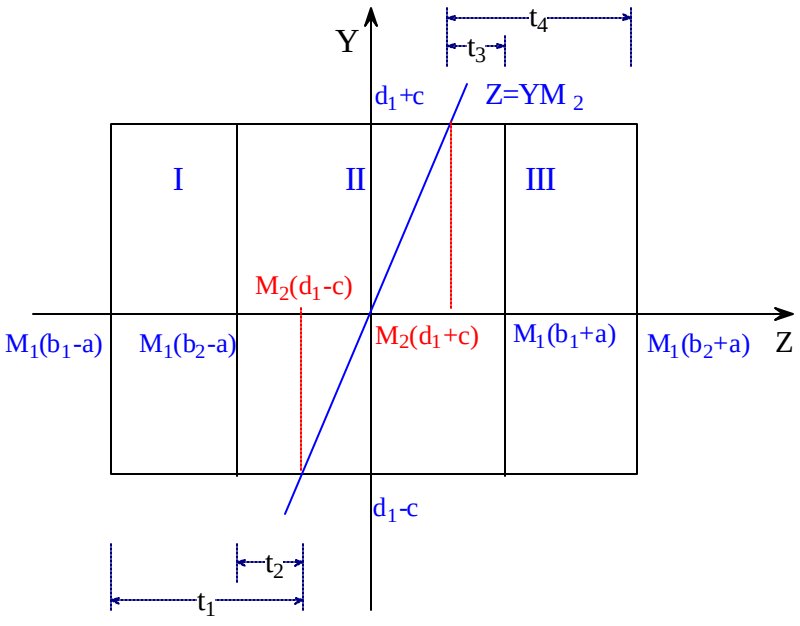

Figure 3.5 Illustration of the intersection of the line $Z=YM_2$ and the three density regions.

The signs of the t values can be used to describe the conditions for the 9 cases (in Table 3.2). For example, positive t_1 and t_2 and negative t_3 and t_4 represent a case that the two intersection points are on the bottom and top boundaries of region II, respectively (case (a)). Similar conditions (different definitions for t_1, t_2, t_3, t_4, just replace d_1+c with d_2+c and d_1-c with d_2-c) can be constructed for the right side bin.

Table 3.2 Conditions for the 9 cases

	t_1	t_2	t_3	t_4
case (a)	+	+	-	-
case (b)	+	-	-	-
case (c)	-	-	-	-
case (d)	+	+	+	-
case (e)	+	-	+	-
case (f)	-	-	+	-
case (g)	+	+	+	+
case (h)	+	-	+	+
case (i)	-	-	+	+

For the first case, we have the following recovery models:

The recovery to the left side bin:

$$\frac{\{(g_3-g_1)[Y(h_2)-Y(h_1)]-(h_2-h_1)[Y(g_3)-Y(g_1)]\}}{2(g_2-g_1)(h_2-h_1)r_{1,m}} \tag{3.29a}$$

The recovery to the right side bin:

$$1-\frac{(g_3-g_1)[Y(h_4)-Y(h_3)]-(h_4-h_3)[Y(g_3)-Y(g_1)]}{2(g_4-g_3)(h_4-h_3)r_{1,m}} \tag{3.29b}$$

where h is defined as below:

$$h_1=\frac{M_2(d_1-c)-m}{\sqrt{2}s} \qquad h_2=\frac{M_2(d_1+c)-m}{\sqrt{2}s} \tag{3.30}$$

$$h_3 = \frac{M_2(d_2 - c) - m}{\sqrt{2}s} \qquad h_4 = \frac{M_2(d_2 + c) - m}{\sqrt{2}s}$$

The complete recovery model for the 2nd stage is shown Table 3.3.

Table 3.3 The recovery models for the 2nd stage (Left side bin)

Case (a)	$\frac{\{(g_3 - g_1)[Y(h_2) - Y(h_1)] - (h_2 - h_1)[Y(g_3) - Y(g_1)]\}}{2(g_2 - g_1)(h_2 - h_1)r_{1,m}}$
Case (b)	$\frac{\{(g_3 - g_1)Y(h_2) + (h_2 - h_1)Y(g_1) + g_1Y(h_1) - h_2Y(g_3) + \frac{erf(h_1) - erf(g_3)}{2}\}}{2(g_2 - g_1)(h_2 - h_1)r_{1,m}}$
Case (c)	$\frac{\{(g_3 - g_1)Y(h_2) + h_2[Y(g_1) - Y(g_3)] + \frac{erf(g_1) - erf(g_3)}{2}\}}{2(g_2 - g_1)(h_2 - h_1)r_{1,m}}$
Case (d)	$\frac{(g_3 - g_1)[Y(h_2) - Y(h_1)] - (h_2 - h_1)[Y(g_3) - Y(g_1)] + g_2Y(h_2) - h_2Y(g_2) + \left[\frac{erf(h_2) - erf(g_2)}{2}\right]}{2(g_2 - g_1)(h_2 - h_1)r_{1,m}}$
Case (e)	$\frac{g_1Y(h_1) - h_2Y(g_3) + g_4Y(h_2) - h_2Y(g_2) + (h_2 - h_1)Y(g_1) + \frac{erf(h_1) - erf(g_2) - erf(g_3) + erf(h_2)}{2}}{2(g_2 - g_1)(h_2 - h_1)r_{1,m}}$
Case (f)	$\frac{h_2Y(g_1) - h_2Y(g_3) + g_4Y(h_2) - h_2Y(g_2) + \frac{erf(g_1) - erf(g_2) - erf(g_3) + erf(h_2)}{2}}{2(g_2 - g_1)(h_2 - h_1)r_{1,m}}$
Case (g)	$\frac{h_2[Y(g_1) - Y(g_2) - Y(g_3) + Y(g_4)] + [h_1Y(g_3) - g_3Y(h_1) + g_1Y(h_1) - h_1Y(g_1)] - \frac{erf(g_2) - erf(g_4)}{2}}{2(g_2 - g_1)(h_2 - h_1)r_{1,m}}$
Case (h)	$\frac{h_2[Y(g_1) - Y(g_2) - Y(g_3) + Y(g_4)] + [g_1Y(h_1) - h_1Y(g_1)] + \frac{erf(h_1) - erf(g_2) - erf(g_3) + erf(g_4)}{2}}{2(g_2 - g_1)(h_2 - h_1)r_{1,m}}$
Case (i)	$\frac{h_2[Y(g_1) - Y(g_2) - Y(g_3) + Y(g_4)] + \frac{erf(g_1) - erf(g_2) - erf(g_3) + erf(g_4)}{2}}{2(g_2 - g_1)(h_2 - h_1)r_{1,m}}$

3.4 Optimizing the designs and operations

For the design of electrostatic separators, the degrees of freedom are:

1) Plate length: L (m)
2) Feed gap between plates: d (m)
3) Plate angle: q
4) Feeder opening: $2a$ (m)
5) Collection bin positions: b_1 and b_2 (m)
6) Voltage: V (V)
7) Plate width: W (m)
8) Recycle rate: R (between 0 and 1, for design (b) only)

The complete optimization model for 1-stage (no recycle) separators is shown in Table 3.4. The cost models and the capacity constraint were developed from industrial data. For the objective function which is the maximization of total profit, the 1st term is the revenue from selling recycled products; the 2nd term represents the annual unit capital cost which is assumed to be a function of plate area LW, and the 3rd term is the operating cost (energy consumption) which is a function of plate area (LW) and the voltage V. For the 3rd constraint, it is assumed that each slice (with width ΔW and gap Δd) of the separator has constant capacity. Therefore the linear relationship of the flowrate and the feed area (Wd) of the separator was developed.

It is easy to modify the model in Table 3.4 for the other design options. For design (b), the feed rate F_0 is replaced by the sum of the fresh feed rate and the flowrate in the recycle, which is the product of the recycle rate and the middling rate. For design (c), the unit capital cost and operating cost are the sum of two separators, respectively; the feed flowrate and composition for the 2nd separator are the same as those in the middling of

the 1st stage, respectively; the charge distribution of the feed to the 2nd stage is the same as that in the 1st stage. For design (d), the objective function is the same as in option (c), except that there is no cost of charging device for the 2nd stage. The feed flowrate, composition and charge distribution are the same as those in the middling of the 1st stage.

Table 3.4 Model for optimizing 1-stage (no recycle) separators

<u>*Objective*</u>:

$$max \quad \left[C_0 F_0 (s^A f_0^A r_1^A + s^B f_0^B r_2^B)\right] - \frac{1}{Depn}\left[C_1 + C_2 \times (WL)^{0.6}\right] - \left[C_0 \times C_4 \times C_3 \times \left(WL\,V^2\right)\right]$$

<u>*Constraints*</u>

1. Recovery model: Equations (3.22) and (3.23)
2. Product purity requirement: ≥ 0.995
3. Upper bound on capacity F_0: $F_0 \leq 5215.8(Wd) - 1055.8$
4. Design specifications:
   - Plate length: $0.9 \leq L \leq 2$
   - Plate gap: $d \geq 0.3$
   - Plate angle: $0 \leq q \leq 15^o$
   - Plate width: $0.6 \leq W \leq 1.5$
   - Ratio of gap to length: $d \leq L/3$
   - Voltage: $V \leq 80$ kV

<u>*Notation*</u>

F_0	Feed rate (kg/hr)
f_0^A, f_0^B	Initial fraction of type A and B plastics in the feed
s^A, s^B	Prices of two types of plastics
r_1^A, r_2^B	Recoveries of type A and B particles to left and right bins, respectively
C_0	Coefficient used to convert the units from hour to year. In this case, it is 1600, based on 8 hrs/day and 200 days/yr
C_1	Fixed investment cost of the unit (=$26,060)
C_2	Coefficient for the variable design cost (=$73,690)
C_3	Coefficient for energy consumption (=4e-9)
C_4	Electricity price (=$0.06/kWh)
Depn	Number of years depreciation (=5 yrs)

The above models were optimized using AMPL, which is a mathematical programming language developed by Fourer et al., (1993) and SNOPT 5.3.4 which is a nonlinear optimization solver developed by Gill, et al., (1997) under various feed flow

rates, charge mean values and standard deviations. The initial feed ratio was chosen as 50/50, and the two types of particles are assumed to have the same absolute value of charge mean and the same standard deviation. Different design options are compared and analyzed below.

- *Parallel v.s diverging plates*

For the various conditions considered in this work, a parallel-plate design is always better than the diverging one (i.e., angle θ=0) since the latter has a weaker electrical field and there are no compensating advantages. However, some industrial designs do use diverging plates to alleviate the rebound of particles after colliding with the walls. The issue was neglected in this work by assuming inelasticity of the walls. Since the angle is usually small in these industrial designs, the angle should not have any influence on the following comparisons of various design options.

- *Influence of particle mean charge and standard deviation on design choices:*

(1) design (a) v.s. design (b) *(the unit is mC/kg for all figures below)*

The profit ratio is a normalized objective value which is defined as the ratio of the objective value of the design to that of the reference design indicated at the caption section of each figure.

From Figure 3.6 (a), the difference is small when the standard deviation is small or high; however, recycling becomes preferable when the standard deviation is in a moderate range. The difference is small at low standard deviation is because the recovery is good and the amount in the recycle is too small to make any significant difference; the difference is small at high standard deviation is because the particles in the middling are

not separable hence recycling does not help to improve the overall recovery. The product prices and feed flowrate do not have much influence on the above conclusion.

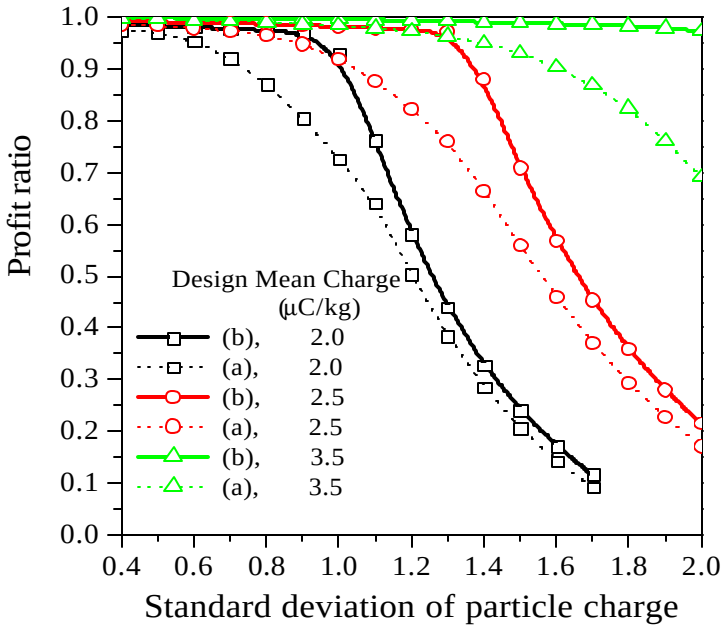

Figure 36 (a) Comparison of design (a) and (b) at feed flowrate 1000 kg/hr and product prices 0.4/0.4 $/kg (The reference design is design (b) at mean charge 3.5 μC/kg and standard deviation 0.4)

From Figure 3.6 (b), the recycle rate is one when the standard deviation is small and then decreases with the standard deviation; as the mean charge increases, the range of the standard deviation at which the recycle rate is one is larger. The recycle rate decreases because the particles in the recycle become more inseparable and the amount of the middling is larger due to the increased number of particles with overlapping charges.

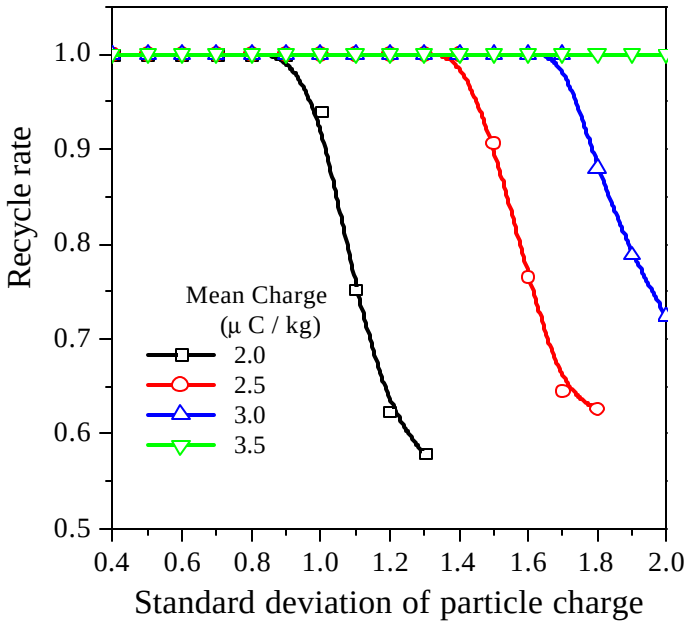

Figure 3.6 (b) Effect of charge mean and standard deviation on the recycle rate at the same condition as in part (a)

(2) design (a) v.s. design (d)

From Figure 3.7(a), 1-stage separation is always better than two-stage separation since the revenue from recovering more particles by adding one more stage is not high enough to cover the cost of the 2nd stage. As the mean charge increases, the objective value is more robust to the variation of the standard deviation of charges (curve becomes flatter). Initially two-stage separation results are the same as one-stage separation because one stage is enough to recover all particles. As the standard deviation of particle charge increases, there is a transition point, where one stage is not enough to recover all particles and the 2nd stage starts to take effect.

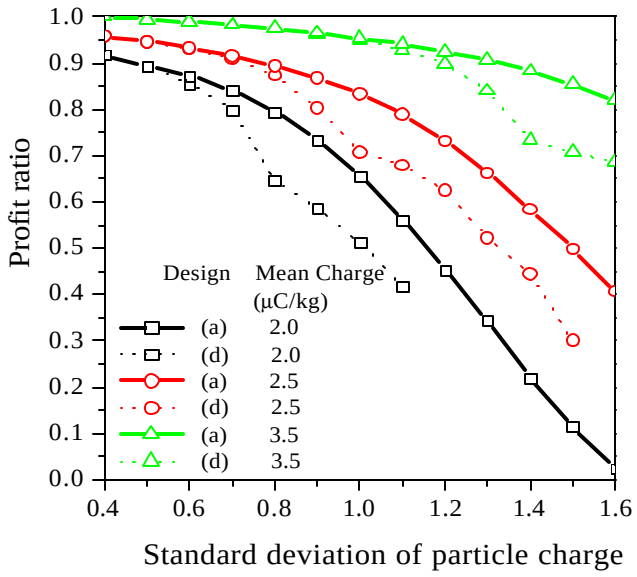

Figure 3.7 (a) Comparison of design (a) and design (d) at feed flowrate 200 kg/hr and product prices 0.4/0.4 $/kg (The reference design is the design (a) at mean charge 3.5 μC/kg and standard deviation 0.4)

Figure 3.7(b) represents a higher feed flowrate. 2-stage separation may be better than 1-stage separation at moderate standard deviation of particle charges. At mean charge 2.0 μC/kg, 2-stage separation is better than 1-stage separation for standard deviation of particle charge between 0.7 and 1.2. The 1st value (0.7) of standard deviation represents a transition at which the revenue from recovered plastics from the 2nd stage just balances the cost of the 2nd stage. At standard deviations lower than this value, the 1-stage separation is better than 2-stage separation because 1-stage can provide enough recovery hence the cost of the 2nd stage exceeds the added revenue. The 2nd value (1.2) of standard deviation represents another transition at which the recovery at the 2nd stage becomes poor and again the revenue from recovered plastics just balances the cost of the 2nd stage.

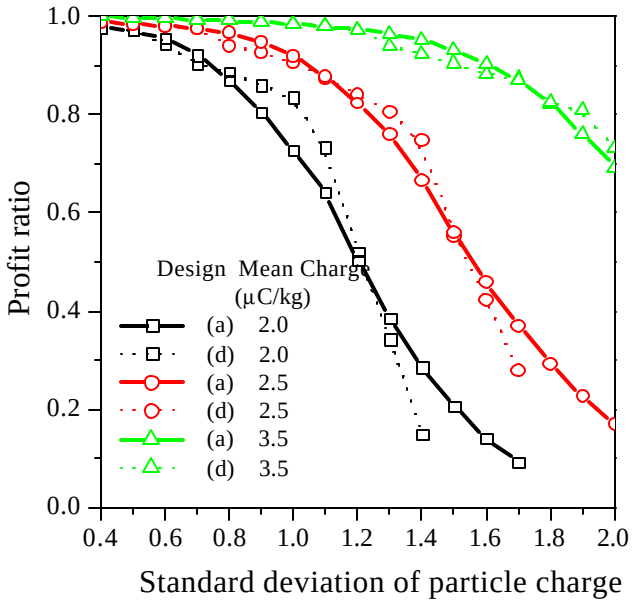

Figure 3.7 (b) Comparison of design (a) and design (d) at feed flowrate 1000 kg/hr and product prices 0.4/0.4 $/kg (the reference design is the design (a) at mean charge 3.5 μC/kg and standard deviation 0.4)

At standard deviations higher than this value, 1-stage separation is better than 2-stage separation because particles fed to the 2nd stage are almost inseparable hence additional stages do not help to improve the overall recovery. As the mean charge increases, the transition points shift towards higher values of standard deviation.

By comparing the fraction of the product rate recovered by each stage of design (d), the relative contribution of each stage to the overall recovery can be seen. From Figure 3.7(c), at high standard deviation of particle charge (>1.5), the 2nd stage recovers more particles than the 1st stage does. At the 2nd stage, with the same voltage, the plates are generally longer or more narrowly separated than the 1st stage, which means a stronger electrical field and longer separation time. This explains why the 2nd stage is able to separate particles from the middling of the 1st stage without recharging them.

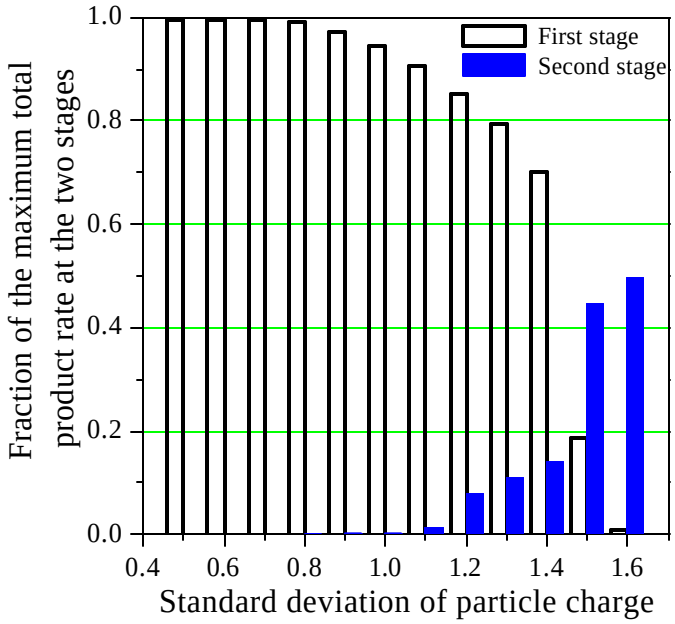

Figure 3.7(c) Product weight recovered by each stage (for design d) at flowrate 1000 kg/hr and product prices 0.4/0.4 $/kg (at mean charge 2.5 μC/kg, the maximum total product rate is 1000 kg/hr)

(3) design (c) v.s. design (d)

From Figure 3.8, at low standard deviation, the two design options provide similar results. If the charging process is expensive, the 2-stage separation without recharging is preferable. As the standard deviation increases, the 2nd stage without recharging is not of much help in separating the particles and 2-stage separation with recharging is better. Therefore, recharging is preferable only at high standard deviation. The product prices and feed flowrate do not have much influence on the above conclusion.

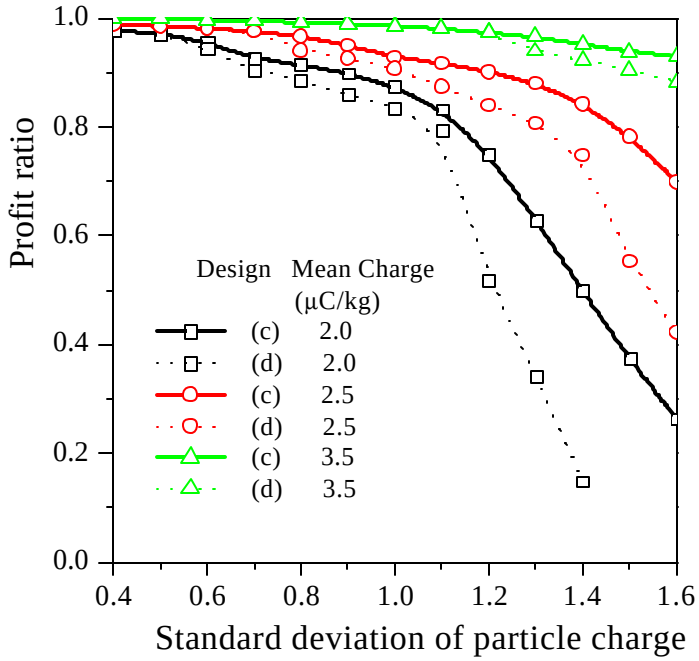

Figure 3.8 Comparison of 2-stage separations (no recharge v.s. recharge) at feed flowrate 1000 kg/hr and product prices 0.4/0.4 $/kg (the reference design is the objective value of design (c) at mean charge 3.5 μC/kg and standard deviation 0.4)

- *A simple guide to the selection of designs under different particle mean charge and standard deviation*

As a summary for the above comparisons, Figure 3.9 provides a general guide for selecting an appropriate design (at high feed flowrate or product prices) under various values of charge mean and standard deviation.

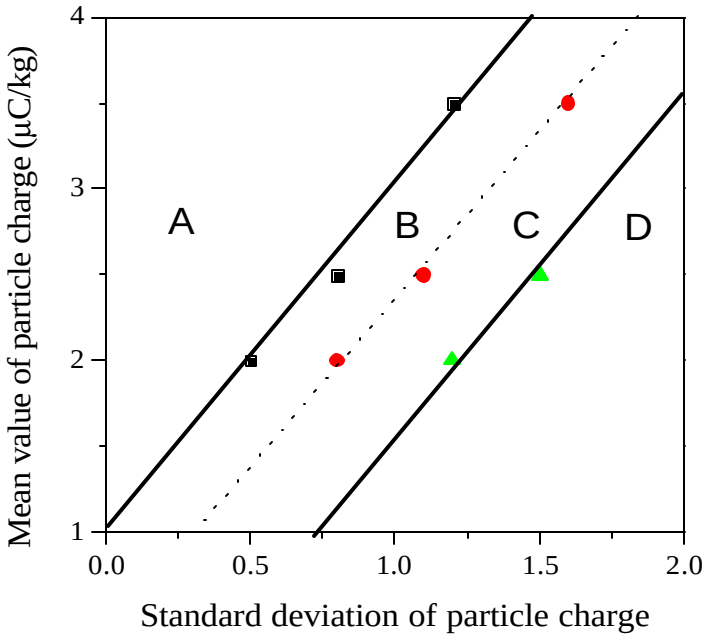

Figure 3.9 Selection guide for choosing an appropriate design
Region A: (a) ≈ (b) ≈ (c) ≈ (d) Region B: (b) > (c) ≈ (d) ≈ (a)
Region C: (b) > (c) > (d) > (a) Region D: (c) > (b) > (a) > (d)

The two-dimensional space is divided into four regions. In region A, where the standard deviation of charge is very low, the four designs provide similar results but design (a) is the cheapest one. In region B where the standard deviation of particle charge is moderately low, recycling becomes helpful to improve the recovery. In region C where the standard deviation is moderate, 2-stage separations are better than 1-stage separation (without recycle), but 1-stage separation with recycle is still the best one. In region D, due to the high standard deviation, recycling is not as efficient as adding a 2nd stage with recharging, therefore design (c) is the best one. The diagram of the best design for each region is also shown in the Figure 3.9. If the flowrate and product prices are both low, 2-

stage separations should not be used and recycling should be used if the standard deviation of particle charges is moderate.

3.5 Conclusions

In this chapter, a general design methodology is presented for free-fall electrostatic separators. First, a trajectory model was derived so that the final position of particles at arbitrary starting locations and with arbitrary low charge can be computed. Second, the recovery models for 4 design options were derived based on probability theory. Finally, optimization models with the objective of maximizing the total profit were proposed and the designs were optimized and compared under various flowrate, charge mean values and standard deviations. Therefore, the models proposed in this chapter can be used to optimize this class of separators and derive information about the separator size, operating conditions such as the voltage and feed flowrate and also whether recycling or a 2^{nd} stage (with or without recharging) is helpful.

It was found that a 2^{nd} stage is preferable at high feed flowrate or product prices and recharging is helpful if the standard deviation of particle charge is not small. At low feed rate or product prices, recycling is preferable at moderate standard deviation. As a summary, a simple guide for selecting an appropriate design was given.

Although this work is based on free-fall separators, the effect of charge mean and standard deviation on the choice of different design may be also applicable to the drum-type separators except that the critical values (for low, moderate and high values of charge mean and standard deviation) might be different. In next chapter, a systematic approach (trajectory modeling and recovery modeling) will be extended to other

trajectory-based separation processes for particles with different densities, sizes, and polarities etc. in various fields (electric or liquid/gas flow etc.).

CHAPTER 4

UNIT MODELING 2

¾ A UNIFIED PROBABILISTIC APPROACH FOR MODELING TRAJECTORY-BASED SEPARATIONS

4.1 Introduction

Mechanical separation of solids is of growing importance in the new domain of recycling processes, for example, the separation of a mix of different plastics (Cui, J. and Forssberg, E., 2002). The differences in various particle properties such as density, size, charge etc are utilized to differentiate them. Unlike the equilibrium-based separations such as distillation and adsorption, the particle trajectory is the ultimate differentiating factor in mechanical separation of solids. However, the trajectory is usually not a constant even for identical particles due to hydrodynamic interactions and random initial conditions. Moreover, there exist distributions of particle properties caused by preprocessing units. For example, the size reduction units such as a shredder or a grinder generate a particle size distribution (Kelly and Spottiswood, 1982) and the charging devices such as a rotating drum or a fluidized bed produce a wide charge distribution (Lowell and Rose-Innes, 1980). Due to the reasons stated above, the separation is usually nonsharp.

The inspiration for many of the recycling separation methods is the mineral processing industry, where mechanical separations are widely used. For many of the mineral processing steps, an S-shaped partition curve (Figure 4.1) is a common

representation of the separation efficiency.

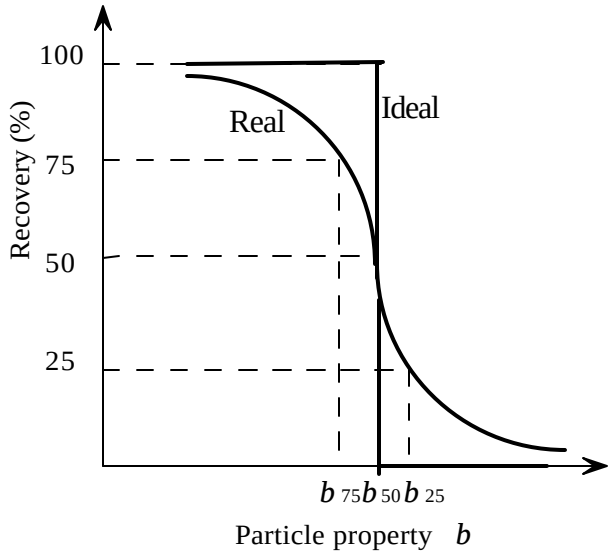

Figure 4.1 Partition curve

While many forms of mathematical functions (Napier-Munn, 1991) have been used to fit the curve, there are usually two parameters: one for the curve position, another for the slope of the curve. For example, the logistic function is of the following form:

$$R = \frac{1}{1 + e^{\frac{1.0986}{Ep}(b - b_{50})}} \tag{4.1}$$

where Ep is the probable error ($= \frac{b_{25} - b_{75}}{2}$), and β_{75}, β_{50}, β_{25} denote the particle properties corresponding to 75%, 50% and 25% recovery, respectively. Therefore, Ep represents the separation efficiency. Various empirical Equations have been proposed for Ep and β_{50} as functions of design and operating variables for different separation methods. Usually the experimental data were obtained by varying the material property, but each

time the property is a constant. In other words, the empirical equation can not be used if the feed material property has a distribution. In such a case, one needs the curve to be represented as a function of the mean value of the property, with the variance information in the Ep value. Such empirical relationships have not been presented in the literature to date and it is the purpose of this work to present a systematic methodology for their construction and use in a design procedure.

If an approach based on first principles is used to develop a model then the usual starting point is to pose and solve differential equations for the concentration profile. For example:

i) for solids sedimentation in liquids: an axial dispersion model for concentration profiles C(t,y):

$$\frac{\partial C}{\partial t} = \frac{\partial}{\partial y}\left(D \frac{\partial C}{\partial y} \right) - \frac{\partial}{\partial y}(vC) \tag{4.2}$$

where D is diffusion coefficient and v is the settling velocity ;

ii) or for the elutriation of fines in gas fluidized beds (Kunii and Levenspiel, 1991): a 1st order ODE for the concentration at the exit

$$\frac{\partial C}{\partial t} = -kC \tag{4.3}$$

where k is a rate constant

iii) or for column flotation (Finch and Dobby, 1990): a combination of them:

$$\frac{\partial C}{\partial t} = \frac{\partial}{\partial y}\left(D \frac{\partial C}{\partial y} \right) - \frac{\partial}{\partial y}(vC) - kC \tag{4.4}$$

When there exists a distribution of particle property, say particle size, individual particles with different sizes would have different settling velocities. Thus even if the diffusion

coefficient can be assumed constant, the concentration profile can not be obtained through solving a single differential equation due to the distribution of settling velocities.

The major reason that causes both approaches (empirical correlations and the differential equations of concentration) fail here is that they are macroscopic methods that do not reveal the real separation mechanisms. It has been shown experimentally that long time behavior of the sedimentation velocity variance is characteristic of a diffusion process (Ham and Homsy, 1988; Nicolai et al.; 1995, Tory, 2000). This can also be verified mathematically through the transformation of a Fokker-Planck Equation to a stochastic differential equation (Laso, 1994). Therefore, the recovery is the probability of the stochastic particle trajectories reaching a certain separation boundary. Thus, situations where distributions of particle properties and hydrodynamic interactions coexist can be modeled. To demonstrate this, several different applications will be presented in the next few sections.

Another objective of this work is to build a connection between the partition curve model (Equation 4.1) and the recovery model derived from probabilistic considerations. Recovery models for different separation methods have various formats. However, the partition curve model has a general form. Thus, if explicit relationships of Ep and β_{50} with the random variables as well as other deterministic design and operating variables can be determined from the probabilistic approach, we can easily find which parameters should be adjusted to achieve the required separation efficiency.

4.2 A Motivating Example (sedimentation in sink-float tank)

In this section, the particle sedimentation in a sink-float tank (Figure 4.2) in which

the particle size distribution and hydrodynamic diffusion cause the particle trajectories to exhibit random perturbations. The separation is mainly based on the difference of particle density, however, particle size also has an influence on the settling velocity. It is assumed that particles that do not settle below the separation boundary Hc, within residence time τ, will report to the overflow.

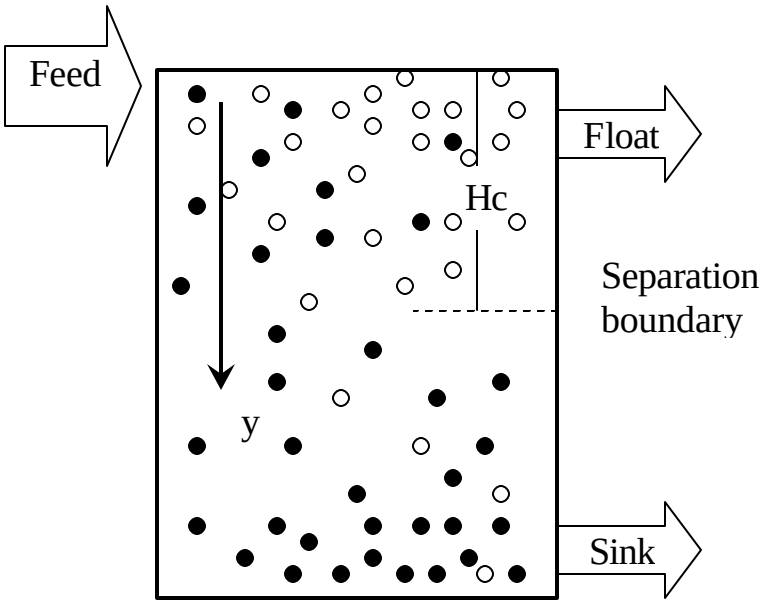

Sink-Float Tank

Figure 4.2 Schematic of a sink-float tank

Consider a case where the particle size is normally distributed with mean m_{dp} and standard deviation s_{dp}. It is assumed that particles are spherical, diffusion coefficient D is a constant and particles quickly reach their terminal velocity. Also assume the flow is in the turbulent region (drag coefficient C_d=0.44), so we have for the terminal velocity

$$v_\infty = b\sqrt{3.03gm_{dp}} \tag{4.5}$$

$$b = sign\left(r_p - r_l\right)\sqrt{\left|\frac{r_p - r_l}{r_l}\right|} \tag{4.6}$$

where $sign(x) = \begin{cases} 1, & if\ x \geq 0 \\ -1, & if\ x < 0 \end{cases}$, ρ_p and ρ_l are solid and liquid densities, respectively.

One can start from the view at the particle level and describe the system using stochastic differential equations. It has been shown that the sedimentation process is a Markov process that is the solution of the following stochastic differential equation (SDE) (Tory, 2000):

$$dY_t = v_\infty dt + BdW_t \tag{4.7}$$

where Y_t is the particle vertical position at time t, $D = B^T B$ and W is a vector of independent Wiener processes. The Wiener process is a continuous-time stochastic process for $t \geq 0$ with W(0)=0 and such that the increment W(t)-W(s) is Gaussian with mean 0 and variance (t-s) for any $0 \leq s < t$, and increments for non-overlapping time intervals are independent. Brownian Motion is the most common example of a Wiener process. The 1st term on the right hand side of equation (4.7) describes a deterministic settling of a particle in a infinite dilute suspension and the 2nd term accounts for the velocity fluctuations caused by particle-particle interactions. Each particle moves independently, in each time step, according to the stochastic process defined by equation (4.7).

The SDE can be solved by discretizing the time τ into N intervals (each Δt) and the space variable

$$Y(t + \Delta t) = Y(t) + v_\infty \Delta t + \sqrt{2D\Delta t}\, y \tag{4.8}$$

where ψ is a random number from the standard normal distribution N(0,1). Since,

$\sum \Delta t = \tau$, $\sum \psi \sim N\left(0, \sqrt{N}\right)$, $\sqrt{2D\Delta t}\sum \psi \sim N\left(0, \sqrt{2D\tau}\right)$, after adding a series of equation (4.8) from Y(0) to Y(τ), and assuming Y(0)=0, we have

$$Y(t) \sim N(v_\infty t, \sqrt{2Dt}) \tag{4.9a}$$

or

$$v = Y/t \sim N(v_\infty, \sqrt{2D/t}) \tag{4.9b}$$

Thus, the diffusion process corresponds to a stochastic process with mean velocity v_∞ and standard deviation $\sqrt{2D/t}$.

The relationship in (4.9a) is a trajectory model that can be used to derive the recovery model. The recovery is simply the probability of particles whose final vertical positions Y(τ) are no larger than the separation boundary position Hc:

$Pr\{Y \le Hc\} = Pr\left\{b\sqrt{3.03 g m_{dp}}t + B \le Hc\right\}$, where $B \sim N\left(0, \sqrt{2D\tau}\right)$

For simplicity, it is assumed that particle size dp only has an influence on the mean settling velocity but not on the variance of velocity (i.e., D is independent of dp), therefore, the distributions of particle size dp and B are independent. The recovery is a joint probability:

$$R = \int_0^\infty \int_{-\infty}^{Hc - bt\sqrt{3.03 g m_{dp}}} \left(\frac{e^{-\frac{1}{2}\left(\frac{B}{\sqrt{2Dt}}\right)^2}}{\sqrt{2p}\sqrt{2Dt}} \frac{e^{-\frac{1}{2}\left(\frac{d_p - m_{dp}}{s_{dp}}\right)^2}}{\sqrt{2p}\, s_{dp}} \right) dB dd_p \tag{4.10}$$

It is impossible to derive an analytical formula for the joint probability. Therefore, a numerical calculation of (4.10) was performed to generate Ep data to fit the following empirical model:

$$Ep = Ep_1 + Ep_2 - \frac{c_{12}}{\left(1+\frac{a_{12}}{Ep_1}\right)\left(1+\frac{b_{12}}{Ep_2}\right)} \tag{4.11}$$

where a_{12}, b_{12} and c_{12} are constants, and Ep_1 and Ep_2 are the Ep values of cases where only the 1st random variable (velocity) or the 2nd random variable (size) exists, respectively.

This form of the model is chosen because it satisfies the general requirements:

(i) $Ep \rightarrow Ep_2$, as $Ep_1 \rightarrow 0$,

(ii) $Ep \rightarrow Ep_1$, as $Ep_2 \rightarrow 0$,

There might be some other forms that also satisfy the above requirements, for example:

$$Ep = Ep_1 + Ep_2 - a_{12} Ep_1^{b_{12}} Ep_2^{c_{12}} \tag{4.12}$$

However, practical calculations in a number of applications indicated that this form is worse than the one in (4.12).

Next, the expressions for Ep_1 and Ep_2 are derived, respectively.

(i) For Ep_1: only velocity distribution, constant particle size

From Equation (4.9), we have

$$R = Pr\{Y \le Hc\} = \frac{1}{2}\left[1 + erf\left(\frac{Hc/t - v_\infty}{\sqrt{2}\sqrt{2D/t}}\right)\right] \tag{4.13}$$

To find the expressions for Ep and β_{50} from (4.13),

let R=0.5, 0.75 and 0.25, we have

$\frac{Hc/t - v_\infty}{\sqrt{2}\sqrt{2D/t}} = 0$, $\frac{Hc/t - v_\infty}{\sqrt{2}\sqrt{2D/t}} = 0.4769$, $\frac{Hc/t - v_\infty}{\sqrt{2}\sqrt{2D/t}} = -0.4769$, respectively

From (4.5), we have

$$b_{50} = \frac{Hc/t}{\sqrt{3.03gm_{dp}}} \tag{4.14}$$

$$b_{75} = -\frac{0.6745\sqrt{2D/t}}{\sqrt{3.03gm_{dp}}} + \frac{Hc/t}{\sqrt{3.03gm_{dp}}} \tag{4.15}$$

$$b_{25} = \frac{0.6745\sqrt{2D/t}}{\sqrt{3.03gm_{dp}}} + \frac{Hc/t}{\sqrt{3.03gm_{dp}}} \tag{4.16}$$

Hence,

$$Ep_1 = \frac{b_{25} - b_{75}}{2} = \frac{0.6745\sqrt{2D/t}}{\sqrt{3.03gm_{dp}}} \tag{4.17}$$

(ii) For Ep_2: Only size distribution, no velocity distribution

$$R = \frac{1}{2}\left[1 + erf\left(\frac{\frac{Hc^2}{3.03gt^2b^2} - m_{dp}}{\sqrt{2}s_{dp}}\right)\right] \tag{4.18}$$

With a similar procedure in i), we have

$$Ep_2 = \frac{Hc\left(\sqrt{m_{dp} + 0.6745s_{dp}} - \sqrt{m_{dp} - 0.6745s_{dp}}\right)}{2t\sqrt{3.03g}\sqrt{m_{dp}^2 - 0.455s_{dp}^2}} \tag{4.19}$$

With expressions for Ep_1 and Ep_2, we are now ready to fit the Ep values to the model (4.12). Values of design variables (Hc, τ) and distribution parameters (D, μ_{dp}, σ_{dp}) are varied within the ranges shown in Table 4.1 to obtain a number of Ep values.

The least square method is used and the values of the coefficients are a_{12}= 0.1446, b_{12}=0.0387, c_{12}=0.1866, with root mean squared error (RMSE) = 0.0029 and relative root

mean squared error (RRMSE)=3.03%.

Table 4.1. Ranges of parameter and variable values in regression for sink-float separation

Hc (m)	0.1 ~ 2.0	D (m^2/s)	0.002 ~ 0.2
τ (s)	1 ~ 60	μ_{dp} (m)	0.004 ~ 0.015
		σ_{dp} (m)	0.001 ~ 0.004

So, we have obtained a recovery model (4.1, 4.11, 4.14, 4.17, 4.19) for solids sedimentation in a sink-float tank.

4.3 A Unified Probabilistic Approach for Trajectory-based Separations

The unified probabilistic modeling approach is a microscopic view of the separation problem in which the nonsharpness is caused by random effects, especially the particle properties, represented as random variables with known distributions. The motivating example above clearly indicates a three-step approach:

1) Modeling the single-particle trajectory based on a force balance and other first principles modeling
2) Modeling the recovery based on a probability calculation
3) Deriving expressions for Ep and β_{50} for the partition curve model.

Often obtaining an analytical solution of the particle trajectory and/or an analytical formula for the probability integral is not possible. In this case, a numerical solution of the differential equation and/or a numerical integration is necessary.

β_{50} can be derived from the corresponding deterministic case. For the Ep value, when one only has numerical solutions of the probability integral, one can use the

following empirical model:

$$
\begin{aligned}
Ep = {} & Ep_1 + Ep_2 + \cdots Ep_n \\
& - \sum_{i_1 < i_2} \sum \frac{c_{i_1 i_2}}{\left(1 + \frac{a_{i_1 i_2}}{Ep_{i1}}\right)\left(1 + \frac{b_{i_1 i_2}}{Ep_{i_2}}\right)} \\
& - \sum_{j_1 < j_2 < j_3} \sum\sum \frac{g_{j_1 j_2 j_3}}{\left(1 + \frac{d_{j_1 j_2 j_3}}{Ep_{j_1}}\right)\left(1 + \frac{e_{j_1 j_2 j_3}}{Ep_{j_2}}\right)\left(1 + \frac{f_{j_1 j_2 j_3}}{Ep_{j_3}}\right)} \\
& - \cdots \\
& - \sum_{k_1 < k_2 < \cdots < k_n} \sum\sum\cdots\sum \frac{s_{k_1 k_2 \cdots k_n}}{\left(1 + \frac{p_{k_1 k_2 \cdots k_n}}{Ep_{k_1}}\right)\left(1 + \frac{q_{k_1 k_2 \cdots k_n}}{Ep_{k_2}}\right)\cdots\left(1 + \frac{r_{k_1 k_2 \cdots k_n}}{Ep_{k_n}}\right)}
\end{aligned}
\tag{4.20}
$$

where Ep_i is the Ep value when only the i-th random variable exists and $a_{i_1 i_2}, b_{i_1 i_2}, c_{i_1 i_2}, d_{j_1 j_2 j_3}, e_{j_1 j_2 j_3}, f_{j_1 j_2 j_3}, g_{j_1 j_2 j_3}, \cdots, p_{k_1 k_2 \cdots k_n}, q_{k_1 k_2 \cdots k_n}, \cdots, r_{k_1 k_2 \cdots k_n}$, $s_{k_1 k_2 \cdots k_n}$ are correlation parameters. While some other forms might be simpler with fewer number of parameters, this form does provide some convenience. With equation (4.20) in which the overall Ep value is broken down into a function of individual Ep models which are much easier to find, one does not need to worry about what form of the empirical model should be used. Also note that, if any random variable K becomes deterministic (i.e., Ep_K is zero), any terms containing Ep_K vanish and the model is reduced to a case with (n-1) random variables. Therefore, instead of fitting the whole lot at once, the parameters can actually be found by a multi-stage approach: first determine the values of $a_{i_1 i_2}, b_{i_1 i_2}, c_{i_1 i_2}$ by only allowing two random variables to exist, second,

determine the values of $d_{j_1 j_2 j_3}, e_{j_1 j_2 j_3}, f_{j_1 j_2 j_3}, g_{j_1 j_2 j_3}$ by allowing three random variables to exist, and so on. For example, with 3 random variables, the model looks like:

$$Ep = Ep_1 + Ep_2 + Ep_3 - \frac{c_{12}}{\left(1+\frac{a_{12}}{Ep_1}\right)\left(1+\frac{b_{12}}{Ep_2}\right)} - \frac{c_{13}}{\left(1+\frac{a_{13}}{Ep_2}\right)\left(1+\frac{b_{13}}{Ep_3}\right)} - \frac{c_{23}}{\left(1+\frac{a_{23}}{Ep_1}\right)\left(1+\frac{b_{23}}{Ep_3}\right)} - \frac{g_{123}}{\left(1+\frac{d_{123}}{Ep_1}\right)\left(1+\frac{e_{123}}{Ep_2}\right)\left(1+\frac{f_{123}}{Ep_3}\right)} \tag{4.21}$$

Note that when the any one of the 3 random variables becomes deterministic, the model (4.21) is reduced to the model (4.12). Therefore, the parameter values of a_{12}, b_{12}, c_{12} can be found by fixing the 3rd random variable to a constant, and similarly for a_{23}, b_{23}, c_{23} and a_{13}, b_{13}, c_{13} by fixing the 1st and 2nd random variable, respectively. After finding the values of all a_{ij}, b_{ij}, c_{ij} (i<j), the parameters $d_{123}, e_{123}, f_{123}, g_{123}$ can be found from the case with all 3 random variables. A diagram of the three-step unified probabilistic approach is shown in Figure 4.3.

While the description of the approach is simple, it can be applied to many other physical separation problems, as described in the next section.

4.4 Applications

The first example here shows that the first order equation (4.3), which is applied in some cases where a series of discrete events happen, can be arrived at through a probability calculation.

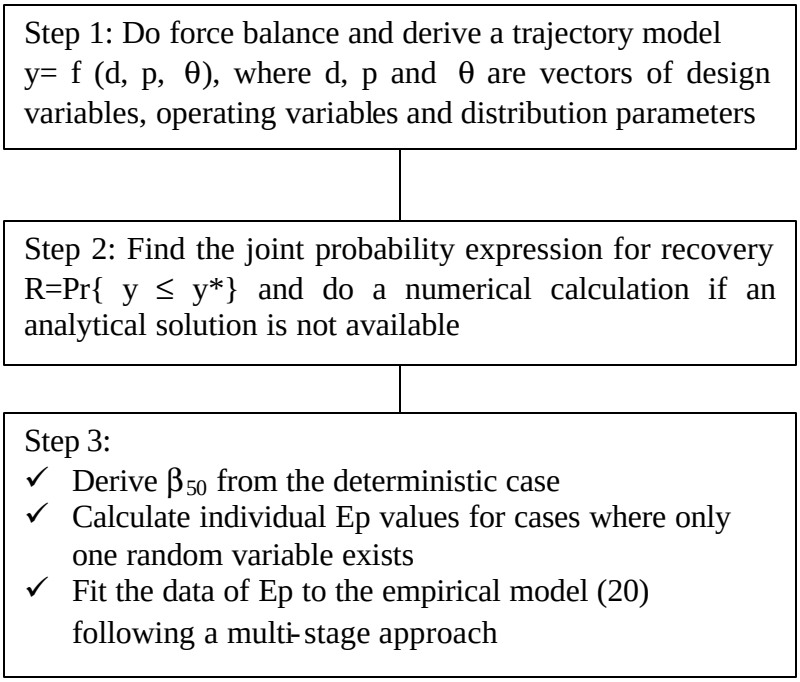

Figure 4.3 Diagram of the three-step approach

4.4.1 **Elutriation in gas fluidized beds**

A fluidized bed usually has two zones (Kunii and Levenspiel, 1991): a dense bubbling phase and a dispersed phase. Solids carried in the bubble wake are partly thrown into the freeboard.

It is assumed that the probability of the particle being caught in a bubble wake is p, the probability of staying in the bed within time t (not caught in any bubble wake) is a binomial distribution, i.e., exactly 0 success out of N Bernoulli trials $(1-p)^N$. Hence the probability of the particle entrained to the freeboard is the probability of being caught in at least one bubble wake:

$$R = 1-(1-p)^N \tag{4.22}$$

It is known that as N→ ∞, $\lim_{N\to\infty}(1-p)^N = e^{-pN}$. The above can be approximated by a Poisson process:

$$R = 1 - e^{-pN} \tag{4.23}$$

The number of trials N is the total number of bubble burstings within time t:

$$N = N_b A t \tag{4.24}$$

where N_b is the bubble bursting rate (i.e., number of bursts per unit time per unit area), A is the cross-sectional area of the bed. N_b can be computed from:

$$N_b = \frac{g(u_0 - u_{mf})}{(1-f_w)V_b} \tag{4.25}$$

where u_0 is the superficial gas velocity and u_{mf} is the minimum fluidization velocity, f_w is the fraction of the wake volume in a bubble, V_b is the bubble volume and γ is a function of Archimedes number. Assume the value of probability p is the ratio of the wake volume that is actually effective in throwing particles (V_{mw}) to the bed volume (V_{bed}): $p = V_{mw} / V_{bed}$. We then have

$$R = 1 - e^{-\frac{g\, f_{mw}(u_0 - u_{mf})}{H_{mf}(1-f_w)}t} \tag{4.26}$$

where $f_{mw} = V_{mw}/V_b$, $H_{mf} = V_{bed}/A$. This is exactly the same as in Smolders (1997) where the derivation is based on the first order equation (4.3) (Leva, 1951).

If we view the entrainment of particles to the freeboard as a trajectory with two discrete values, the above derivation is another example of the unified probabilistic approach.

4.4.2 Froth flotation

The objective of this example is to show an application with 3 random variables. The schematic of a flotation tank is similar to the sink-float tank shown in Figure 4.2 except that there is a third phase (bubbles) and particles are fed from the lower section of the tank. Froth flotation is based on the difference of particle wettability: hydrophobic particles have a higher probability of reporting to the overflow. Froth flotation of large particles is believed to be different from that of small particles (Shen et al., 2001). In the former, for example, the flotation of plastics (Shen et al., 1999), more than one bubble attach to a large particle hence the flotation of particle depends on the aggregate density, while, in the latter, small particles attach to one bubble hence the floatability is irrespective of the density or size of the particles.

In this work, the first case, flotation of large particles, is studied. Shen et al. (2001) proposed a model for the particle-bubble aggregate density ρ_{pb}:

$$\frac{r_{pb}}{r_p} = \frac{1.59}{1.59 + 4K\dfrac{d_b}{d_p}} \tag{4.27}$$

where ρ_p is the particle density, d_b and d_p are bubble diameter and particle diameter, respectively and K is the bubble coverage percentage of the particle surface.

The behavior of the particle-bubble aggregates is the similar to the particle sedimentation in the sink-float tank. Due to the various uncertainties such as conditioning and particle-bubble collisions, it is highly unlikely for particles of the same size to carry exactly the same number of bubbles, therefore, the parameter K is a random variable. Therefore three random variables are considered in this application:

1) random velocity $v \sim N(v_\infty, s_v)$, where $s_v = \sqrt{2D/t}$

2) bubble coverage $K \sim N(m_K, s_K)$

3) particle diameter $d_p \sim N(m_{dp}, s_{dp})$

The trajectory model is similar to the one for sedimentation:

$$Y = sign(r_l - r_{pb})\sqrt{3.03 g d_p \left|\frac{r_l - r_{pb}}{r_l}\right|}t + B \tag{4.28}$$

where B is a random variable with normal distribution $N(0, \sqrt{2Dt})$, and the origin of the Y axis starts from the tank bottom and the direction is upwards.

Let $b = m_K$. It is easy to show that:

$$b_{50} = \frac{1.59}{4}\frac{m_{dp}}{d_b}\left(\frac{r_p / r_l}{1 - \frac{Hc^2 / t^2}{3.03 g m_{dp}}} - 1\right) \tag{4.29}$$

An analytical solution for Ep can not be found, hence the empirical model in equation (4.21) is used.

First the individual Ep values are determined.

(i) For Ep1: (only velocity distribution)

$$Ep_1 = \frac{1.59}{8}\frac{m_{dp}}{d_b}\left(\frac{r_p / r_l}{1 - \frac{\left(Hc + 0.6745\sqrt{2Dt}\right)^2 / t^2}{3.03 g m_{dp}}} - \frac{r_p / r_l}{1 - \frac{\left(Hc - 0.6745\sqrt{2Dt}\right)^2 / t^2}{3.03 g m_{dp}}}\right) \tag{4.30}$$

(ii) For Ep2: (only K distribution)

$$Ep_2 = 0.6745 s_K \tag{4.31}$$

(iii) For Ep3: (only dp distribution)

$$Ep_3 = \frac{b_{75} - b_{25}}{2} \tag{4.32}$$

where

$$b_{75} = \frac{1.59}{4}\left[\frac{r_p / r_l}{1 - \dfrac{(Hc/t)^2}{3.03g\left(m_{dp} + 0.6745 s_{dp}\right)}} - 1\right]\frac{\left(m_{dp} + 0.6745 s_{dp}\right)}{d_b} \tag{4.33}$$

$$b_{25} = \frac{1.59}{4}\left[\frac{r_p / r_l}{1 - \dfrac{(Hc/t)^2}{3.03g\left(m_{dp} - 0.6745 s_{dp}\right)}} - 1\right]\frac{\left(m_{dp} - 0.6745 s_{dp}\right)}{d_b} \tag{4.34}$$

Ranges of design and operating variables (Hc, τ, d_b) and distribution parameters (D, μ_{dp}, σ_{dp}, μ_K and σ_K) are in Table 4.2. Following a 2-stage regression approach described in the previous section, the following result is obtained: the parameter values are in Table 4.3, the RMSE is 0.015 and the RRMSE is 3.7%.

Table 4.2 Ranges of variables and parameters values in regression for froth flotation

H_c (m)	0.4 ~ 2.0	μ_{dp} (m)	0.002 ~ 0.015
τ (s)	1 ~ 30	σ_{dp} (m)	0.0005~0.003
d_b (m)	0.001 ~ 0.005	μ_K	0.15 ~ 0.95
		σ_K	0.02 ~ 0.2
		D (m^2/s)	0.1 ~ 5.0

Table 4.3 Values of model parameters in equation (4.21)

A_{12}	0.0018	a_{13}	0.0000	a_{23}	0.1679	d_{123}	6.9838
B_{12}	0.4802	b_{13}	6.4745	b_{23}	0.3583	e_{123}	0.0593
C_{12}	0.5524	c_{13}	5.7021	c_{23}	1.7663	f_{123}	0.0856
						g_{123}	10.6837

The partition curves (recovery v.s. mean bubble coverage) at different particle size distributions are shown in Figure 4.4. Apparently, with the same bubble coverage, it is easier to float smaller particles. While it is impossible to find experimental data in literature to prove our model, Figure 4.5(a) and (b), which show the influence of particle size and flotation time on the recovery, are qualitatively consistent with Figure 7 and Figure 10 in Shen et al. (2001).

4.4.3 Electrostatic separation

The purpose of this example is to illustrate separation by using an electrical field. Electrostatic separation is based on the difference of particle charges, hence can be used for particles with overlapping densities. Two types of separators are considered: free-fall separators are usually used in laboratories and drum-type separators, which have larger throughput, are used industrially. In both cases, the drag force (valid for large particles in air), inter-particle collisions and influence of particle charges on the electric field are neglected.

(a) Free-fall separators (Wei and Realff, 2003 (a))

In the previous chapter, we have derived an analytical solution for the particle horizontal position at the bottom x:

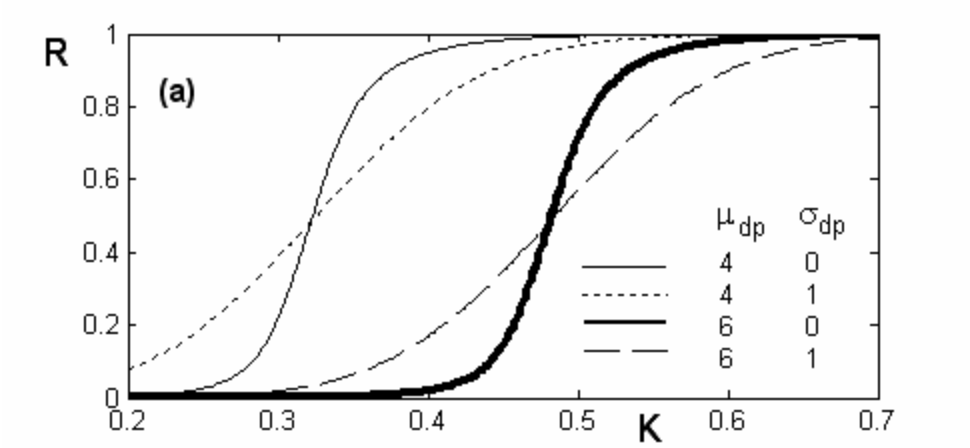

Figure 4.4 Partition curve for froth flotation (μ_{dp} and σ_{dp} are in mm)

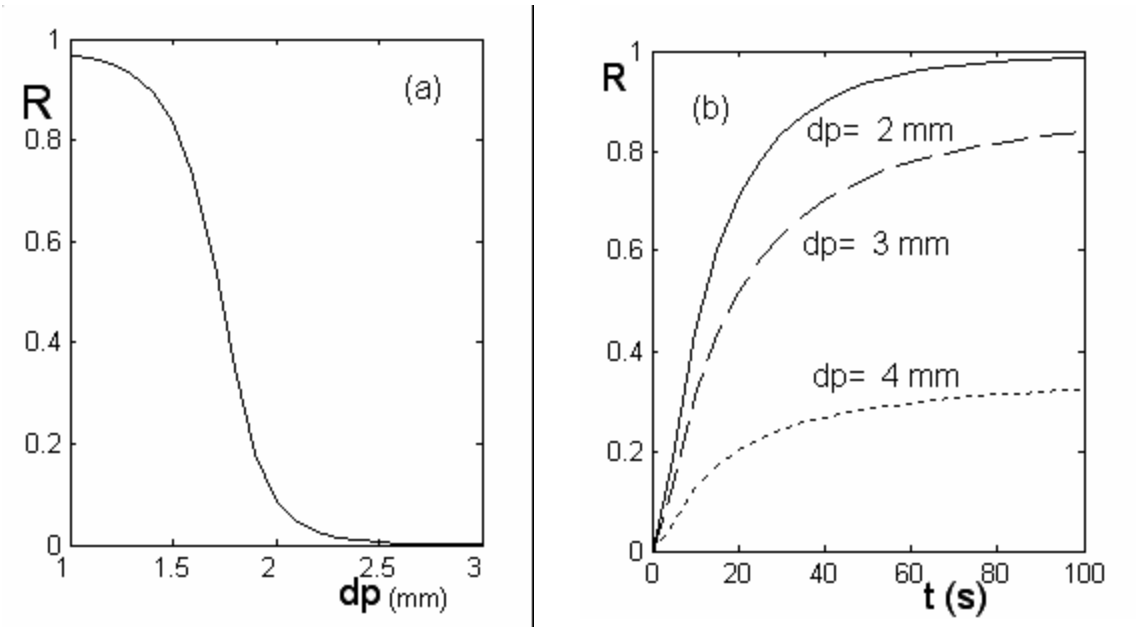

Figure 4.5 Influence of (a) particle size and (b) flotation time on recovery

$$x = x_0 + 2\frac{A}{B}\left[\sqrt{B}\,arctan\sqrt{B} - ln\sqrt{1+B}\right] \tag{4.35}$$

where $A = \left(\frac{2V}{d} q_m\right) / g$ and $B = 2\,tanq / d$, x_0 is the initial position, and q_m is the particle charge-to-mass ratio.

An analytical recovery model has also been obtained:

$$r_{1,I} = \frac{1}{2} + \frac{Y(g_2) - Y(g_1)}{2(g_2 - g_1)} \tag{4.36}$$

where

$$g_1 = \frac{M(b_1 - a) - m}{\sqrt{2}s}, g_2 = \frac{M(b_1 + a) - m}{\sqrt{2}s} \tag{4.37}$$

$$M = \begin{cases} \dfrac{1}{\dfrac{2V}{g\tan q}\left[\sqrt{B}\arctan\sqrt{B} - \ln\sqrt{1+B}\right]}, & q > 0 \\ \dfrac{gd}{2VL}, & q = 0 \end{cases} \tag{4.38}$$

and

$$\Psi(x) = x \cdot erf(x) + \frac{1}{\sqrt{p}} e^{-x^2} \tag{4.39}$$

The Ep and cut charge for partition curve (recovery v.s. mean charge-to-mass ratio) is:

$$Ep = 0.5Ma + 0.6745s_q - \frac{2.8725}{\left(1 + \frac{1.0513}{Ma}\right)\left(1 + \frac{2.3784}{s_q}\right)} \tag{4.40}$$

$$q_{50} = Mb_1 \tag{4.41}$$

with RMSE = 0.0316, RRMSE=2.33%.

And the ranges of design and operating variables (M and a) and distribution parameter σ_q are in Table 4.4:

Table 4.4. Ranges of variables and parameters values in regression for free-fall electrostatic separations

M ($\mu C \cdot kg^{-1} \cdot m^{-1}$)	1 ~ 50
a (m)	0 ~ 0.2
σ_q ($\mu C \cdot kg^{-1}$)	0.01 ~ 4.5

(b) Drum-type separators (Wei and Realff, 2003 (b))

Figure 4.6 is a schematic of a drum-type separator without the tribo-electrification part. It usually consists of a rotating drum (partly charged with high voltage) and an outer plate (either straight or with some curvature, also charged with high voltage). Particles are transported on a belt or dropped directly from above the rotating drum. Particles detach from the drum surface if the sum of forces (gravitational, centrifugal and electrostatic forces) is positive in the radial direction (i.e., outwards). Therefore, particles that are attracted by the outer plate detach earlier and their final positions are further from the drum.

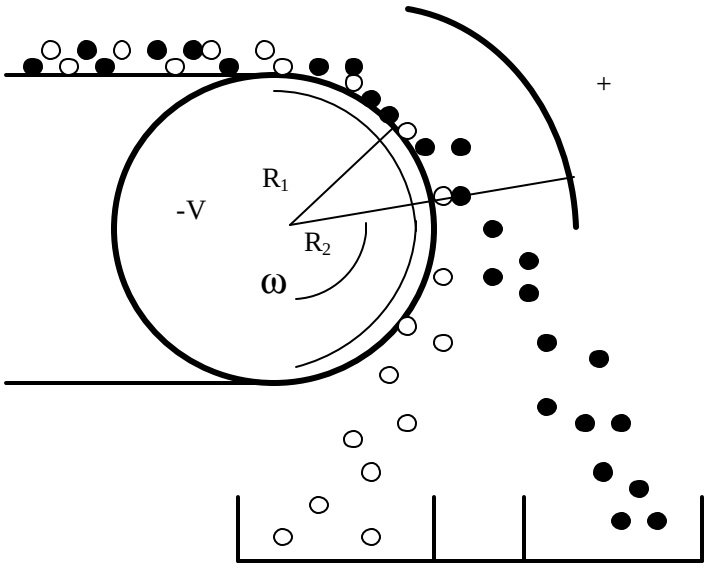

Figure 4.6 Schematic of drum-type electrostatic separators

The only random variable is then the charge-to-mass ratio. Only numerical solutions can be obtained from a system of 2-dimensional 2nd order non-linear ODEs. The following empirical trajectory model has been obtained:

$$\tilde{x}_b = b_4 e^{b_1\tilde{x}_1 + b_2\tilde{x}_2 + b_3\tilde{x}_3} + b_5 \tag{4.42}$$

where b_1 to b_5 are model parameters and

$$\tilde{x}_1 = \frac{-2Vq_m}{R_1 g\, ln(R_2 / R_1)} \tag{4.43}$$

Which is the ratio of electrostatic force to gravitational force

$$\tilde{x}_2 = w^2 R_1 / g \tag{4.44}$$

Which is the ratio of centrifugal force to gravitational force

$$\tilde{x}_3 = y_c / R_1 \tag{4.45}$$

Which is dimensionless height of the collection bin

$$\tilde{x}_b = x_b / R_1 \tag{4.46}$$

Which is dimensionless particle horizontal position

where ω is the drum angular velocity. The variables are varied in the ranges shown in Table 4.5. The parameter values are in Table 4.6, in which case (a) has a curved outer-plate (1/4 circle) that is concentric with the inner drum and case (b) has a straight outer-plate that is assumed infinitely long and inclined at a 45^o angle.

Table 4.5. Ranges of variables and parameters values in regression for drum-type electrostatic separations

$\tilde{x}_1$	- 1.134 ~ 0.783
$\tilde{x}_2$	0.0306 ~ 0.925
$\tilde{x}_3$	- 2.667 ~ 0.909
$\tilde{x}_b$	0.623 ~ 2.784

Table 4.6 Parameter values in Equation (4.42)

	b_1	b_2	b_3	b_4	b_5
Case (a)	1.6453	0.9663	-0.1251	0.5098	0.3715
Case (b)	1.6323	1.1050	-0.1941	0.3581	0.5138

Since there is only one random variable, the derivations of the recovery model and the partition curve model are straightforward:

$$r = \frac{1}{2}\left[1 - erf\left(\frac{\tilde{z} - 1}{\sqrt{2}s_q / m_q}\right)\right] \tag{4.47}$$

where

$$\tilde{z} = \frac{ln\left(\frac{\tilde{x}_c - b_5}{b_4}\right) - b_2\tilde{x}_2 - b_3\tilde{x}_3}{b_1\tilde{x}_1} \tag{4.48}$$

$$Ep = 0.6745s \tag{4.49}$$

$$q_{50} = \frac{ln\left(\frac{\tilde{x}_c - b_5}{b_4}\right) - b_2\tilde{x}_2 - b_3\tilde{x}_3}{b_1\left(\frac{-2V}{R_1 g\, ln(R_2 / R_1)}\right)} \tag{4.50}$$

As summarized in Table 4.7, several applications with various random variables have been demonstrated. The trajectory models, dependent on the physics of the problem, can be analytical or empirical. When an analytical recovery model can not be derived from the joint probability calculation, a numerical calculation is used and numerical values of Ep are found to fit the expression for Ep directly. Even if a recovery model is analytic, the Ep model could still be empirical and Equation (4.20) is a suggested form of the model.

Table 4.7 Summary of the models for different applications

	Random Variables	Trajectory Model	Recovery Model	Ep and β_{50} Models
Sink-float	Velocity, particle size	Analytical	--	Empirical
Froth flotation	Velocity, particle size, bubble coverage	Analytical	--	Empirical
Free-fall Electrostatic	Initial position, Particle charge	Analytical	Analytical	Empirical
Drum-type electrostatic	Particle charge	Empirical	Analytical	Analytical

4.5 Design Analysis by Manipulating the Partition Curve

The purpose of this section is to provide a simple procedure to choose the appropriate Ep and cut values.

Consider a separation of two materials (initial fractions: f_1 and $1-f_1$, respectively) with purity requirements ($p_1 \geq \alpha_1$ and $p_2 \geq \alpha_2$) for each product. Our task is to find the corresponding requirements for Ep and β_{50} in terms of known parameters: f_1, α_1,α_2, β_1 and β_2.

The purity requirement can be formulated as:

$$\begin{cases} p_1 = \dfrac{f_1 R_1}{f_1 R_1 + (1-f_1) R_2} \geq a_1 \\ p_2 = \dfrac{(1-f_1)(1-R_2)}{f_1(1-R_1) + (1-f_1)(1-R_2)} \geq a_2 \end{cases} \tag{4.51}$$

where R_i is the recovery of material i to product 1.

It can be shown that the feasible region defined by the inequalities (4.51) in the 2-

dimensional coordinates (R1, R2) can be approximated by a rectangle.

In Figure 4.7, the line PB represents a contour for $p_1 = a_1 = 0.95$, and the line PD represents a contour for $p_2 = a_2 = 0.95$. The quadrilateral PBCD is the feasible region defined by constraints (4.51) for R1 and R2. The coordinates of the points B, D and P are:

$$R_1(B) = \frac{a_2 + f_1 - 1}{a_2 f_1},\ R_2(B) = 0 \tag{4.52}$$

$$R_1(D) = 0,\ R_2(D) = \frac{f_1(1 - a_1)}{(1 - f_1)a_1} \tag{4.53}$$

$$R_1(P) = R_1(B') = \frac{a_1(a_2 + f_1 - 1)}{f_1(a_1 + a_2 - 1)} \tag{4.54}$$

$$R_2(P) = R_2(D') = \frac{(1 - a_1)(a_2 + f_1 - 1)}{(1 - f_1)(a_1 + a_2 - 1)} \tag{4.55}$$

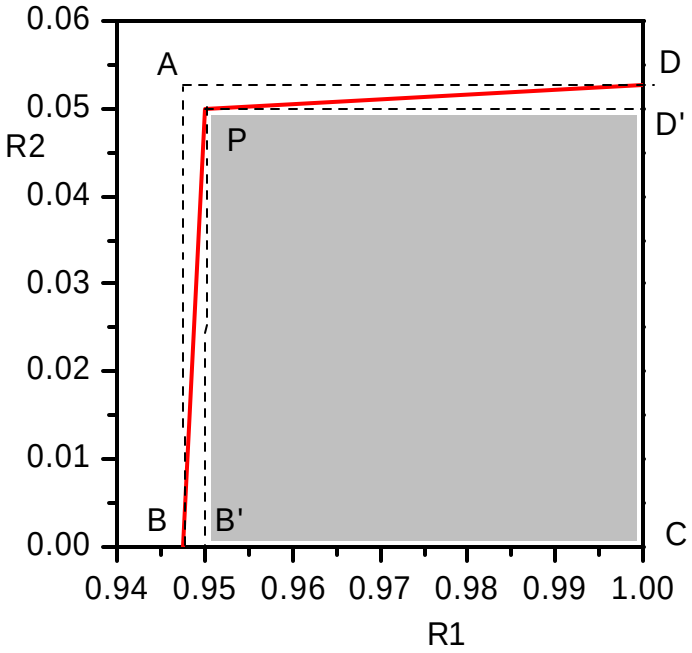

Figure 4.7. Feasible region for R1 and R2

It can be shown that:

if $1-a_2 \le f_1 \le a_1$ and $a_1 + a_2 - 1 > 0$, we have

$$\Delta B = R_1(B') - R_1(B) = \frac{(1-a_1)(1-a_2)(a_2 + f_1 - 1)}{a_2 f_1 (a_1 + a_2 - 1)} \ge 0 \tag{4.56}$$

and

$$\Delta D = R_2(D) - R_2(D') = \frac{(1-a_1)(1-a_2)(a_1 - f_1)}{a_1 (a_1 + a_2 - 1)(1 - f_1)} \ge 0 \tag{4.57}$$

It can also be shown that for $a_1, a_2 \ge 0.95$, $\Delta B_{max} = 0.00277$ and $\Delta D_{max} = 0.00277$. Since ΔB and ΔD are sufficiently small, the rectangle PB'CD' is a good approximation to the feasible region PBCD. Hence the constraints (4.51) are decoupled to:

$$R_1 \ge \frac{a_1(a_2 + f_1 - 1)}{f_1(a_1 + a_2 - 1)} \text{ and } R_2 \le \frac{(1-a_1)(a_2 + f_1 - 1)}{(1 - f_1)(a_1 + a_2 - 1)} \tag{4.58}$$

Note that although two materials are separated in the same separator, they may have different partition curve models. Let Ep_1, $\beta_{1,50}$ and Ep_2, $\beta_{2,50}$ be the Ep value and cut property for material 1 and material 2, respectively.

From

$$e^{\frac{1.0986}{Ep_1}(b_1 - b_{1,50})} = \frac{1}{R_1} - 1 \le \frac{1}{\frac{a_1(a_2 + f_1 - 1)}{f_1(a_1 + a_2 - 1)}} - 1 = \frac{(a_1 - f_1)(1 - a_2)}{a_1(a_2 + f_1 - 1)} \tag{4.59}$$

we have $b_{1,50} \ge b_1 + g_1$, where

$$g_1 = \frac{Ep_1}{1.0986} \ln\left[\frac{a_1(a_2 + f_1 - 1)}{(a_1 - f_1)(1 - a_2)}\right] \tag{4.60}$$

Similarly from

$$e^{\frac{1.0986}{Ep_2}(b_2 - b_{2,50})} = \frac{1}{R_2} - 1 \geq \frac{1}{\frac{(1-a_1)(a_2 + f_1 - 1)}{(1 - f_1)(a_1 + a_2 - 1)}} - 1 = \frac{a_2(a_1 - f_1)}{(1 - a_1)(a_2 + f_1 - 1)} \tag{4.61}$$

We have $b_{2,50} \leq b_2 - g_2$, where

$$g_2 = \frac{Ep_2}{1.0986} \ln\left[\frac{a_2(a_1 - f_1)}{(1 - a_1)(a_2 + f_1 - 1)}\right] \tag{4.62}$$

The decoupled requirements for R_1 and R_2 can be translated to the following requirements for the cut points $\beta_{1,50}$ and $\beta_{2,50}$.

$$b_1 + g_1 \leq b_{1,50} \text{ and } b_{2,50} \leq b_2 - g_2 \tag{4.63}$$

where

$$g_1 = \frac{Ep_1}{1.0986} \ln\left[\frac{a_1(a_2 + f_1 - 1)}{(a_1 - f_1)(1 - a_2)}\right], \quad g_2 = \frac{Ep_2}{1.0986} \ln\left[\frac{a_2(a_1 - f_1)}{(1 - a_1)(a_2 + f_1 - 1)}\right] \tag{4.64}$$

We divide the problem into two cases for simplicity of explanation.

1) If β_{50} is a function of only design and operating variables, such as in electrostatic separation, $b_{1,50} = b_{2,50}$. In such cases, inequalities (4.63) become:

$$b_1 + g_1 \leq b_{50} \leq b_2 - g_2 \tag{4.65}$$

The above inequalities imply a necessary condition for Ep values:

$$\left(\frac{a_1}{1-a_2}\right)^{Ep1}\left(\frac{a_2}{1-a_1}\right)^{Ep2}\left(\frac{a_2+f_1-1}{a_1-f_1}\right)^{Ep1-Ep2} \le e^{1.0986|\Delta b|} \qquad (4.66)$$

where $|\Delta b| = |b_1 - b_2|$.

The explanation for inequalities (4.65, 4.66) is: Ep value (sharpness) must be less (greater) than certain value which is determined by the purity requirements α_1, α_2 and the difference of the material properties Δb. Once the Ep value is fixed, the cut value β_{50} must fall in an interval $(b_1 + g_1, b_2 - g_2)$. Since the interval width is proportional to $-Ep_1$ and $-Ep_2$, the smaller the Ep values are, the larger the interval is allowed. Figure 4.8 illustrates the feasible region for β_{50} for an example with f_1=0.5, $\alpha_1=\alpha_2$=0.95, β_1= -0.477, β_2= 0.477 and equal Ep values ($Ep_1=Ep_2$=0.16) which satisfies the requirement in (4.66). From (4.65), the feasible interval for β_{50} is (-0.018, 0.018).

For $a_1 = a_2$, there are three cases with regard to the relative position of feasible interval for β_{50} between β_1 and β_2.

(**case I**): when f_1=0.5 and $Ep_1=Ep_2$, $g_1 = g_2 = \frac{Ep}{1.0986} ln\left(\frac{a}{1-a}\right)$

When the initial fractions and Ep values are equal, respectively, the feasible interval lies in the middle between β_1 and β_2 (as in Figure 4.8).

(**case II**): When f_1>0.5 or $Ep_1>Ep_2$, $g_1 > g_2$. This can be explained from purity requirements (4.51) as follows: as f_1 increases from 0.5, if β_{50} is kept the same, the purity of product 1 increases, however, the purity of product 2 decreases below the requirement. To increase the purity, an efficient way is to decrease the fraction of material 1 in product 2, i.e., increase the recovery of material 1 in product 1. Therefore, the interval needs to be shifted to the right at the cost of reduced recovery of material 2 in product 2. The

explanation is similar for the situation when $Ep_1 > Ep_2$.

(**case III**): When $f_1 < 0.5$, $g_1 < g_2$, the interval shifts to the left. This can be explained similarly as in case II.

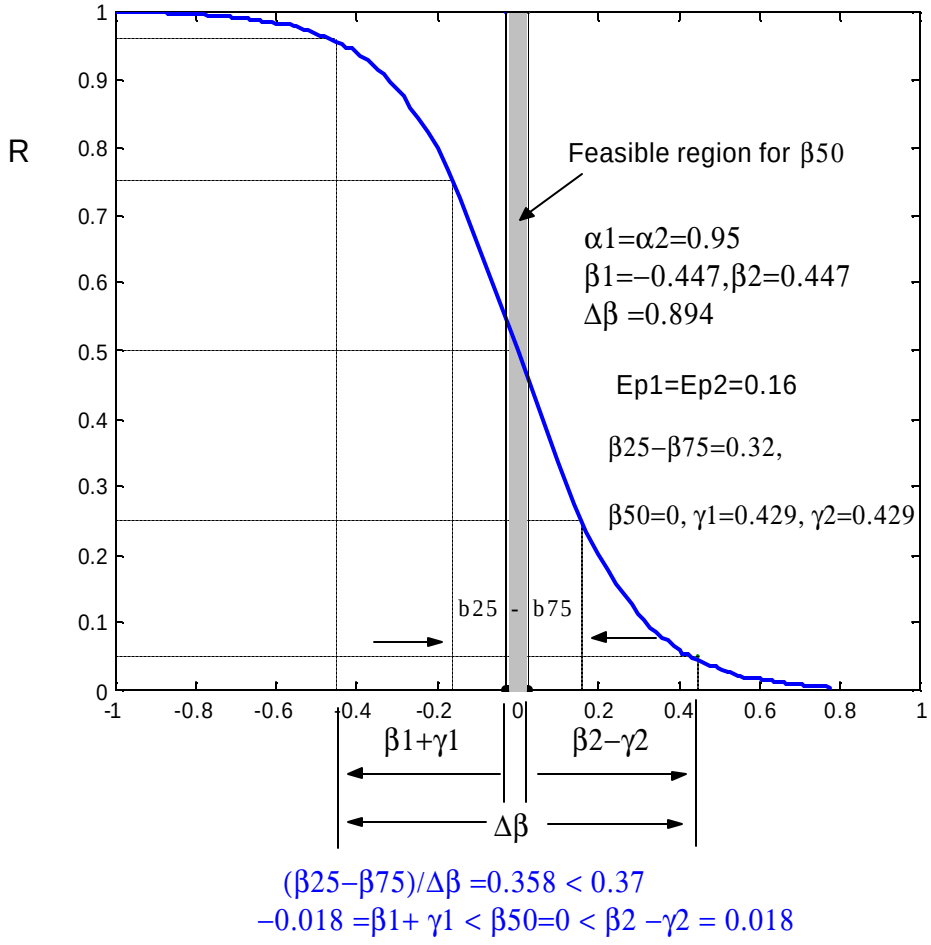

Figure 4.8 Illustration of the feasible region for β_{50}

2) β_{50} can also be a function of some material property φ which is different for two materials, such as in sink-float separation and froth flotation, in which the cut point functions (4.14) (4.29) contain the mean particle size. If the two materials in the feed

have different mean particle size, we then have $b_{1,50} \neq b_{2,50}$. We can write $b_{50} = f(Q, j)$, where Q is a vector of design and operating variables. After transformation, we have:

$$h(b_1 + g_1, j_1) \leq g(Q) \leq h(b_2 - g_2, j_2) \tag{4.67}$$

where g and h are some functions. Therefore inequalities (4.56) define a feasible region for function g(Q), and a similar analysis can be done. For example, if the two materials in a sink-float tank have different mean particle size μ_1, μ_2, plug the cut point function (4.14) into (4.63), we then have

$$(b_1 + g_1)\sqrt{3.03 g m_1} \leq Hc/t \leq (b_2 - g_2)\sqrt{3.03 g m_2} \tag{4.68}$$

which define a feasible region for the ratio of two design variables Hc/τ.

When the design model (4.63) is combined with the expressions for Ep and β_{50}, we have a very simple design procedure. This is briefly illustrated using the free-fall electrostatic separator as an example. From Equation (4.40), the Ep value increases with both the standard deviation of particle charge σ_q and the value of M^*a. If any one of them is significantly greater than the upper bound, it has to be reduced. If Ma dominates in Ep, we will have:

$$\frac{m_{q_1}}{b_1 - \dfrac{0.5a}{1.0986} ln\left[\dfrac{a(a + f_1 - 1)}{(a - f_1)(1 - a)}\right]} \leq M \leq \frac{m_{q_2}}{b_1 + \dfrac{0.5a}{1.0986} ln\left[\dfrac{a(a - f_1)}{(1 - a)(a + f_1 - 1)}\right]} \tag{4.69}$$

Similarly, if σ_{q1} and σ_{q2} dominate in Ep_1 and Ep_2, we will have:

$$\frac{m_{q_1} + \frac{0.6745 s_{q_1}}{1.0986} ln\left[\frac{a(a + f_1 - 1)}{(a - f_1)(1 - a)}\right]}{b_1} \le M \le \frac{m_{q_2} - \frac{0.6745 s_{q_2}}{1.0986} ln\left[\frac{a(a - f_1)}{(1 - a)(a + f_1 - 1)}\right]}{b_1}$$

(4.70)

If Ma , $\sigma_{q1,}$ σ_{q2} are in the same magnitude, one can substitute Equations (4.40) (4.41) into (4.67) to solve quadratic equations for an upper and a lower bound of M.

The inequality constraint for M makes the design procedure fairly simple. M can be adjusted by controlling the voltage V and the plate geometry d/L, depending on which one results in a lower cost. The feasible region of M can be adjusted by moving the bin position $b_{1.}$

4.6 Conclusions

In this chapter, it has been shown that how trajectory-based solid-solid separations can be modeled with a unified (microscopic) approach based on a joint probability calculation of recovery, which is a departure from a traditional differential-equation based (macroscopic) approach. One advantage of the unified approach is its ability to handle the randomness of individual particle properties. A connection between the probabilistic recovery model and the empirical partition curve model was also built that simplifies the design to a procedure that changes two parameters.

The accuracy of the recovery model depends mainly on the physics of the trajectory model used at the Step1 of the modeling approach (Figure 4.3) and the distributions assumed for the random variables. Given these are sufficiently accurate, the calculations at Step2 and Step3 should not bring significant errors. The proposed empirical Ep model (Equation 4.20) has been validated with four applications.

Although the probabilistic approach interprets the separations from a microscopic perspective, this does not mean the macroscopic method can be completely abandoned. The microscopic parameters such as the velocity deviation or bubble coverage deviation sometimes need to be calculated from experimentally determined macroscopic quantities such as the concentration. For example, Martin, et al., (1995) proposed to use a solid-liquid fluidized bed, in which the upward flowing solvent counterbalances gravity, to overcome sedimenting suspension and polydispersity problems. Thus a steady state is obtained and the concentration profile, from which the diffusion coefficient and hence the velocity deviation can be calculated, is measured.

CHAPTER 5

AN OVERALL DESIGN STRATEGY

The purpose of this chapter is to develop an overall design strategy, with a combination of heuristics and mathematical programming, which will assist in the design of an entire bulk recycling system for a given feed specification. The Douglas' (1988) hierarchical design method can be used to decompose the problem into several levels. Since this is a solid processing process, the hierarchy of decisions is different from that of a typical chemical process. Wibowo and Ng (1999) proposed a systematic procedure for synthesis of bulk solids processing systems to generate flowsheet alternatives. The step by step procedure is as follows:

Step 1. Selection of function structure

Step 2. Selection of equipment for functional structure

Step 3. Generation of flowsheet configurations

Step 4. Selection of storage and transportation equipment

Step 5. Evaluation of alternatives

The rules proposed for this procedure by Wibowo and Ng (1999) should in general be still applicable to the bulk recycling system. Therefore our work will focus on the specific issues for the bulk recycling systems, such as how to decompose the interactions between size reduction and separation.

5.1 The interactions between size reduction and separation

The interactions between size reduction and separation are shown in the following diagram (Figure 5.1).

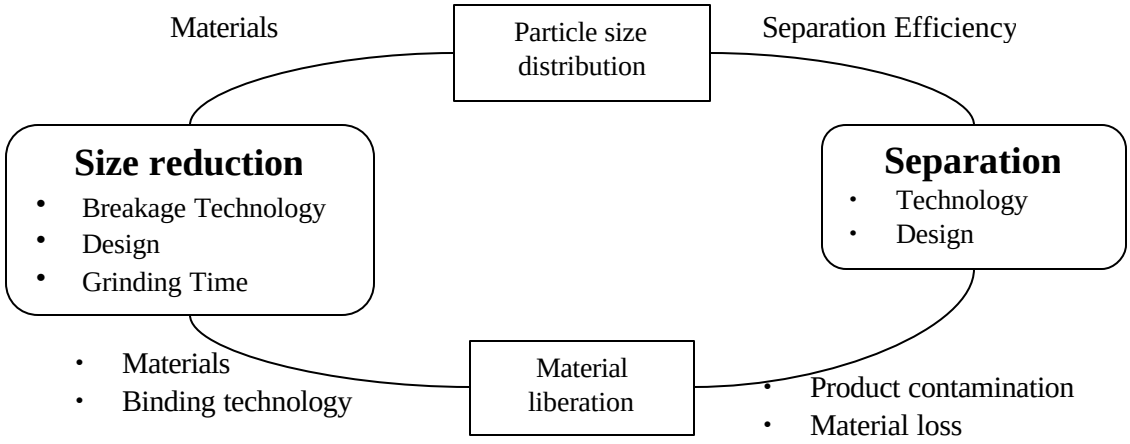

Figure 5.1 Interaction between size reduction and separation

The size reduction step has influence on the separation through both the particle size distribution and the degree of material liberation. The former affects the separation in terms of separation efficiency and costs; the latter can result in product contamination or additional cost of removing unliberated pieces. The particle size distribution is dependent of not only the size reduction equipment (technology, design) but also the materials to be processed. Also, the distribution changes with processing time. The degree of material liberation depends on how different materials are bound together and how the breaking force/energy is applied.

Therefore, many decisions have to be made to synthesize a cost effective system. These decisions include: choices of size reduction and separation units; use of classifiers for particle size control; use of detection equipment for unliberated pieces; processing time in the size reduction units.

Next, the interactions are discussed, covering the following aspects: (1) Influence of size reduction on the particle size distribution (2) Influence of size reduction on the degree of material liberation, and (3) influence of particle size distribution on separation.

5.2 Influence of size reduction on the particle size distribution

5.2.1 Evolution of particle size distribution with time

Batch grinding experiments such as grinding dolomite by a stirred ball mill (Gao and Forssberg, 1995), polystyrene by a shaker bead mill (Molina-Boisseau and Bolay, 2000), various minerals by a standard ball mill (Aksani and Sonmez, 2000) and limestone by three ball mills (Datta and Rajamani, 2002) have observed qualitatively similar change of cumulative size distribution with time, shown in Figure 5.2.

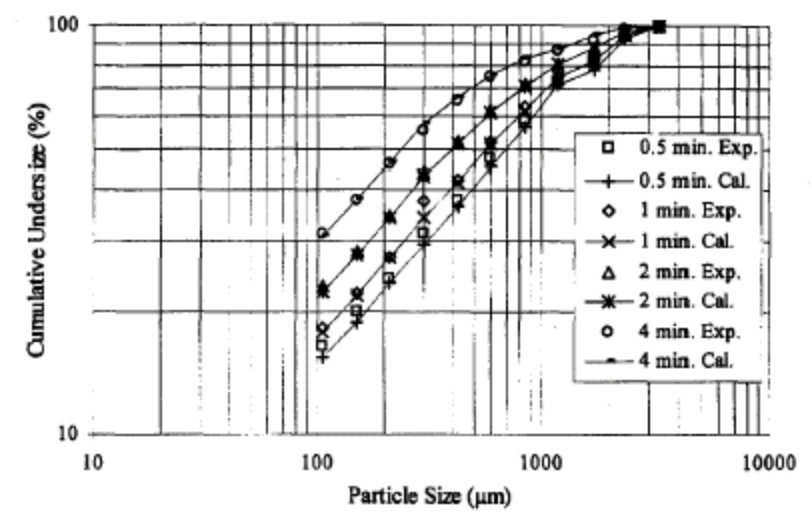

Fig. 1 Experimental and calculated particle size distribution of copper ore.

Figure 5.2 Experimental and calculated particle size distribution
(from Figure 1 of Aksani and Sonmez, 2000, page 675)

Theoretically, the following Population Balance Equation (PBE) has been widely used to solve for the dynamic particle size distribution (Ramkrishna, 1971, 1985).

$$\frac{\partial F(d,t)}{\partial t} = \int_d^\infty S(d')B(d,d')f(d',t)\mathrm{d}d' \tag{5.1}$$

where

$F(d,t)$: Fraction of particles whose size is less than d at time t (c.d.f)

$f(d,t)$: Corresponding density function

$B(d,d')$: Amount of particles less than size d broken out of particle size d'

$S(d)$: Breakage rate

There is no general closed-form analytical solution of the above equation. For a special case (King, 1972) in which it is assumed:

$$S(d')b(d,d') = a\ k_0\ d^{a-1} \tag{5.2}$$

and by definition $B(d,d') = \int_0^d b(d,d')\mathrm{d}d$, an analytical solution can be obtained:

$$F(d,t) = 1 - [1 - F(d,0)]e^{-k_0 d^a t} \tag{5.3}$$

$$f(d,t) = \left[k_0 t a d^{a-1}(1 - F(d,0)) + f(d,0)\right] e^{-k_0 t d^a} \tag{5.4}$$

where *F(d,0), f(d,0)* are the initial cumulative distribution function and probability density function, respectively. The case in which the initial particle size is a constant value d_0 and α=1 is considered,

$$F(d,0) = \begin{cases} 1 & d \geq d_0 \\ 0 & d < d_0 \end{cases} \tag{5.5}$$

$$f(d,0)=\begin{cases}1 & d=d_0\\ 0 & d\neq d_0\end{cases} \tag{5.6}$$

then we have

$$F(d,t)=\begin{cases}1-e^{-k_0 td} & d<d_0\\ 1 & d\geq d_0\end{cases} \tag{5.7}$$

The mean and the variance of the particle size are

$$E[d]=\int_0^{d_0} d\cdot k_0 te^{-k_0 td}\,dd+d_0e^{-k_0 td_0}=\frac{1}{k_0 t}\left(1-e^{-k_0 td_0}\right) \tag{5.8}$$

$$V[d]=\frac{1-2k_0 td_0e^{-k_0 td_0}-e^{-2k_0 td_0}}{(k_0 t)^2} \tag{5.9}$$

The mean size is a monotonic decreasing function of time (Figure 5.3a), while the variance (Figure 5.3b) increases initially and then decreases. The maximum variance occurs when k_0td_0=1.1265.

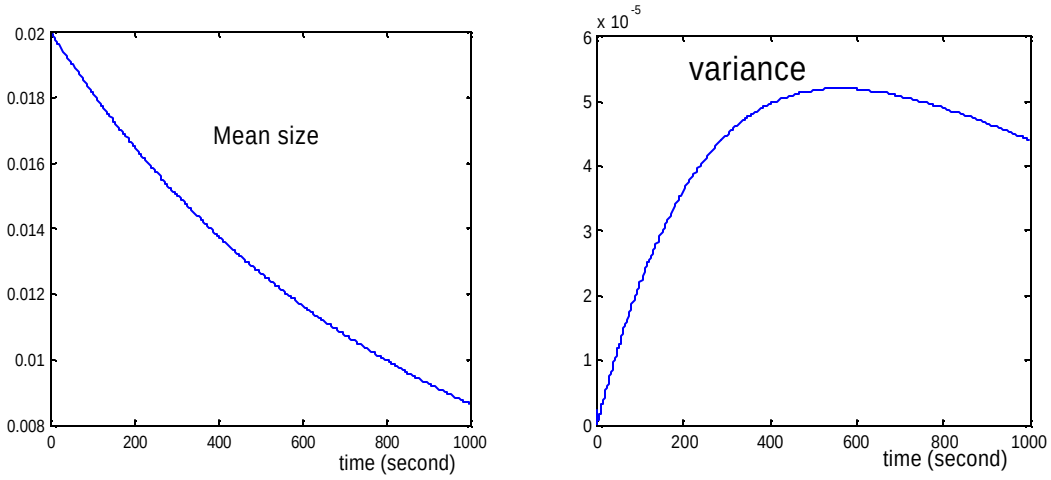

(a) (b)

Figure 5.3 The evolution of the (a) mean and (b) variance of particle size.

5.2.2 Selection of size reduction equipment

The following table (Table 5.1) is a brief summary of different types of equipment in terms of the size control, energy use, costs and applications. More information can be found from Kelly and Spoottiswood (1982).

5.3 Influence of size reduction on the degree of material liberation

The bond between different materials of manufactured products is generally weaker than in natural ores, therefore its not energy intensive to liberate materials having distinctive mechanical properties (Zhang and Forssberg, 1999).

Loehr and Melchiorre (1996) classified the liberation procedure into three types:

i) Chopping: Chopping is independent of its composition or structure, such as cutting cables

ii) Dividing: Dividing bonded materials along their interface, such as breaking coated materials by shearing in a cone crusher.

iii) Stripping: Stripping specific components from a composite by only disintegrating the rest, such as the disintegration of non-metals from scrap cars.

In selective comminution such as dividing and stripping, the difference of brittleness can be enhanced in the cryogenic condition, which is often used in breaking bonded plastics.

Based on some experimental observations, it is reasonable to assume the curve of liberation fraction L v.s. mean particle size dp has an "S" shape (i.e., when $dp \rightarrow 0$, $L \rightarrow 1$; when $dp \rightarrow \infty$, $L \rightarrow 0$). So we use the following empirical function to represent the relationship. The values of α and β depend on the size reduction equipment, the properties of materials and the binding methods.

Table 5.1 Comparison of different size reduction equipment

	Size control	Energy use	Costs	Applications
Crushers: by Compression or Impact				
Jaw Crushers Gyratory Crushers	Limited reduction ratio due to the fixed size of input and output openings;	Cause fracture by compression; Apply energy directly to particles. Internal stresses in material broken by compression which can cause later cracking.	Gyratory crushers have larger capacity. The capital and maintenance costs of a jaw crusher are slightly less than those of the gyratory. But the latter have lower installation costs.	Jaws perform better than gyratories on plastic materials, while the latter are found to be particularly suitable for hard, abrasive material.
Roller Crushers		Some fracture may occur by cleavage in toothed machines, but most is by shatter. Unlike jaw and gyratory crushers, where reduction is progressive by repeated pressure, the crushing in rolls is one of single pressure.	Have highest capital cost of all crushers because very large rolls are required in relation to the feed particles.	
Hammer mills	The exit from the mill is perforated, so that material that is not broken to the required size is retained and swept up again by the rotor for further impacting.	Cause fracture by impact; Impact causes immediate fracture with no residual stresses. Some fracture by abrasion, which leads to little control on product size and a much higher proportion of fines than with compressive crushers.		Limited use to relatively non-abrasive materials. Have extensive use in limestone quarrying and coal crushing.
Grinders: 1) As opposed to crushing, grinding is a more random process and is subject to the laws of probability. 2) Mechanisms: Compression or Impact or Chipping or Abrasion 3) Control of particle sizes is exercised by the type of medium used, the speed of rotation of the mill, the nature of the material and type of circuits 4) Most of the tumbling load is dissipated as heat, only a small fraction being expended in actually breaking the particles				
Rod mills Ball mills Autogenous	little restriction on the feed and product size; exert limited amount of control on product size ; Products from an open-circuit ball mill exhibits a wide range of particle size	Predominantly shatter fracture; Energy is consumed in keeping the mill shell, the media and the particles in motion. Fracture occurs as a by-product of passage through the mill and is a statistical process.	Medium consumption in Ball mills can be up to 40% of total milling cost.	often operated in closed circuit with an external classifier;

$$L = e^{-a d_p{}^b} \tag{5.10}$$

5.4 Influence of particle size distribution on separation

In this section, the influence of the particle size distribution on the separation efficiency is discussed based on the unit models developed in chapter 4. Qualitative diagrams of how the partition curve evolves with time will be shown.

5.4.1 Electrostatic separation

A. Charging Process

The particle size affects the charge-to-mass ratio through the surface-to-volume ratio. A linear relationship between the mean charge versus the particle area was observed by Trigwell et al. (2003) who used an Electronic Single Particle Aerodynamic Relaxation Time (ESPART) analyzer to measure the charge-to-mass ratio of materials, such as Epoxy, Toner, Polyester, Acrylic Class, charged by milling with stainless steel beads. The inverse relationship between charge-to-mass ratio and particle size is also supported by Rowely (2001) who used a cyclone with interchangeable contact surfaces of steel and polymers to charge lactose particles for size range from 90 to 500 μm.

Therefore, for particles with the same material, it is assumed that the total charge it can acquire is linearly proportional to their surface area or the square of the diameter, i.e. $q \propto d_p^2$. Since the particle mass is linearly proportional to the cube of the diameter, the charge-to-mass ratio is proportionally to $1/dp$, i.e., $q_m = \frac{a}{dp}$, where a is a constant. It can be seen that finer particles can acquire higher mean charge-to-mass ratio.

B. Separation Process

The particle size can influence the separation process through its influence on the charge-to-mass ratio.

First, we derive the distribution function of the charge-to-mass ratio.

From the c.d.f. of particle size,

$$F_d(d) = \begin{cases} 1 - e^{-k_0 t\ d}, & d < d_0 \\ 1, & d \geq d_0 \end{cases} \tag{5.11}$$

the c.d.f. for particle charge-to-mass ratio (for the case of $q_m \geq 0$) is

$$\begin{aligned} F_q(z) &= Pr\{q_m \leq z\} = Pr\left\{\frac{b}{d} \leq z\right\} \\ &= \begin{cases} Pr\left\{d \geq \frac{b}{z}\right\} = 1 - F_d\left(\frac{b}{z}\right) = \begin{cases} e^{-k_0 t \frac{b}{z}}, & z > \frac{b}{d_0} \\ 0, & 0 < z \leq \frac{b}{d_0} \end{cases} \\ 0, z \leq 0 \end{cases} \\ &= \begin{cases} e^{-k_0 t \frac{b}{z}}, & z > \frac{b}{d_0} \\ 0, & z \leq \frac{b}{d_0} \end{cases} \end{aligned} \tag{5.12}$$

so the p.d.f. of charge-to-mass ratio is:

$$f_q(z) = \begin{cases} \frac{k_0 t b}{z^2} e^{-k_0 t \frac{b}{z}}, & z > \frac{ß}{d_0} \\ e^{-k_0 t d_0}, & z = \frac{ß}{d_0} \\ 0, & z < \frac{ß}{d_0} \end{cases} \tag{5.13}$$

From the c.d.f. of charge-to-mass ratio:

$$z_{75} = 3.4761 k_0 t b \ , \ z_{25} = 0.7213 k_0 t b \tag{5.14}$$

so

$$Ep = \frac{z_{75} - z_{25}}{2} = 1.3774 k_0 t b \tag{5.15}$$

Therefore, as time increases, Ep increases or the separation efficiency decreases because particle charge-to-mass ratios are more widely spreaded as particles become finer. In other words, the partition curve is flatter as time increases (Figure 5.4).

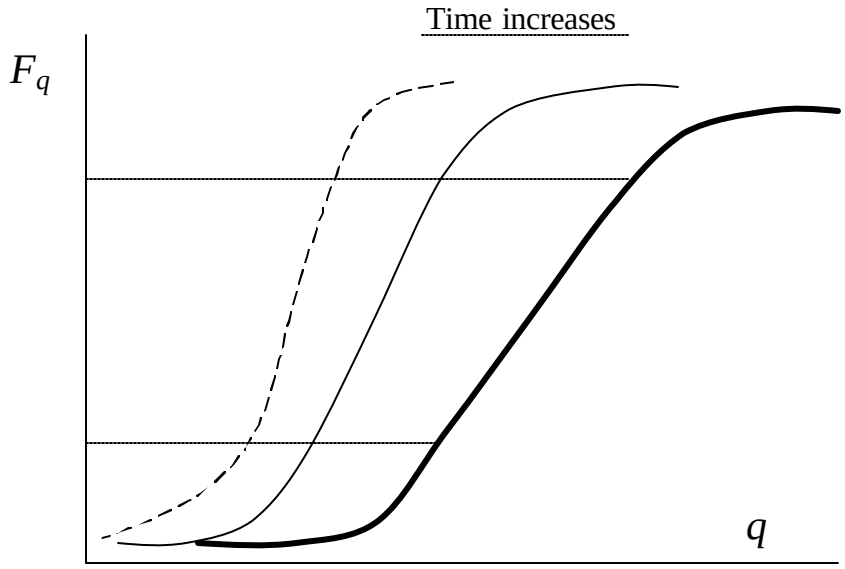

Figure 5.4 Evolution of partition curve with time for electrostatic separation

5.4.2 Sink-float separation

The mean particle size μ_{dp} can influence the separation efficiency through partition curve model parameter Ep. Based on Equation 4.19 (assuming particle size has a normal distribution),

$$Ep_2 = \frac{Hc\left(\sqrt{m_{dp} + 0.6745 s_{dp}} - \sqrt{m_{dp} - 0.6745 s_{dp}}\right)}{2t\sqrt{3.03g}\sqrt{m_{dp}^2 - 0.455 s_{dp}^2}}$$

Ep decreases with increasing μ_{dp} and increasing σ_{dp}, respectively, which means that the separation efficiency (slope of partition curve) increases with μ_{dp}, but decreases with $\sigma_{dp.}$

To see how grinding time influences the separation efficiency, let's use the particle size distribution model developed in this chapter. Other random variables are neglected and only the influence of the size distribution is studied.

$$R = Pr\left\{b\sqrt{3.03gd}t \geq Hc\right\} = Pr\left\{d \geq \frac{Hc^2}{3.03gt^2}\frac{1}{b^2}\right\} = 1 - F_d\left(\frac{Hc^2}{3.03gt^2}\frac{1}{b^2}\right)$$

$$= \begin{cases} e^{-k_0 t\frac{Hc^2}{3.03gt^2}\frac{1}{b^2}}, & if \ \frac{Hc^2}{3.03gt^2}\frac{1}{b^2} < d_0 \\ 0, & if \ \frac{Hc^2}{3.03gt^2}\frac{1}{b^2} \geq d_0 \end{cases} \tag{5.16}$$

$$b_{75} = 1.071\frac{Hc}{t}\sqrt{k_0 t/g}\ ,\ b_{25} = 0.4879\frac{Hc}{t}\sqrt{k_0 t/g}\ , \tag{5.17}$$

so,

$$Ep = 0.292\frac{Hc}{t}\sqrt{k_0 t/g} \tag{5.18}$$

Since Ep is proportional to the grinding time t, the separation efficiency decreases with time. The evolution of the partition curve with time is similar to that in electrostatic separation (Figure 5.4).

Combining the results from the two models, it can be seen that the decreasing mean particle size with time has a major contribution to the reduced separation efficiency. This result implies that, less grinding favors the SF separation.

5.4.3 Froth flotation

From the model developed in the previous chapter (Equations 4.33 and 4.34), for the case when the particle size is the only random variable, we have

$$b_{75} = \frac{1.59}{4}\left[\frac{r_p / r_l}{1-\frac{(Hc/t)^2}{3.03g\left(m_{dp}+0.6745s_{dp}\right)}}-1\right]\frac{\left(m_{dp}+0.6745s_{dp}\right)}{d_b} \tag{4.33}$$

$$b_{25} = \frac{1.59}{4}\left[\frac{r_p / r_l}{1-\frac{(Hc/t)^2}{3.03g\left(m_{dp}-0.6745s_{dp}\right)}}-1\right]\frac{\left(m_{dp}-0.6745s_{dp}\right)}{d_b} \tag{4.34}$$

Some numerical calculations show that for typical values of particle/medium densities and separator size, Ep increases with the mean and the variance of the particle size. So small particle sizes with small variance favor the separation.

To see the influence of grinding time on the separation efficiency, again the particle size distribution model developed in this chapter is used.

$$\begin{aligned} R &= Pr\left\{\sqrt{3.03gd_p\left(1-\frac{1.59r_p}{1.59r_l+4K\frac{d_b}{d_p}r_l}\right)}\,t \le Hc\right\} \\ &= Pr\left\{1.59\left(\frac{r_p}{r_l}-1\right)d_p^2-\left[4Kd_b-\frac{1.59(Hc/t)^2}{3.03g}\right]d_p+\frac{(Hc/t)^2}{3.03g}4Kd_b \le 0\right\} \\ &= Pr\left\{d_{p,1} \le d_p \le d_{p,2}\right\} \end{aligned} \tag{5.19}$$

where

$$d_{p,1} = \frac{\left[4Kd_b - \frac{1.59(Hc/t)^2}{3.03g}\right] - \sqrt{\left[4Kd_b - \frac{1.59(Hc/t)^2}{3.03g}\right]^2 - 4*1.59\left(\frac{r_p}{r_l} - 1\right)*\frac{(Hc/t)^2}{3.03g}4Kd_b}}{2*1.59\left(\frac{r_p}{r_l} - 1\right)}$$

(5.20a)

$$d_{p,2} = \frac{\left[4Kd_b - \frac{1.59(Hc/t)^2}{3.03g}\right] + \sqrt{\left[4Kd_b - \frac{1.59(Hc/t)^2}{3.03g}\right]^2 - 4*1.59\left(\frac{r_p}{r_l} - 1\right)*\frac{(Hc/t)^2}{3.03g}4Kd_b}}{2*1.59\left(\frac{r_p}{r_l} - 1\right)}$$

(5.20b)

Assuming $d_{p,1}$ is sufficiently small such that $Pr\{d_{p,1} \le d_p \le d_{p,2}\} \approx Pr\{d_p \le d_{p,2}\}$

$$R = \begin{cases} 1 - e^{-k_0 t d_{p2}}, & d_{p,2} < d_0 \\ 1, & d_{p,2} \ge d_0 \end{cases} \quad (5.21)$$

Since $d_{p,2}$ increases monotonically with K, the evolution of partition curve with time (Figure 5.5) is reversed compared to that in electrostatic and sink-float separations The separation efficiency increases with grinding time, therefore longer grinding time favors the separation.

However, to limit the carry-over of fine particles by rising bubbles despite of their densities, the particle size should not be too small, hence over-grinding should be avoided to limit the fraction of fines.

5.5 The Overall Design Strategy

Figure 5.6 gives a summary of the size control at each step through the system.

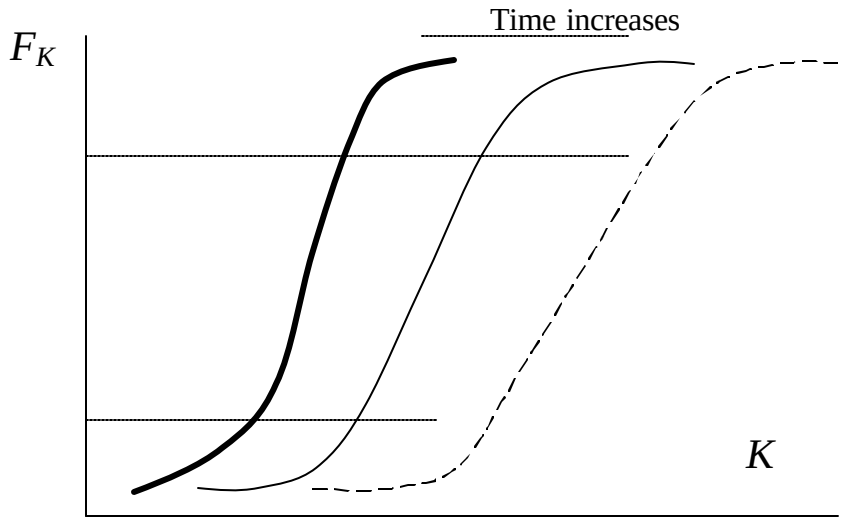

Figure 5.5 Evolution of partition curve with time for froth flotation

The sink-float separation should be placed before electrostatic and froth flotation separation because that larger particles favor the sink-float separation and also they are cheaper. After the density-based separation, a secondary-grinding might be needed and the ratio of size reduction depends on the subsequent separation methods to be used.

Our objective is to maximize the total profit which is the difference of the recovered value and the total cost. As shown in Figure 5.7, the recovered value drops sharply as the output particle size is increased to a certain value due to the large fraction of unliberated pieces causing contamination of products. The recovered value has a similar shape to that of the liberation percentage function. The total cost is a monotonically decreasing function of output particle size. The total profit is expected to show a transition point for the particle size at which the profit reaches the maximum. This defines the optimal average output particle size.

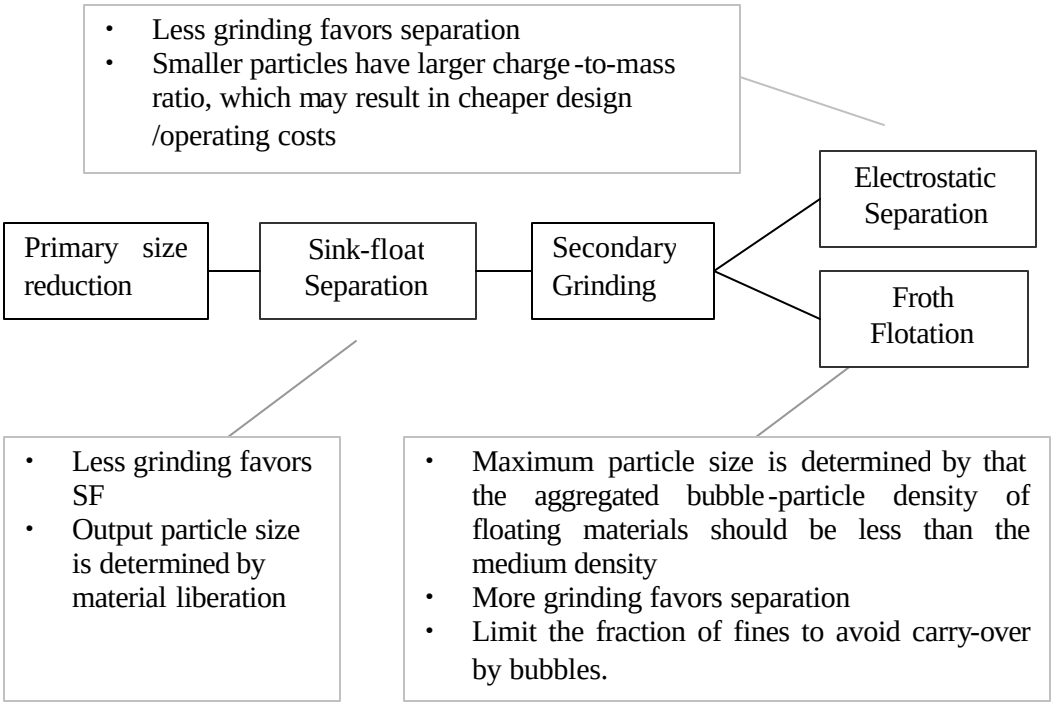

Figure 5.6 A step-by-step size control strategy

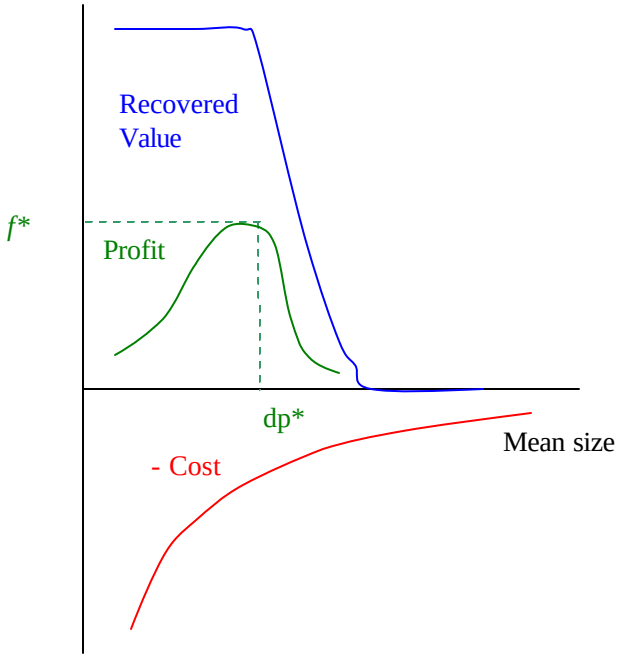

Figure 5.7 Overall economic analyses

Theoretically, one can find the optimal output size and the associated grind time by optimizing the profit function given that the above relationships have been mathematically defined. In such an approach, particle size is treated as a variable and the size reduction steps are incorporated into the superstructure as optional units. Thus, the superstructure size is further increased. Moreover, it might not be easy to find some of the relationships. Therefore, such an optimization approach is not easy to implement.

Due to the difficulty of incorporate size reduction into the superstructure optimization, the following procedure with heuristic rules is presented to help to make decisions regarding the selection of size reduction equipment and the appropriate particle size.

The step-by-step design hierarchy

In this design procedure, it is assumed that the characteristics of the size reduction units are known or available from the manufacture. The information needed include the evolution of the degree of liberation and the output particle size distribution with grinding time.

Step 1: Preliminary flowsheet optimization of the separation system.

Since the separation units operated in different conditions (particle properties, medium density, feed composition) will have different requirements for the particle sizes, a flowsheet is needed to start with for the analysis of particle size requirements. Therefore first the size reduction units are neglected and particle size distribution is assumed to be fixed through the separation system. With an estimated particle size distribution, find an

optimal flowsheet based on the average condition (i.e., neglect the uncertainties). This estimated size distribution is a starting point and will be adjusted later. The size distribution that can generate a nearly complete material liberation is a good choice.

Step 2: Determination of appropriate mean particle size for each separation unit

Based on the flowsheet found from step 1, find the appropriate particle size range for each separation unit used in the flowsheet according to the following methods:

(1) *for sink-float tanks*: use the largest particle size that is acceptable for the units.

(2) *for froth-flotation tanks*: use the following procedure to find the minimum and maximum particle sizes.

(i) Since the particle-bubble aggregates for float and sink particles should in general be lighter and heavier than the medium, respectively, we have:

$$\frac{1.59}{1.59+4K_1\dfrac{d_b}{d_p}}\,r_{p1} \le a_1 r_l \qquad a_1 \approx 0.95 \qquad \text{for float material}$$

$$\frac{1.59}{1.59+4K_2\dfrac{d_b}{d_p}}\,r_{p2} \ge a_2 r_l \qquad a_2 \approx 1.05 \qquad \text{for sink material}$$

After rearrangement, we have $\dfrac{4a_2K_2d_b}{1.59\left(\dfrac{r_{p2}}{r_l}-a_2\right)} \le dp \le \dfrac{4a_1K_1d_b}{1.59\left(\dfrac{r_{p1}}{r_l}-a_1\right)}$

Taking account of the bubble coverage distribution, the above is rewritten as :

$$\frac{4a_2(K_2+3s_K)d_b}{1.59\left(\dfrac{r_{p2}}{r_l}-a_2\right)} \le dp \le \frac{4a_1(K_1-3s_K)d_b}{1.59\left(\dfrac{r_{p1}}{r_l}-a_1\right)} \qquad (5.22)$$

(ii) To avoid carry-over by bubbles, the particles should not be larger than bubbles.

(3) *for electrostatic separators*: Assuming the particle charge-to-mass ratio is inversely proportionally to the particle diameter. Then the short-cut design procedure can be used to calculate the maximum particle size allowed in the electrostatic separation:

Assume $q_{m1} = -\frac{a_1}{dp}$ $q_{m2} = \frac{a_2}{dp}$, we have $q_{m2} - q_{m1} = \frac{a_2 + a_1}{dp}$

Based on the short cut design model: $q_{m1} + g_1 \le q_{m50} \le q_{m2} - g_2$, we should have at least: $q_{m1} + g_1 < q_{m2} - g_2$

Therefore,

$$q_{m2} - q_{m1} > g_1 + g_2 \text{ , which gives } dp < \frac{a_2 + a_1}{g_1 + g_2} \tag{5.23}$$

where

$$g_1 = \frac{Ep_1}{1.0986} \ln\left[\frac{a_1(a_2 + f_1 - 1)}{(a_1 - f_1)(1 - a_2)}\right] \text{ and } g_2 = \frac{Ep_2}{1.0986} \ln\left[\frac{a_2(a_1 - f_1)}{(1 - a_1)(a_2 + f_1 - 1)}\right] \tag{5.34}$$

Step 3: Selection of size reduction units and determination of grinding time.

The complete system is divided into two phases: (1) primary size reduction – sink/float separation (Figure 5.8), and (2) secondary size reduction- electrostatic/froth flotation separation (Figure 5.9).

(1) *Primary Size Reduction – Sink/float separation*

This phase mainly consists of a primary size reduction unit, possibly a classifier to

remove fines and a sub-network of sink-float units.

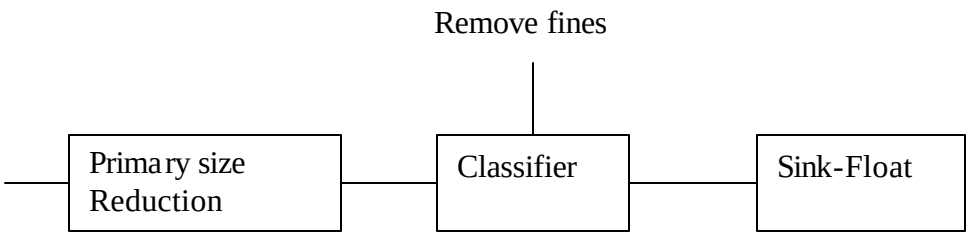

Figure 5.8 Phase 1: Primary size reduction – density-based separation

Rules:

1) Find the maximum of the mean particle size that can provide nearly complete material liberation and is acceptable to all sink-float units.
2) Find the grinding time that is needed to achieve this mean particle size. Select a size reduction unit that provides a good balance of size distribution and cost, using Table 5.1 as a guide. To enhance the materials liberation, one should choose one or two units in which fractures are generated by a combination of shear, impact, pressure etc.
3) Use classifier to remove fines if necessary. Fine particles can report to wrong exit due to carry-over by large particles.

(2) *Secondary size reduction- Froth flotation/Electrostatic separation*

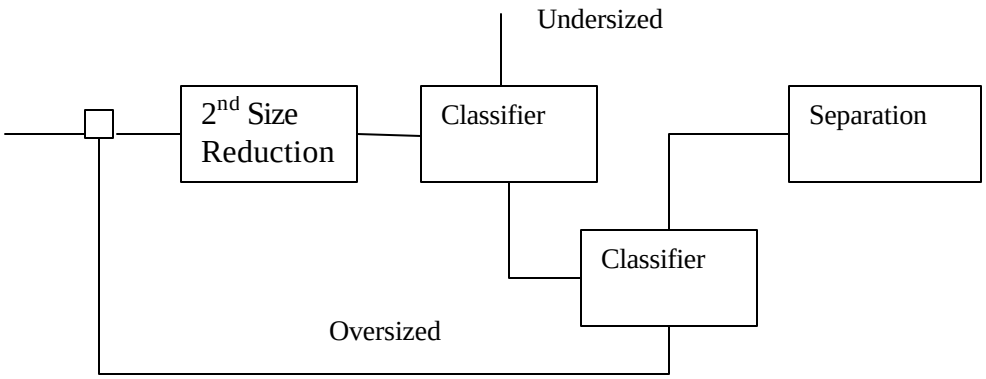

Figure 5.9 Phase 2: Secondary size reduction – non-density based separation

Rules:

1) Find the maximum particle size d_m with which inequalities (5.22 - 5.24) are all satisfied.

2) Find the appropriate particle size distribution that gives

$$Pr\{d_p \le d_m\} \ge 0.99 \tag{5.35}$$

and the resulting grinding time. Select a size reduction unit that provides a good balance of achieving this size distribution and cost, using Table 5.1 as a guide.

3) Use classifiers to remover undersized particles and recycle oversized particles for regrinding.

Step 4: Improving the flowsheet

With the particle size distribution determined from Step 3, run the superstructure optimization with the uncertainties for the separation system to generate a new flowsheet. If the flowsheet does not change, the design process is finished; otherwise, return to Step1 and repeat.

5.6 Conclusions

The overall design method proposed in this chapter focus on decomposing the interactions between the size reduction and separations. The unit models developed in Chapters 3 and 4 are used to find the limits for the particle size for each type of separation methods. The step-by-step method decomposes the procedure by first fixing the size distribution to find a preliminary optimal flowsheet, then fixing the flowsheet to find the appropriate size distribution needed for each unit by some heuristics and finally adjusting the appropriate size distribution for the two phases of size reduction and re-optimize the separation flowsheet.

CHAPTER 6

A CASE STUDY

The main purpose of this case study is to demonstrate the application of the SAA-MINLP method to solving a large plastics separation system design problem under uncertainty, using the unit models developed in Chapter 3. The size reduction units are not included in the superstructure due to the lack of appropriate models. Heuristic rules are used to select size reduction units and determine the appropriate particle sizes. Once the size reduction units are chosen, the cost is considered as a fixed value. Therefore, this case study considers only the selection, sequencing and sizing of the separation units themselves.

6.1 Problem description

In this case study, the flow stream to be processed is a mixture of TV and Computer products. The components of a TV or a computer are assumed to be fixed, respectively. However, the fraction of TVs or Computers is uncertain, which makes the fraction of each component in the feed stream also a random number. The total feed flow rate is fixed at 3600 kg/hr (=1 kg/s) and the fraction of TVs has a normal distribution with mean 74% and standard deviation 17% (APC report, 2000). In TVs, HIPS is the dominant material, while in computers, ABS dominates. The data are shown in Table 6.1.

Table 6.1 Feed components and fractions (APC report, 2000)

		PE	HIPS	ABS	PPO	PC/ABS
Feed	Total: 3600 kg/ hr, TV (Mean: 74%; STD 17%) + Computer					
Components	For TV	5%	75%	8%	12%	0%
	For Computer	0%	5%	57%	36%	2%

The product prices are also uncertain and correlated. Due to the lack of historical data, they are assumed to have normal distributions, with their respective mean and standard deviation and the correlation coefficient matrix shown in Table 6.2.

Table 6.2 Product price distribution

		PE	HIPS	ABS	PPO	PC/ABS
Price ($/kg)	Mean	0.4	0.6	0.6	1.5	1.5
	S.T.D.	0.02	0.04	0.04	0.1	0.1
	Correlation Coefficient	1	0.2	0.2	0.2	0.2
			1	0.5	0.3	0.3
				1	0.3	0.7
					1	0.4
						1

The material properties for each component, such as density, distribution of particle size, distribution of bubble coverage and charge-to-mass ratio are presented in Table 6.3.

Table 6.3 Material properties

			PE	HIPS	ABS	PPO	PC/ABS
Density (g/cm^3)			0.92	1.05	1.06	1.07	1.20
Particle size (mm)			Normal distribution N (6, 0.3)				
Bubble coverage	Mean	Unit 5	0.7	0.9	0.8	0.1	0.1
		Unit 6	0.7	0.9	0.1	0.1	0.1
	S.T.D.		0.02				
Charge -to-mass	Mean (μC/kg)	Unit 7,9	4	4	3	-5	-4
		Unit 8,10	4	3	-4	-5	-4
	S.T.D. (μC/kg)		0.2				

For bubble coverage and charge-to-mass ratio, no quantitative data have been reported in literature. Moreover, such properties depend on the type of units and operating conditions. Therefore, for a specific problem, the users will need to find these data, by either seeking help from the manufacture or experimenting on the materials to be processed themselves.

The following superstructure (Figure 6.1) is proposed, which consists of 10 optional units (4 sink-float tanks (SF), 2 froth flotation tanks (FF), 2 free-fall electrostatic separators (FE) and 2 drum separators (DE)). The superstructure has the following features:

1) First of all, in this structure, a top level separation sequence has been specified: density-based separations first, followed by the non density based separations. The reasons are the follows:

   a) First, existing research on plastics separation technologies does not support an arbitrary cut for a mix of 4 or more plastics and has focused on mainly binary or tertiary mixtures with overlapping densities. For a mix of 4 plastics (ordered as ABCD in terms of floatability), it does not seem that a mix of ABCD conditioned by some agent resulting in a bubble coverage order of 100% for A, 70% for B, 30% for C and 0% for D can be efficiently separated. Therefore, it would require a conditioning method by using a different agent at a time to differentiate A from BCD by making A floatable and BCD non-floatable, and then B from CD by making B floatable and CD non-floatable, and so on. However, such a conditioning method has not been seen in literature. Therefore, the application of non density-based separations is limited to a mixture with 2 or 3 plastics only and assume the

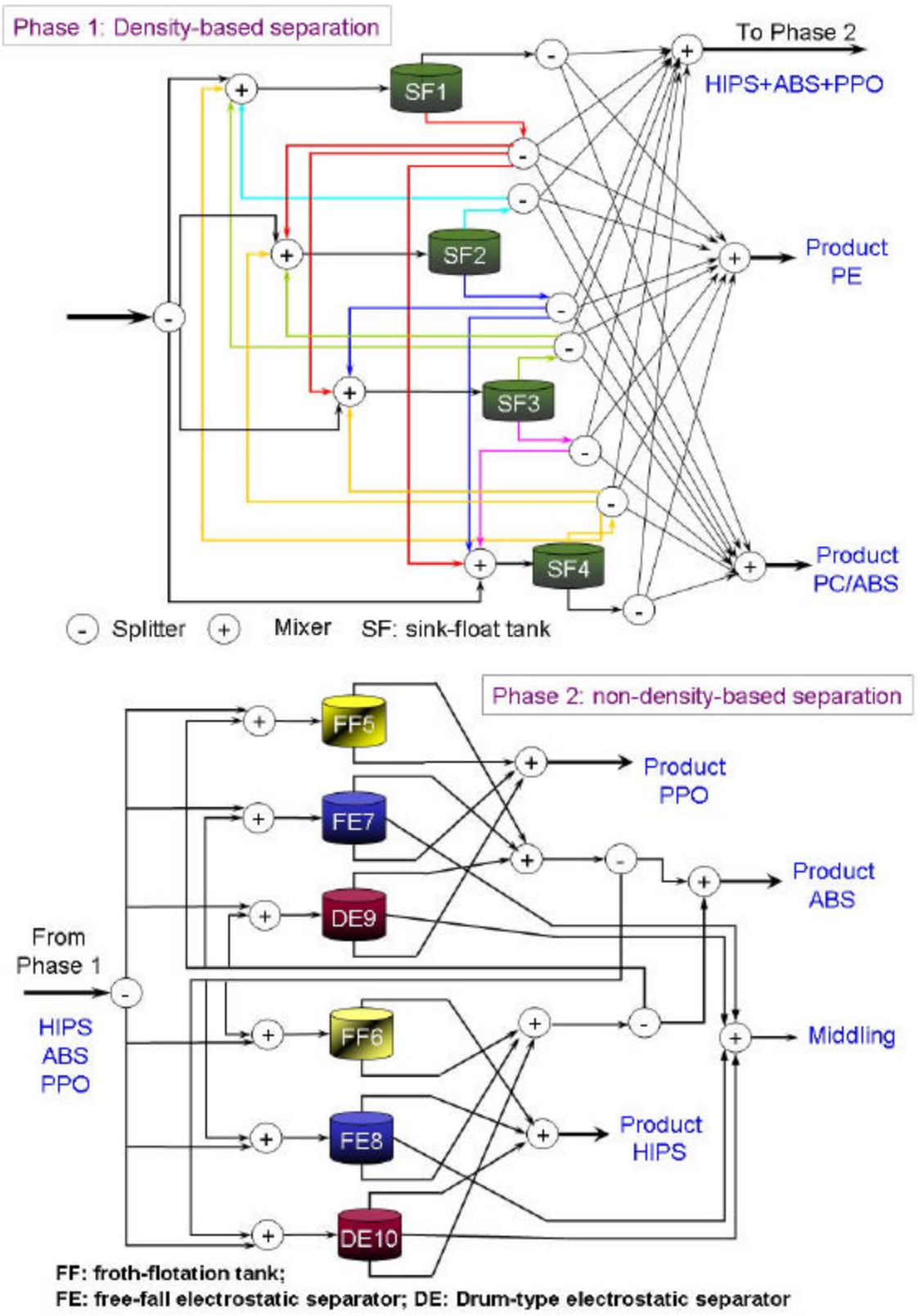

Figure 6.1 The superstructure for the case study.

conditioning or charging technologies exist to change the floatability/charge of component B such that B is non-floatable/ negatively charged in the A/BC or A/B cut and floatable/ positively charged in the AB/C or B/C cut.

b) Second, since the non density-based separations are generally more expensive and complicated, one would want to use as many of the density-based separations as possible and implement them as early in the flowsheet as possible.

c) Third, considering that the sink-float tanks can accept larger particles than the other two separations do, placing the sink float tanks before the froth flotation and electrostatic separations is consistent with the requirement of the order of size reduction steps.

2) For the density-based separation part, the 4 SFs are connected with a combination of parallel and recycle streams, separating the feed into 3 streams based on their density ranges: (A): PE, (BCD): HIPS + ABS+PPO and (E): PC/ABS. This structure allows a choice of the separation sequence: A/BCDE, followed by BCD/E or ABCD/E, followed by A//BCD, and if necessary, a two-stage separation for each cut.

3) Then, the HIPS+ABS+PPO mix is processed further by a non density-based separation system consisting of two subsystems, each equipped with an FF, an FE and a DE, and connected in parallel and recycle fashion. This structure allows the choices of the separation sequence (B/CD+C/D or BC/D+ B/C) and the separation unit (FF, FE or DE) for each cut.

The unit operating conditions, including the medium density, bubble size and diffusion coefficient, and the cost coefficients are shown in Table 6.4.

Table 6.4 Unit operating conditions and cost constants

Unit number		1	2	3	4	5	6	7	8	9	10
Medium density (g/cm^3)		0.98	0.98	1.10	1.12	0.85	0.85	-	-	-	-
Diffusion Coefficient		0.01				0.01					
Bubble size (mm)		-				1.0		-		-	
										-	
Cost	FC ($)	5.0×10^4				7.0×10^4		6.6×10^4		8.5×10^4	
	DC ($/(kg·s^{-1}))	3.5×10^4				4.0×10^4		5.0×10^4		5.5×10^4	
	OC ($/(kg·s^{-1}))	0.06				0.1		0.04		0.05	

6.2 Model Equations and design/operating constraints:

The design and operating variables in the system are shown in Table 6.5.

Table 6.5 The design and operating variables

Unit	Design variables		Operating Variables	
Sink-float	Hc	Height to overflow (m)	Q	Volume flowrate (m^3/s)
	V	Tank volume (m^3)	τ	Residence time (s)
	F_{max}	Maximum flowrate (kg/s)		
Froth flotation	Hc	Height to underflow (m)	Q	Volume flowrate (m^3/s)
	V	Tank volume (m^3)	t	Residence time (s)
	F_{max}	Maximum flowrate (kg/s)		
Free-fall Electrostatic separation	L	Plate length (m)	D	Plate gap (m)
	a	Feeder opening	$Volt$	Voltage (kV)
	W	Plate width (m)	c_l	Left collection bin position (m)
	F_{max}	Maximum flowrate (kg/s)	c_r	Right collection bin position (m)
Drum Electrostatic separation	R_1	Drum radius (m)	ω	Rotating angular velocity (s^{-1})
	W	Drum width (m)	$Volt$	Voltage (kV)
	F_{max}	Maximum Flowrate (kg/s)	R_2	Outer plate radius (m)
			c_l	Left collection bin position (m)
			c_r	Right collection bin position (m)

Table 6.6 shows the notations for variables and parameters that will be used to describe the objective function and constraints in this section.

Table 6.6 Notation for the case study

C_a [i]	The base design cost of unit i at capacity 1000 kg/hr. Therefore, a conversion factor 3.6 appears in the cost term.
C_b [i]	The operating cost of unit i per kg/s of feed processed.
C_c [i]	The fixed capital cost ($) of unit i
D_e	The depreciation (year)
F_p [l,s]	The flowrate (kg/s) of product l at sample s. l=1…6. l=6 for the middling
f_p [p,j,s]	The fraction of component j in product p at sample s.
F_I [i,s]	The feed flowrate (kg/s) to unit i at sample s.
$f_I[i,j,s]$	The fraction of component j in the feed to unit i for sample s
$F_O[i,k,s]$	The flowrate from outlet k of unit i for sample s
$f_O[i,j,k,s]$	The fraction of component j from outlet k of unit i for sample s
$F_{dn}[i_1,i_2,s]$	Downward recycle flowrate from unit i_1 to unit i_2 for sample s
$F_{up}[i_1,i_2,s]$	Upward recycle flowrate from unit i_1 to unit i_2 for sample s
$F_{fresh}[i,s]$	The flowrate of the stream to unit i coming from the fresh feed
F_0	Flowrate of feed to phase 1 (Initial fresh feed)
$f_0[j,s]$	Fraction of component j in the feed to phase 1
$F_2[s]$	Flowrate of feed to phase 2 (also the intermediate stream of HIPS+ABS+PPO)
$f_2[j,s]$	Fraction of component j in the feed to phase 2
$F_{t2}[i,k,s]$	Flowrate of the stream from outlet k of unit i to the intermediate stream of HIPS+ABS+PPO.
F_{max}[i]	The capacity (kg/s) of unit i.
K	The number of outlets K=2 for SFs (i=1 to 4) and 3 for FFs, FEs and DEs (i=5 to 10).
k	Index for outlets (1 for overflow, 2 for underflow, 3 for middling)
M	The number of units (=10 in this case)
N	The number of samples
v[l,s]	The price ($/kg) of product l at sample s.
y_i	Binary variables representing the selection of unit i
γ	A conversion factor to convert the flowrate from kg/s to kg/yr. In this case study, it is assumed that the process is run for 8 hours per day and 200 days per year. Then, γ=3600*8*200.
β	A large number.

Objective function:

The objective is to maximize the average profit, which is the difference of the revenue and the sum of the capital and operating costs. The revenue is the average annual income from selling the recycled products. The capital cost is the annual investment (averaged by depreciation), including a fixed cost plus a design cost which is a function of the capacity. The operating cost is a linear function of the feed flowrate. The interest issue is neglected in this case.

Maximize Profit = Revenue- (Capital cost + Operating cost)

$$Revenue = \frac{1}{N}\sum_{s=1}^{N}\sum_{l=1}^{5} v[l,s]\times F_p[l,s]\times g$$

$$Capital\ cost = \frac{1}{N}\sum_{s=1}^{N}\sum_{i=1}^{M}\frac{1}{D_e}\left\{C_c[i]\times y[i] + C_a[i]\times 3.6\times F_{max}[i]^{0.7}\right\}$$

$$Operating\ cost = \frac{1}{N}\sum_{s=1}^{N}\sum_{i=1}^{M}\left\{C_b[i]\times F_I[i,s]\times g\right\}$$

During the SAA algorithm implementation, the maximization problem is transformed to a minimization problem by placing a minus sign before the objective function. Therefore, in the section, the results reported are negative values.

Constraints:

1) Flow rate balances

<u>For the units</u>:

$$F_I[i,s]\cdot f_I[i,j,s] = \sum_{k}^{K} F_O[i,k,s]\cdot f_O[i,j,k,s], \quad i=1\ldots M;\ \ j=1\ldots 5;\ \ s=1\ldots N$$

$$\sum_{j=1}^{5} f_I[i,j,s] = 1, \qquad i=1\ldots M;\quad s=1\ldots N$$

$$\sum_{j=1}^{5} f_O[i,j,k,s] = 1, \qquad i=1\ldots M;\ \ k=1\ldots4;\ \ s=1\ldots N$$

For the mixers

There are two types of mixers. One is the "feed mixers", mixers to combine the fresh feed and recycles before each unit. Another is the "product mixers", mixers to combine the streams from different outlets to before each product.

For the feed mixers

$$F_I[i,s]\cdot f_I[i,j,s] = F_{fresh}[i,s]\cdot f_0[j,s] + \sum_{i_1=1}^{i-1} F_{dn}[i_1,i,s]\cdot f_O[i_1,j,2,s] + \sum_{i_1=M}^{i+1} F_{up}[i_1,i,s]\cdot f_O[i_1,j,1,s],$$

$i=1,\ldots,M; \quad j=1,\ldots,5; \quad s=1,\ldots,N$

For the product mixers

$$F_p[l,s]\cdot f_p[l,j,s] = \sum_{i=1}^{10} F_{tp}[i,k,l,s]\cdot f_O[i,j,k,s],$$

$l=1,\ldots,6; \quad j=1,\ldots,5; \ k=1,\ldots,4; \quad s=1,\ldots,N$

$$\sum_{j=1}^{5} f_p[l,j,s] = 1 \qquad l=1,\ldots,6; \quad s=1,\ldots,N$$

$$F_2[s]\cdot f_2[j,s] = \sum_{i=1}^{4} F_{t2}[i,k,s]\cdot f_O[i,j,k,s]$$

$$\sum_{j=1}^{5} f_2[j,s] = 1 \qquad s=1,\ldots,N$$

For the splitters

There are also generally two types of splitters. One is the "feed splitter", splitters

to separate the fresh feed to several streams fed to the units. Another is the "outlet splitter", splitters to separate each unit outlet stream into an upward or downward recycle and a stream to each product.

For the feed splitter

$$F_0 = \sum_{i=1}^{4} F_{fresh}[i,s] \qquad s=1,..,N$$

$$F_2[s] = \sum_{i=5}^{10} F_{fresh}[i,s] \qquad s=1,..,N$$

For the outlet splitter

$$F_O[i,k,s] = \sum_{i_2=i+1}^{10} F_{dn}[i,i_2,s] + \sum_{i_2=1}^{i-1} F_{up}[i,i_2,s] + \sum_{l=1}^{6} F_p[l,s],$$

$$i=1,..,M;\ k=1,..,4;\ s=1,..,N$$

Note: The above equations for mixers and splitters are just general representations and should be modified appropriately for each one according to the superstructure used.

2) Unit design models (Equations from chapter 4)

For sink-float units: Equations (4.1) (4.11) (4.14) (4.17) (4.19)

For froth-flotation units: Equations (4.1) (4.29-4.34)

For free-fall electrostatic separation units: Equations (4.1) (4.38) (4.40-4.41)

For drum electrostatic separation units: Equations (4.1) (4.42-4.46) (4.49- 4.50)

3) Other design and operating specifications

Solid volume fraction: *F/Q /1000 £ 0.3*

Height to overflow (m): *0.5 £ Hc £ 2.0*

Tank volume (m^3)	$0.5 \pounds V \pounds 10$
Volume flowrate (m^3/s)	$0 \pounds Q$
Residence time (s)	$5 \pounds t$
Tank height (m):	$0.5 \pounds H \pounds 3.0$
Plate width (m):	$0.5 \pounds W \pounds 2.0$
Plate gap(m):	$0.1 \pounds D \pounds 1.0$
Voltage (kV):	$10 \pounds Volt \pounds 100$
Angular velocity (rad/s)	$0.1 \pounds w \pounds 50$
Drum radius (m)	$0.1 \pounds R_1 \pounds 1.0$
Outer plate radius (m)	$0.2 \pounds R_2 \pounds 3.0$
Half-feeder width (m)	$0.1 \pounds a$
Capacity (kg/s)	$F_{max} \pounds 2$

4) Product purity requirement: $f_p[l,l,s] \geq 0.95, \quad l=1,\ldots,5; \ s \text{ in } 1,\ldots,N$

5) Selection of units: $F_I[i,s] \leq y_i b, \quad i=1 \ldots M; s=1 \ldots N$

6) Capacity: $F_I[i,s] \leq F_{max}[i], \quad i=1 \ldots M; s=1 \ldots N$

6.3 The non-convexity issue

The nonconvexities of this problem mainly come from the bilinear terms of flow rate balances for the units and the mixers, and also the unit models. Then, it can not be guaranteed that the global optimum of the solution found for NLP subproblems by SNOPT. Moreover, the linearizations in the master problem may not give a valid lower bound. One approach to solve the issue is to use the methods of global optimization. In

our research, the heuristic strategy (Viswanathan and Grossmann, 1990) with the aim of reducing the effect of nonconvexities on generating lower bounds in master problems is applied.

This approach introduced slack variables in the master problem which has the following form shown in (MILP-APER)

$$
\begin{aligned}
& min\ Z^K = a + \sum_{k=1}^{K} w_p^k p^k + w_q^k q^k \\
& s.t. \quad a \geq f\left(x^k, y^k\right) + \nabla f\left(x^k, y^k\right)^T \begin{bmatrix} x - x^k \\ y - y^k \end{bmatrix}, \quad k = 1,...,K \\
& \quad T^k \nabla h\left(x^k, y^k\right) \begin{bmatrix} x - x^k \\ y - y^k \end{bmatrix} \leq p^k, \quad k = 1,...,K \\
& \quad \mathrm{g}\left(\mathrm{x}^k, y^k\right) + \nabla g\left(x^k, y^k\right)^T \begin{bmatrix} x - x^k \\ y - y^k \end{bmatrix} \leq q^k, \quad k = 1,...,K \\
& \quad \sum_{\mathrm{i} \in \mathrm{B}^k} y_i - \sum_{i \in N^k} y_i \leq \left|B^k\right| - 1, \quad k = 1,...,K \\
& \quad x \in X, y \in Y, p^k, q^k \geq 0
\end{aligned}
\qquad \text{(MILP-APER)}
$$

Where w_p^k, w_q^k are weights that are chosen sufficiently large; $T^k=\{\mathrm{sign}(\lambda_i^k)\}$ in which λ_i^k is the multiplier associated with the equation $h_i(x,y)=0$.

6.4 Lagrangian decomposition

The smaller NLP problems have the following form with the discrete variables already fixed.

$$
\begin{aligned}
& \underset{x, z_i}{min} \ \frac{1}{N} \sum_{i=1}^{N} f\left(x, z_i\right) \\
& s.t. \quad g_i\left(x, z_i\right) \leq 0 \quad \mathrm{i} = 1, \cdots, \mathrm{N} \\
& \quad x \in X, z_i \in Z
\end{aligned}
$$

Due to the existence of the continuous decision variables x, the scenarios are coupled and

the problem has a block diagonal structure shown in Figure 6.2. Solving such a problem as a whole without any decomposition is time-consuming and may result in out of memory errors if the sample size, number of constraints and variables are very large.

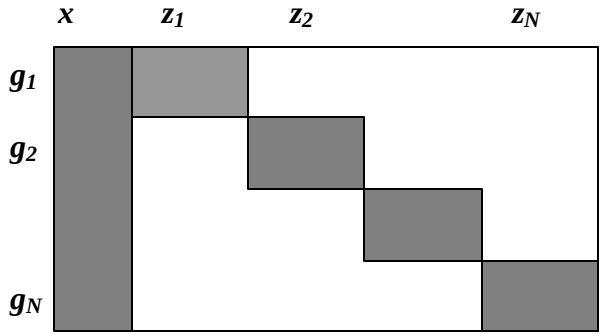

Figure 6.2 The block diagonal structure of the smaller NLPs

However, the special structure of the problem can be exploited to decouple the scenarios and solve the problem in an iterative way until the decision variables x solved at each scenario converge to the same value. This can be done by first splitting the decision variable x into N variables x_i ($i=1, \cdots, N$) and then applying Lagrangian Relaxation (Fisher, 1981; Guignard and Kim, 1987) to the copy constraints $x = x_i$. This is called Lagrangian Decomposition .

$$\begin{aligned} \min_{x,x_i,z_i} \ & \frac{1}{N}\sum_{i=1}^{N} f_i(x_i, z_i) \\ s.t. \ & g_i(x_i, z_i) \le 0, \ i = 1,\cdots,N \\ & x = x_i, \ i = 1,\cdots,N \\ & x, x_i \in X, z_i \in Z \end{aligned}$$

The Lagrangian of the above problem is

$$L = \frac{1}{N}\sum_{i=1}^{N} f_i(x_i, z_i) + \sum_{i=1}^{N} m_i g_i + \sum_{i=1}^{N} p_i(x - x_i)$$

Theoretically, if the problem is convex and the variables are continuous, the original

problem is equivalent (in terms of the optimal objective value) to solving the following LD problem:

$$\max_{p_i}\left[\min_{x_i,x}\left\{\frac{1}{N}\sum_{i=1}^{N} f_i(x_i,z_i)+\sum_{i=1}^{N} p_i(x-x_i)\;\middle|\; g_i(x_i,z_i)\le 0, x, x_i\in X, z_i\in Z\right\}\right] \qquad \text{(LD)}$$

However, a duality gap might exist in this case due to the non-convexities of the problem. Therefore the solution of LD provides a lower bound to the original problem. Any feasible solution to the original problem is an upper bound. Typically a sub-gradient method is used to update the multipliers to provide the tightest lower bound.

Then, the problem can be solved in an iterative way (Wu and Ierapetritou, 2003):

Step1: Pick any π_i values, for i=1,…,N, solve the following decoupled sub-problems and denote the solutions for x_i as $\hat{x}_i$

$$\begin{aligned} P_i = \min_{x_i,z_i}\ & \frac{1}{N} f_i(x_i,z_i) - p_i x_i \\ s.t.\ \ & g_i(x_i,z_i)\le 0 \\ & x_i\in X, z_i\in Z \end{aligned}$$

and solve the following problem for x and denote the solution as $\hat{x}$

$$\begin{aligned} Q = \min_{x}\ & \sum_{i=1}^{N} p_i x \\ s.t.\ \ & x\in X \end{aligned}$$

Therefore $LB=\sum_i^N P_i + Q$ provides a lower bound. The initial π_i values used in the case study are 0.01.

Step2: Find a feasible solution as the upper bound UB. If the difference of the upper and

lower bound is sufficiently small:

$$\left|\frac{UB-LB}{LB}\right| < e\,, \qquad \varepsilon=0.02 \text{ in this case study}$$

or the maximum iteration number (=10 in this case study) is reached, the algorithm stops; otherwise go to Step3 to update the multipliers.

Step 3: Use the subgradient method to update the multipliers:

$$p_i^{k+1} = p_i^k + t_k\left(\hat{x} - \hat{x}_i\right)$$

$$t_k = \frac{b^k\left(UB-LB\right)}{\sum_{i=1}^{N}\left(\hat{x}-\hat{x}_i\right)^2}$$

where b^k is a scalar (0~1) and is decreased (by a factor of 1.05 in this case study) when there is no improvement of the objective value (i.e., LB). Return to Step 1 and repeat with new values of π_i.

(End)

A smaller MILP can be solved as a whole within relatively reasonable time, compared to the solution time of a smaller NLP, therefore, the above decomposition method was applied to the smaller NLPs only.

6.5 Results

The problem was solved with AMPL CPLEX 8.1 and SNOPT 5.3-4 on a PC with 2.53GHz CPU and 1G memory. All the objective values reported below have been scaled by 1E-6 (i.e., have the units of million dollars). Starting with (0110111111) for the binary

variables, the optimal solution was reached at the 2nd iteration (0100001100) with an optimal objective value -3.622. One sink-float tank and two free-fall electrostatic separators are selected and the corresponding optimal design is shown in Table 6.7.

Table 6.7 Case study result – Design variables

	SF2	FE7	FE8
Hc (m)	0.5	-	-
V (m^3)	10	-	-
F_{max} (kg/s)	1	0.758	0.996
R_1 (m)	-	-	-
W (m)	-	2	2
a (m)	-	0.3	0.23
L (m)	-	3	3

Lagrangian decomposition result

The Lagrangian decomposition problems can in general converge within 2 iterations with initial multiplier values 0.01. For example, at the first iteration, the lower bound generated by Lagrangian decomposition is -3.592 and the upper bound by the heuristic rule is -3.481. The stopping rule is not satisfied so the multipliers are adjusted by the subgradient method described in the previous section. At the second iteration, the lower bound is -3.524 and the upper bound is -3.500. Since the relative difference of these two values is with 2%, the Lagrangian decomposition procedure is considered to have converged. Therefore, despite of the nonconvexities in the nonlinear problems, the duality gaps are negligible.

As a heuristic rule to find an upper bound, the variables *x* are fixed at the maximum of the $\hat{x}_i$ values found in step1 and then the problem is solved again. This heuristic rule can provide a fairly tight upper bound and also the values of the decision

variables for the larger NLP.

If the initial multiplier values are increased to 0.1, the number of iterations for the convergence will increase to 6. Due to the fact that the previous Lagrangian multiplier values are used as the starting point for all next replications, they converge only after one iteration.

Comparison between the uncertain and the average conditions

The deterministic case under the average condition (feed fraction and product prices) is also solved and the optimal flowsheet is shown in Figure 6.3.

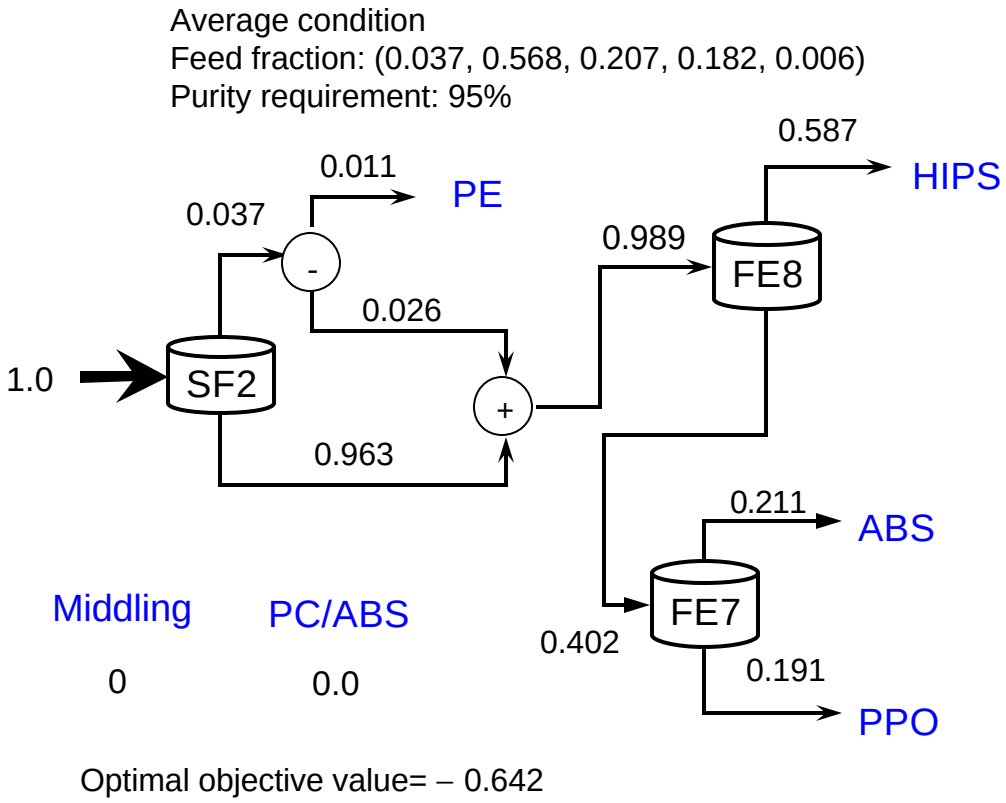

Figure 6.3 Optimal flowsheet of the deterministic case with 95% purity

The optimal objective value is -3.642, which is slightly better than that of the uncertain case, and the choices of the units are the same as in the uncertain case (Table 6.8). Clearly there is no difference between the uncertain and the average conditions in terms of the choice of units (i.e., flowsheet structure) because the variation in the feed composition has no influence on the unit separation efficiencies. However, from Table 6.8 it can be seen that the capacity (F_{max}) of the second free-fall electrostatic separator designed under the average condition is not feasible for the uncertain case since in the latter this unit processes much larger volumes of flow for many scenarios than in the average condition.

Table 6.8 Comparison of the uncertain and average condition

	Under uncertainty	Average condition
Objective value	-3.622	-3.642
Choice of units	(0100001100)	(0100001100)
Capacity of unit 2	1.0	1.0
Capacity of unit 7	0.758	0.402
Capacity of unit 8	0.996	0.989

SAA Computational efficiency and the confidence of the solution

The computational time with the SAA method was 5 hours and 45 minutes. The computational saving is apparent compared with using a fixed sample size of 2000. Since at each OA iteration, the former requires solving 3400 single-size NLPs/MILPs (assuming the Lagrangian decomposition converges with 2 iterations for the first replication and 1 iteration for all other replications) and the latter requires solving 8000 single-size NLPs/MILPs (assume the Lagrangian decomposition converges with 2

iterations) .

Intuitively one would think that such a problem with uncertainty dimension=10 should require very large sample sizes. However, our calculation result (Table 6.9) showed that the problem can be solved with small sample sizes (smaller sample size N=100, number of replications M=6, and larger sample size N'=2000) but still achieve high solution quality. The confidence intervals (99%) of the upper and lower bound at both iterations are less than 0.077, which is only around 2% of the optimal objective value. This is due to the fact that the variances of the feed component fractions in this case study do not have a significant impact on the configuration of flowsheet and costs.

Table 6.9 Case study result – confidence intervals of optimality gaps
(with N=100, M=6, N'=2000)

		Iteration 1 (0110111111)	Iteration2 (0100001100)
S-NLP	Mean of UB	-3.556	-3.660
	Variance of UB	0.0018	0.0023
L-NLP	Mean of UB	-3.545	-3.622
	Variance of UB	0.0891	0.0881
	Mean of UB gap	0.011	0.038
	CI of UB gap	**0.0708**	**0.103**
S-MILP	Mean of LB	-3.775	-3.675
	Variance of LB	4.09e-4	4.11e-4
L-MILP	Mean of LB	-3.753	-3.583
	Variance of LB	0.00893	0.00917
	Mean of LB gap	0.022	0.092
	CI of LB gap	**0.0576**	**0.0761**

6.6 Conclusions

The case study is an attempt to solve a plastics flowsheet optimization problem with the SAA method. It is also a good example to show that some apparently large

problems actually do not require large sample sizes if the variance of solutions is small. The SAA method helps to evaluate the solution and make a decision whether it is necessary to increase the sample sizes. In this case study, since ABS and HIPS dominate in both TV and computer products, and PE and PC/ABS are in relatively small fractions, the uncertainty in the feed fraction caused by the variation in the volumes of the products does not change the flowsheet structure compared to the average condition, however, the unit capacities are under-designed in the average condition.

CHAPTER 7

SUMMARY AND FUTURE WORK

7.1 Summary

Before this work, no systematic design methodology has been proposed for the bulk recycling system design problem. Most of existing work has focused on individual experimental technologies or overall recycling strategies without using detailed unit models. The two levels of design, system and unit, were isolated in the past, which is a gap of this research seeks to fill.

The objective of this work is not to provide a single optimal process, since the solution is always problem-specific, but to develop a general methodology for the design of bulk recycling systems that can identify optimal flowsheets with confidence.

While the research scope is limited to the plastics separation part of the flowsheet, it is a real challenge to design a plastics separation system that can separate a mix of various products in arbitrary fractions. Significant uncertainty in the feed is an intrinsic problem in the bulk recycling systems.

Successfully applications of various process systems approaches to typical chemical systems design motivated us to consider bulk recycling process design problems in a similar way. This leads to the use of the superstructure approach to determine the optimal plastics separation sequence. However, the feature of significant uncertainties and use of a combination of different separation methods made extending the classical process systems approaches to bulk recycling a significant challenge.

First, the existence of various uncertain parameters makes the solution of a

stochastic MINLP time-consuming. When the sample size is greater than 100, the stochastic NLP problem can not be solved as a whole, thus, requiring a decomposition method. Moreover, when the uncertainty space is large, it is crucial to make the sample size as small as possible, but still achieve a certain solution quality. Previous work in the MINLP area uses a pre-specified sample size, fixed by the size of the problem, that can be solved in a reasonable time frame. The sample size used could be over or under estimated and there have been no criteria to evaluate this. Therefore, an efficient and reliable solution technique for stochastic MINLP became a focus of this work, both to improve computational efficiencies and thus address more significant problems, and to guarantee the solution quality.

Motivated by existing work of sample average methods in the stochastic LP or IP area (Norkin et al., 1998; Mak et al., 1999; Kleywegt et al., 2001), the sample average method for stochastic MINLPs is proposed, which combines the basic SAA method of constructing the confidence interval of optimality gap and the Outer Approximation method for deterministic MINLPs. The method uses the average of replicates of NLP and MILP solutions at a smaller sample size as the lower estimates of the upper and lower bounds, respectively. Solutions of the NLP and MILP at a larger sample size, with fixed decision variables, are used as the upper estimates of the upper and lower bounds. The difference of the upper and lower estimates provides the mean of the optimality gap, and the confidence interval of the optimality gap can be calculated accordingly, from which the sample sizes can be adjusted. Therefore, computational time can be reduced significantly due to the decoupled larger problems. When the uncertainty space is very large, say the number of parameters is greater than 20, it might be useful to use quasi-

Monte-Carlo sampling, such as the Latin Hypercube Sampling (Mckay et al., 1979) or Latin Supercube Sampling (Owen, 1998). These methods take advantages of the low discrepancy of quasi-Monte-Caro sequences (Sobal sequence, Hammersley Sequence, etc.) to generate samples that converge more rapidly to the true distributions.

When the uncertainty space in bulk recycling problems is further enlarged, for example, including parametric uncertainties such as the correlation coefficients in the empirical unit models, the problem size or the solution time is not expected to increase exponentially. The SAA method allows one to solve larger design under uncertainty problems without intractable computational difficulty.

Another focus of this work is plastics separation unit modeling, which is complicated by the fact that the feed particles do not have the same properties, an inevitable result of size reduction, conditioning and triboelectrification processes. Previous modeling work in this area was mostly empirical, based on experimental results, and ignored the influence of the particle differences. The proposed new models directly relate the particle distribution with the separation efficiency, therefore providing a basis to improve the separation efficiency by particle control. It is not intended to model every possible separation method. Instead, a few typical methods are modeled in a unified approach, which allows others to follow and model units of their own interests.

With the SAA method for MINLPs and unit models developed, more realistic plastics separation systems design problems can be solved. The case study in Chapter 6 shows a successful application of the mathematical programming approach for the design of a plastics separation system for a mixture of TVs and Computers with uncertain mixing fractions and product prices.

The influence of particle size distribution on the separation efficiency is also discussed based on the unit models developed. The result shows that more grinding favors the froth flotation and electrostatic separation, but not the sink-float separation because in the former the influence of the size reduction overcomes that of the size variance on the separation efficiency. This justifies the use of a separation system with density-based separation first, followed by non density-based separations. An overall design strategy is proposed for the size reduction and plastics separation system. In the strategy, the idea of the Douglas' hierarchical design method is used to decompose the problem into two levels. At the level of size reduction design, the short cut design method proposed in Chapter 4 is first used to determine the appropriate mean particle size at each stage. Heuristic rules are then developed to select the size reduction equipment and at last determine the appropriate grinding time by simulation based on population balance equations. At the level of plastics separation, the particle sizes at different stages are fixed, and the mathematical programming approach is used to solve for the optimal flowsheet from the superstructure. Therefore, this overall design strategy is a combination of heuristics and optimization.

In conclusion, this work solved some critical issues (uncertainty, modeling) in the design of bulk recycling problems and developed a design strategy that allows others to find customized optimal processes. This work is not only the first approach of systematic design for bulk recycling problems, but also a successful example of how the process systems approach is extended to the bulk recycling area.

7.2 Recommendations for future work

Future work on the unit modeling, algorithm and overall bulk recycling systems design that could have the most impact include the following issues.

Unit modeling in this research assumes a normal distribution of particle size. Models could be developed with a more accurate description of particle size distribution, such as a lognormal distribution, with possibly the time factor as a parameter to reflect the evolution. If such a mathematical distribution is available, the size reduction units can be incorporated into the superstructure.

A barrier that prevents us to run a case study for a complete bulk recycling system in this work is the lack of particle property data, such as the grinding data (k_0 and α in Equation 5.2), the distribution of particle charges, bubble coverage, diffusion coefficient etc. It would be a great contribution if future experimental work could follow the unified modeling approach and measure the above data.

For SAA algorithm improvement, using quasi-Monte-Carlo sampling for high dimension of uncertainty space could make it converge faster. These methods use the quasi-Monte-Carlo sequences which are actually fixed sequences of points. Some new issues arise and need further study:

(1) Some sequences are not incremental, i.e., they increase the number of samples and discard the samples already drawn. For example, Halton and Sobol sequence are incremental but Hammersley sequence is not. Therefore, the Hammersley sequence is not good for adaptive sampling.

(2) For correlated uncertainties, the random nature of Monte-Carlo sampling allows one to take a part of samples but still maintain the right correlation. This might not be the

case for Quasi-Monte-Carlo sampling. It is would be important to know how samples can be added without disrupting the correlation structure.

(3) It is not clear at this point whether the existing statistical results for Monte-Carlo based SAA can be extended to Quasi-Monte-Carlo based SAA.

For the overall bulk recycling systems design, some strategy is to be developed for making top level decisions, such as the choice (as shown in Figure 1.3) between processing the mix of different products continuously and processing different products in a batch mode without mixing. For a specific problem, basically one can solve the two problems independently and then compare the costs. However, it is probably possible to make a decision based preliminary estimation of the costs of the two options, without solving the strict optimization problems.

REFERENCES

Acevedo, J. and Pistikopoulos, E.N. 1996, Computational studies of stochastic optimization algorithms for process synthesis under uncertainty, *Computers and Chemical Engineering*, 20, S1.

Acevedo, J. and Pistikopoulos, E.N. 1998, Stochastic optimization based algorithms for process synthesis under uncertainty, *Computers and Chemical Engineering*, 22, 647.

Aksani, B. and Sonmez, B., 2000, Simulation of bond grindability test by using cumulative based kinetic model, *Minerals Engineering*, 13, 673.

APC report, 1999, American Plastics Council, Durables Recycling, http://www.plasticsresource.com/s_plasticsresource/sec.asp?TRACKID=&DID=269&CID=164&rcss=print

APC report, 2000, American Plastics Council, Plastics from residential electronics recycling, http://www.plasticsresource.com/s_plasticsresource/view.asp?DID=391&CID=174

Austin, L.G., Bhatia, K., Jindal, V., and Savage, K., 1976, Some results on the description of size reduction as rate process in various mills, *Industrial Engineering Chemistry Process Design and Development*, 15, 187.

Bernardo, F. P., Pistikopoulos E. N. and Saraiva P. M., 1999, Integration and computational issues in stochastic design and planning optimization problems, *Industrial and Engineering Chemistry Research*, 38, 3056.

Birge, J.R. and Louveaux, F., 1997, *Introduction to Stochastic Programming*, Springer Ser. Oper. Res., Springer-Verlag, NewYork, NY.

Botsch M. and Köhnlechner, R., 1997, Electrostatic separation and its industrial application for the processing of different mixtures of recycling materials, *Proceedings of the XX IMPC-Aachen, 21-26 September*, 297.

Buekens and Huang, 1998, Catalytic plastics cracking for recovery of gasoline-range hydrocarbons from municipal plastic wastes, *Resources, Conservation and Recycling*, 23, 163.

CarØe, C. C. and Schultz, R., 1999, Dual decomposition in stochastic integer programming, *Operations Research Letters*, 24, 37.

Coghill, W and Devaney, F.D., 1937, Ball-mill grinding, US Bureau of Mines, Technical paper, 581.

Cui, J. and Forssberg, E. 2002, Mechanical recycling of waste electric and electronic equipment: a review, *Journal of Hazardous Materials*, 99(3), 243.

Das, P.K, 2001, Use of cumulative size distribution to back-calculate the breakage parameters in batch grinding, *Computers and Chemical Engineering*, 25,1235.

Datta, A. and Rajamani, R.K., 2002, A direct approach of modeling batch grinding in ball mills using population balance principles and impact energy distribution, *Int. J. Mineral Processing*, 64, 181.

Douglas, J.M., 1988, *Conceptual Design of Chemical Processes*, New York: McGraw-Hill

Doherty, M.F. and Malone, M.F., 2001, *Conceptual Design of Distillation Systems*, New York: McGraw-Hill.

Duran, M.A. and Grossmann I. E. 1986, An Outer-Approximation algorithm for a class of mixed integer nonlinear programs, *Mathematical Programming*, 36 , 307.

EPA report, 1999, United States Environmental Protection Agency, Analysis of Five Community Consumer/Residential Collections: End-of-life Electronic and Electrical Equipment, April, EPA-901-R-98-003;
http://www.epa.gov/Region1/programs/csifinal.pdf

Finch, J. A. and Dobby, G. S., 1990, *Column Flotation*, Pergamon Press.

Fisher, M.L., 1981, The Lagrangean relaxation method for solving integer programming problems, *Management Science*, 27,1.

Fisher, M.M. and P. Peuch, 1998, "Plastics in Electronic Equipment - Quantifying the US and European Marketplace," presented at the Society of Plastics Engineers Annual Recycling Conference, November 11-13.

Fletcher, R. and Leyffer, S. (1994). Solving mixed integer nonlinear programs by outer approximation, *Mathematical Programming*, 66, 327.

Fourer, R., D. M. Gay, and B. W. Kernighan, 1993, *AMPL, A modelling language for mathematical programming*, Boyd and Fraser, Danvers, MA.

Fraunholcz, N., Dalmijn W.L., 1997, Wetting mechanisms in the flotation of plastics, *Proceedings of the XX International mineral processing congress*, Aachen, Germany, 5, 329.

Gao, M and Forssberg, E., 1995, Prediction of product size distributions for a stirred ball mill, *Powder Technology*, 84, 101.

Guignard, M. and Kim, S., 1987, Lagrangean decomposition: a model yielding stronger Lagrangean bounds, *Mathematical Programming*, 39, 215.

Gill, P.E., W. Murray and M. Saunders,1997, *SNOPT: An SQP algorithm for large-scale constrained optimization,* Report NA 97-2, Department of Mathematics, University of California, San Diego, CA.

Grossmann I. E. and K. P. Halemane, 1982, Decomposition strategy for designing flexible chemical plants. *AIChE J.* 12, 686.

Grossmann I. E., K. P. Halemane and R. E. Swaney, 1983, Optimization strategies for flexible chemical Processes, *Computers and Chemical Engineering*, 7, 439.

Grossmann, I. E. and R. W. H. Sargent, 1978, Optimum design of heat-exchanger networks, *Computers and Chemical Engineering,* 2, 1

Guern, C. L., Conil, P. and Houot R., 1997, Physico-chemical separation (flotation) of plastic waste before cycling, *Proceedings of the XX IMPC* –Aachen, Sept., 21-26

Halemane K. P. and Grossmann I. E. 1983, Optimal process design under uncertainty, *AIChE J*., *29*, 425.

Ham, J.M., and Homsy, G.M., 1988, Hindered Settling and hydrodynamic diffusion in quiescent sedimenting suspensions, *Int. J. Multiphase Flow*, 14, 533.

Higashiyama, Y., Y. Ujiie and K. Asano, 1997, Triboelectrification of plastic particles on a vibrating feeder laminated with a plastic film, *Journal of Electrostatics*. 42, 63.

Higle, J.L. and Sen, S. , 1991, Stochastic decomposition: an algorithm for two-stage linear programs with recourse, *Mathematics of Operations Research*, 16, 650.

Hoyer D. I, 1995, Batch grinding simulation – population balance models and self-similar size distributions, *Mineral Engineering*, 8(11) 1275.

Inculet I.I., Castle G.S.P. and Brown J.D., 1998, Electrostatic separation of plastics for recycling, *Particulate Science and Technology*, 16, 91.

Inculet, I. I.,1984, *Electrostatic Mineral Separation*, Research studies press, Wiley & Sons.

Jody B., Arman, B., Karvelas, D.E., Pomykala, J.A., Daniels, E.J., 1997, US patent 5653867, Method for the separation of high impact polystyrene (HIPS) and Acrylonitrile butadiene styrene (ABS) plastics.

Kalagnanam, J. R. and Diwekar, U. M., 1997, An efficient sampling technique for off-line quality control. *Technometrics*, 39, 308.

Kamptner, A., Mientkewitz, O., and Schubert, G., 1997, The electrostatic separation of PVC containing waste, *Proceedings of the XX IMPC*-Aachen, 21-26 September. 403.

Kelly, E.G., and Spottiswood, D.J., 1982, *Introduction to Mineral Processing*, John

Wiley & Son, Inc., New York.

Kesavan, P. and Barton, P.I. 2000. Generalized branch-and-cut framework for mixed-integer nonlinear optimization problems, *Computers and Chemical Engineering*, 24, 1361.

Kim, Ki-Joo and Diwekar, U. M. 2002. Efficient Combinatorial Optimization under Uncertainty. 1. Algorithmic Development, *Industrial and Engineering Chemistry Research*, 41, 1276.

King, A.J. and Rockafellar, R.T., 1993, Asymptotic theory for solutions in statistical estimation and stochastic programming, *Mathematics of Operations Research.*,18, 148.

King, R.P., 1972, An analytical solution to the batch comminution equation, *J. South Afr. Inst. Min. Met.*, 127.

Kleywegt, Anton J., Alexander Shapiro and Tito Homem-De-Mello, 2001, The Sample Average Approximation Method for Stochastic Discrete Optimization, *SIAM Journal On Optimization, 12*, 479.

Kunii, D. and Levenspiel, O., 1991, *Fluidization Engineering*, 2nd ed., Butterworth-Heinemann, Boston, MA.

Kwetkus, B. A.,1998, Particle triboelectrification and its use in the electrostatic separation process, *Particulate Science and Technology*, 16, 55

Laso, M., 1994, Stochastic dynamic approach to transport phenomena, *AIChE J.*, 40(8), 1297.

Leva, M., 1951, Elutriation of fines from fluidized systems, *Chemical Engineering Progress*, 47, 39.

Linderoth, J., Shapiro, A. and Wright, S., 2002, The empirical Behavior of Sampling methods for stochastic programming, *Optimization Online*, http://www.optimization-online.org/DB_HTML/2002/01/424.html

Loehr, K. and Melchiorre, M., 1996, liberation of composite waste from manufactured products, *Int. J. Miner. Processing*, 44-45, 143.

Lowell J. and Rose-Innes, A.C., 1980, Contact electrification, *Advances in Physics*, 29(6), 947.

Mak, W.K. , Morton, D.P. and Wood, R.K. ,1999, Monte Carlo bounding techniques for determining solution quality in stochastic programs, *Operational Research Letters*, 24, 47.

Martin, J., Rakotomalala, N. and Salin, D., 1995, Hydrodynamic dispersion of noncolloidal suspensions: measurement from Einstein's Argument, *Physical Review Letters*, 74(8), 1347.

Mckay M.D., R. J. Beckman and W. J. Conover, 1979, A comparison of three methods of selecting values of input variables in the analysis of output from a computer code, *Technometrics*, 21(2), 239.

Mihailescu, M, A. Samuila, A. Urs, R. Morar, and A. Iuga, 2000, Computer-assisted experimental design for the optimization of electrostatic separation processes, *Conference Record IAS Annual Meeting* v1, IEEE Piscataway NJ USA 687.

Molina-Boisseau, S. and Bolay, N.L., 2000, Size reduction of polystyrene in a shaker bead mill—kinetic aspects, *Chemical Engineering Journal*, 79, 31.

Napier-Munn, T.J., 1991, Modelling and Simulating Dense Medium Separation Processes – A Progress Report, *Minerals Engineering*, 4(3/4), 329.

Nicolai, H., Herzhaft, B., Hinch, E.J., Oger, L., and Guazzelli, E., 1995, Particle velocity fluctuations and hydrodynamic self-diffusion of sedimenting non-Brownian spheres, *Phys. Fluids*, 7(1), 12.

Norbert, R. and S. Ingo, 1997, Tubular free-fall separator for separating plastic mixtures, *U.S. Patent 5687852*, Nov., 18.

Norkin, W. I., Pflug, Georg Ch. and Ruszczynski, A., 1998, A Branch and Bound

Method for Stochastic Global Optimization, *Mathematical Programming*, 83, 425.

Novak Pintaric, Z. and Kravanja, Z., 2000, The two-level strategy for MINLP synthesis of process flowsheets under uncertainty, *Computers and Chemical Engineering*, 24, 195.

Novak, Z. and Kravanja Z., 1999, Mixed-integer nonlinear programming problem process synthesis under uncertainty by reduced dimensional stochastic optimization, *Industrial and Engineering Chemistry Research*, *38*, 2680.

Owen, A.B., 1998, Latin supercube sampling for very high-dimensional simulations, *ACM Transactions on Modeling and Computer Simulation*, 8(1), 71.

Paules, G.E. and Floudas, C. A. ,1992, Stochastic programming in process synthesis: a two-stage model with MINLP recourse for multiperiod heat-integrated distillation sequences. *Computers and Chemical Engineering*, *16*, 189.

Pistikopoulos, E. N., and Grossmann, I. E., 1989a, Optimal retrofit design for improving process flexibility in nonlinear systems—I. Fixed degree of flexibility, *Computers and Chemical Engineering.*, 13, 1003.

Pistikopoulos, E. N., and Grossmann, I. E., 1989b, Optimal retrofit design for improving process flexibility in nonlinear systems—II. Optimal level of flexibility, *Computers and Chemical Engineering*, 13, 1087.

Pistikopoulos, E.N., 1995, Uncertainty in process design and operations. *Computers and Chemical Engineering*, 19, s553

Pistikopoulos, E. N. and Ierapetritou, M. G., 1995, A novel approach for optimal process design under uncertainty, *Computers and Chemical Engineering*, 19, 1089.

Raman, R. and I.E. Grossmann, 1994, Modeling and Computational Techniques for Logic Based Integer Programming, *Computers and Chemical Engineering*, 18, 563.

Ramkrishna, D., 1971, Solutions of population balance equations, *Chemical Engineering Science*, 26, 1134.

Ramkrishna, D., 1985, The status of population balances, *Review Chemical Engineering*, 3, 49.

Raspanti, C. G., Bandoni, J.A. and Biegler, L. T. 2000, New strategies for flexibility analysis and design under uncertainty, *Computers and Chemical Engineering*., 24, 2193.

Reimer, B., Sodhi, M.S. and Knight, W.A., 2000, Optimizing electronics end-of-life disposal costs, *IEEE International Symposium on Electronics and the Environment*, 342.

Rios P, Stuart J.A., and Grant E., 2003, Plastics disassembly versus bulk recycling: Engineering design for end-of-life electronics resource recovery, *Environ. Science and Technology*, 37, 5463.

Shapiro, A. and Homem-de-Mello, T., 2000, On rate of convergence of Monte Carlo approximations of stochastic programs, *SIAM J. Optimization*, 11, 70.

Shapiro, A., 1991, Asymptotic analysis of stochastic programs, *Annals of Operations Research*, 30, 169.

Shen H., Pugh, R.J., Forssberg, E., 1999, A review of plastics waste recycling and the flotation of plastics, *Resources, Conservation and Recycling*, 25, 85.

Shen, H., Forssberg, F. and Pugh, R.J., 2001, Selective flotation separation of plastics by particle control, *Resources, conservation and recycling*, 33, 37.

Shibata, J., Matsumoto S., Yamamoto, H., Kusaka, E., Pradip, 1996, Flotation separation of plastics using selective depressants, *International. Journal of Mineral Processing*, 48, 127.

Smolders, K. and Baeyens, J., 1997, Elutriation of fines from gas fluidized beds: mechanisms of elutriation and effect of freeboard geometry, *Powder Technology*, 92, 35.

Sodhi, M.S, Young, J. and Knight, W.A., 1999, Modeling material separation processes in bulk recycling, *International Journal of Production Research*, 37(10), 2239.

Stahl, I. and Beier, P.M., 1997, Sorting of plastics using the electrostatic separation process, *Proceedings of the XX IMPC-Aachen*, 21-26 September, 395.

Stuart J. A. and Lu Q., 2000(a), A model for discrete processing decisions for bulk recycling of electronics equipment, *IEEE Transactions on Electrical Packing Manufacturing*, 23(4), 314.

Stuart J. A. and Lu Q., 2000(b), A refine-or-sell decision model for a station with continuous reprocessing options in an electronics recycling center, *IEEE Transactions on Electrical Packing Manufacturing*, 23(4), 321.

Stuckrad BTO, Lohr K, Vogt V., 1997, Sorting of waste plastic mixtures by flotation, *Proceedings of the XX international mineral processing congress*, Aachen, Germany, Vol. 5, 307.

Takaretu Imai , Stephan Hamm, and Klaus P. Rothenbacher, 2003, Comparison of the Recyclability of Flame-Retarded Plastics, *Environmental Science and Technology* 37,652.

Tory, E.M., 2000, Stochastic sedimentation and hydrodynamic diffusion, *Chemical Engineering Journal*, 80, 81.

Vehlow, J., Bergfeldt, B., Hunsinger, H, Jay, K., Mark, F.E., Tange, L. Drohmann, D. and Fisch, H., 2002, Recycling of bromine from plastics containing brominated flame retardants in state-of-the-art combustion facilities, A technical paper from APME (Association of plastics manufactures in Europe).
http://www.cefic-efra.com/pdf/TEC%20Report%208040%20GB.pdf

Viswanathan, J. and Grossmann, I.E., 1990, A combined penalty function and outer approximation method for MINLP optimization, *Computers and Chemical Engineering*, 14, 769.

Vlad, S., A. Luga and L. 2000, Dascalescu, Modelling of conducting particle behaviour in plate-type electrostatic separators, *J. Phys. D: Appl. Phys*. 33, 127.

Vogel, L. and Peukert, W., 2003, Breakage behaviour of different materials – construction of a mastercurve of the breakage probability, *Powder Technology*, 129, 101.

Wei, J. and Realff, M.J., 2003 (a), Design and optimization of free-fall electrostatic separators for plastics recycling, *AIChE J*., 49(12), 3138.

Wei, J. and Realff, M.J., 2003 (b), Design and optimization of drum-type electrostatic separators for plastics recycling, submitted to *Industrial & Engineering Chemistry Research*.

Wei, J. and Realff, M.J., 2003 (c), A unified probabilistic approach for modeling trajectory-based solids separations, submitted to *AIChE J*.

Wei, J. and Realff, M.J., 2004, The sample average approximation methods for stochastic MINLPs, *Computers and Chemical Engineering*, 28(3), 333.

Wibowo, C. and Ng, K.M, 1999, Synthesis of bulk solids processing systems, *AIChE J.*, 45 (8), 1629.

Wu, D., and Ierapetritou, M.G., 2003, Decomposition approaches for the efficient solution of short-term scheduling problems, *Computers and Chemical Engineering*, 27, 1261.

Xiao, C., Allen L., Biddle, M.B. and Fisher, M.M., 1999, Electrostatic separation and recovery of mixed plastics, SPE Annual Recycling Conference 1999, http://www.plasticsresource.com/recycling/ARC99/Xiao.PDF

Yan, E. S., Outokumpu Technology Inc, Personal Communication

Yan, E. S., T. J. Grey and T. U. Niitti, 2001, Electrostatic separation apparatus and method using box-shaped electrodes, *U.S. Patent 6329623* B1, Dec., 11

Yanar, D.K. and Kwetkus, B.A., 1995, Electrostatic separation of polymer powders, *Journal of Electrostatics*, 35, 257

Zhang, Shunli and Forssberg, E., 1999, Intelligent liberation and classification of electronic scrap, *Power Technology*, 105, 295.

VITA

Jing Wei was born on October 12, 1974, in Nantong, China, People's Republic of, to Junsheng Wei and Yanyu Feng. She attended the Zhejiang University in 1992, from which she was awarded a Bachelor of Science in 1996 and a Master of Science in 1999, both in Chemical Engineering. She married Jian Gu on March 31, 1999, and left for the United States in August, 1999 to pursue a higher degree at the Georgia Institute of Technology. In the summer of 2004, she was awarded a Doctorate of Philosophy in Chemical Engineering.